RETENTION MECHANISMS OF (BIO)COLLOIDS IN SINGLE FRACTURES

IDENTIFYING THE RETENTION MECHANISMS OF (BIO)COLLOIDS IN SINGLE, SATURATED, VARIABLE-APERTURE FRACTURES

Sandrina N. Rodrigues

B.Eng.

A Thesis

Submitted to the School of Graduate Studies

in Partial Fulfillment of the Requirements

for the Degree

Doctor of Philosophy

McMaster University Copyright

© by Sandrina N. Rodrigues, September 2012

DOCTOR OF PHILOSOPHY (2012)

Civil Engineering

McMaster Univeristy

Canada

TITLE: IDENTIFYING THE RETENTION MECHANISMS OF (BIO)COLLOIDS IN SINGLE, SATURATED, VARIABLE-APERTURE FRACTURES

AUTHOR: Sandrina Nicole Rodrigues
B.Eng. (McMaster University)

SUPERVISOR: Dr. Sarah E. Dickson

NUMBER OF PAGES: xiii, 116

Thesis Abstract

Owing to the lack of knowledge pertaining to the fate and transport of microorganisms in fractured aquifers, the research presented in this thesis was designed to improve the mechanistic understanding of particulate transport in fractures by conducting tracer experiments in natural and epoxy replica fractures. This research demonstrated that particulate retention within fractures is heavily dependent on the equivalent mass balance aperture, followed by the coefficient of variation of the aperture field, and then by the flow conditions. It was also shown that the fracture aperture field alone, not the flow rate or the matrix properties, determines the number of fracture volume flushes required to achieve a 2-3 log decrease in effluent concentration. Moreover, a statistical model was developed that identifies the most important factors affecting particulate retention as the ratio of the ionic strength of solution to the charge of the collector, the ratio of the particle to collector charges, and the Peclet number. The model is able to reasonably predict particulate retention. Finally, tracer experiments conducted in a natural fracture and an epoxy replica of that fracture isolated the effects of matrix properties on attachment, and hence, retention. The transparent nature of the replica fracture was exploited to capture images of *E. coli* RS2-GFP transport. These images reveal preferential transport within the fracture, and also show that the preferential pathway broadens slightly under increasing flow conditions. This broadening is likely due to higher fluid pressures associated with larger specific discharges. In the groundwater field, there is so little fracture-specific information available that coupling the understanding of a critical environmental setting (fractures) with high-quality particulate tracer experiments and associated modeling represents a significant contribution to the body of science.

Acknowledgements

My sincerest gratitude goes to Dr. Sarah Dickson for sharing her expertise, for her guidance, and for her constant faith in my abilities. Sarah is an excellent supervisor, an approachable mentor, and a tireless editor. It has been a pleasure working with her on this research and I cherish the lifelong friendship I have gained as a result of this journey.

I would like to extend a heartfelt thank you to each of my committee members: Dr. Monica Emelko, Dr. Carlos Filipe, and Dr. Bob Pelton. Their insights were always instructional and timely.

I am indebted to Anna Robertson and Peter Koudys for their friendship and laboratory assistance. Many aspects of this work depended on their time, patience, and insight.

I will sincerely miss all of my friends at McMaster, especially the girls in JHE 330 with whom I have had many enlightening conversations and from whom I have learned so much.

To my family and friends, especially my mom, Siddarth, and Katia: Thank you for the love, support, and encouragement. Nothing pleases me more than being able to share this with you.

Contents

1 Introduction **1**

1.1 Impetus and Scope of Research . . . 1

1.2 Background . . . 3

1.2.1 Groundwater and Fractured Rock Aquifers . . . 3

1.2.2 Groundwater Legislation in Ontario . . . 4

1.2.3 Fracture Characterization . . . 5

1.2.4 Concept of 'Equivalent Aperture' . . . 6

1.2.5 Definition of 'Specific Discharge' . . . 8

1.2.6 Colloid Filtration Theory . . . 8

1.2.7 Pore, Charge, and Size Exclusion . . . 10

1.2.8 Colloid Attachment Mechanisms . . . 11

1.2.9 *E. coli*-Specific Attachment Mechanisms . . . 11

1.2.10 Biofilm Formation in Fractures . . . 13

1.2.11 Surrogates for *E. coli* O157:H7 . . . 13

2 Colloid Retention Mechanisms in Single, Saturated, Variable-Aperture Fractures **19**

2.1 Introduction . . . 23

2.1.1 Background . . . 24

2.2 Materials and Methods . . . 27

2.2.1 Fracture Plane Preparation . . . 27

2.2.2 Experimental Setup . . . 28

2.2.3 Fracture Plane Saturation . . . 30

2.2.4 Aperture Field Characterization . . . 30

2.2.5 *E. coli* RS2-GFP Tracer Tests . . . 32

2.3 Results and Discussion . . . 33

2.3.1 Aperture Field Characterization . . . 33

2.3.2 Repeatability of the *E. coli* RS2-GFP Tracer Tests . . . 38

2.4 Conclusions . . . 48

3 A Statistical Model for Particulate Retention Mechanisms in Single, Saturated, Variable-Aperture Fractures 54
3.1 Background . . . 58
3.2 Model Development . . . 59
3.2.1 Dimensionless Numbers . . . 60
3.3 Results and Discussion . . . 62
3.3.1 Regression Diagnostics . . . 64
3.3.2 Model Verification . . . 67
3.4 Conclusions . . . 67

4 The Effect of Matrix Properties and Specific Discharge on *E. coli* RS2-GFP Transport in Single, Saturated, Variable-Aperture Fractures 71
4.1 Background . . . 76
4.2 Materials and Methods . . . 78
4.2.1 Experimental Setup . . . 79
4.2.2 Fracture Plane Saturation . . . 82
4.2.3 Fracture Plane Characterization . . . 82
4.2.4 *E. coli* RS2-GFP Experiments . . . 83
4.3 Results and Discussion . . . 84
4.3.1 Fracture Aperture and Matrix Characterization . . . 84
4.3.2 Quantitative *E. coli* RS2-GFP Tracer Test Results . . . 87
4.3.3 Qualitative *E. coli* RS2-GFP Tracer Test Results . . . 91
4.4 Conclusions . . . 92

5 Conclusions 97
5.1 Conclusions & Implications from Chapter 2 . . . 98
5.2 Conclusions & Implications from Chapter 3 . . . 98
5.3 Conclusions & Implications from Chapter 4 . . . 99
5.4 Concluding Remarks . . . 100

6 Suggestions for Future Work 102

7 Appendix A 104

8 Appendix B 109

9 Appendix C 115

List of Figures

1.1 Concept of equivalent aperture 6

1.2 Mechansisms of colloid attachment (Yao et al, 1971) 9

2.1 Photographs of the top view of the two types of fractures employed in these experiments. 28

2.2 Schematic diagram of the experimental apparatus. 29

2.3 Specific discharge (q) versus ΔH for F1. The least squares simple linear regression trend line is shown. Error bars representing the standard deviation of known concentrations determined in triplicate can not be seen because they are smaller than the symbols. 34

2.4 Bromide BTC from Fracture F1. Error bars representing the standard deviation of concentrations determined in triplicate can not be seen because they are smaller than the symbols. 36

2.5 *E. coli* RS2-GFP BTCs for F1 (dolomitic limestone) at 140 m·day^{-1} (in triplicate). The symbols represent the back-calculated concentration of *E. coli* determined from serial dilutions and standard bacteria plating methods. Error bars were determined using Equation 4.8. 39

2.6 BTCs of □ Bromide and ◯ *E. coli* RS2-GFP for F1 at 140 m·day^{-1}. 40

2.7 *E. coli* RS2-GFP recovery versus mass-balance aperture for each fracture at □ 1.4, ◯ 14, and △ 140 m·day^{-1}. Error bars represent the standard deviation of *E. coli* RS2-GFP recovery from experiments conducted in triplicate. . . . 41

2.8 *E. coli* RS2-GFP recovery versus COV_S of the aperture field for each fracture at specific discharges of □ 1.4, ◯ 14, and △ 140 m·day^{-1}. Error bars represent the standard deviation of *E. coli* RS2-GFP recovery from experiments conducted in triplicate. 42

2.9 Log normalized median *E. coli* RS2-GFP BTCs for □ F1 (dolomitic limestone), ◯ F2 (dolomitic limestone), and △ F3 (granite) at 140 m·day^{-1}. 44

2.10 Specific discharge versus average *E. coli* RS2-GFP recovery for □ F1 (dolomitic limestone), ◯ F2 (dolomitic limestone), and △ F3 (granite). Error bars represent the standard deviation of *E. coli* RS2-GFP recovery from experiments conducted in triplicate. 45

2.11 Log normalized median *E. coli* RS2-GFP BTCs for F1 at □ 1.4, ◯ 14, and △ 140 m·day^{-1}. 47

3.1 Normal probability plot for observed values. 65

3.2 Residual versus a) lnN_{IS}, b) lnN_Q, and c) lnN_{Pe} for the natural logarithm of fraction retained. 66

3.3 Log-normalized values of predicted versus observed retention. 67

4.1 Photographs of the top view of the two types of fractures employed in these experiments. 78

4.2 Schematic diagram of the experimental setup. 80

4.3 Schematic diagram of the epoxy replica compression system. 81

4.4 Schematic diagram of the fracture placed inside the image-capturing setup. . 81

4.5 *E. coli* RS2-GFP tracer tests in a) F at 14 m·day^{-1} (in triplicate) and in b) RF at 15 m·day^{-1} (in duplicate). Error bars represent the range of maximum and minimum concentrations and were determined using Equation 4.8. . . . 87

4.6 Average *E. coli* RS2-GFP recovery at different specific discharges for F and RF. Error bars represent the standard deviation of replicated experiments. The two data points without error bars were not replicated. 88

4.7 *E. coli* RS2-GFP BTCs for F and RF at 14 and 15 m·day^{-1}, respectively. . . 89

4.8 Log normalized median *E. coli* RS2-GFP BTCs in a) F and b) RF at different specific discharges. 90

4.9 *E. coli* RS2-GFP traveling through RF at various specific discharges (rows) captured at different fracture volume flushes (columns). Bulk flow is from left to right. 91

7.1 Log-normalized median *E. coli* RS2-GFP BTCs for F1 at a)1.4m$\cdot$d^{-1}, b)14m$\cdot$d^{-1}, and c) 140m$\cdot$d^{-1} (in triplicate). 106

7.2 Log-normalized median *E. coli* RS2-GFP BTCs for F2 at a)1.4m$\cdot$d^{-1}, b)14m$\cdot$d^{-1}, and c) 140m$\cdot$d^{-1} (in triplicate). 107

7.3 Log-normalized median *E. coli* RS2-GFP BTCs for F3 at a)1.4m$\cdot$d^{-1}, b)14m$\cdot$d^{-1}, and c) 140m$\cdot$d^{-1} (in triplicate). 108

8.1 Matlab code used for processing the photos of *E. coli* RS2-GFP transport through the epoxy fracture. 110

8.2 SAS code used to develop particulate retention model. 111

9.1 *E. coli* RS2-GFP BTC for RF at 30m$\cdot$d^{-1} (in duplicate). 116

List of Tables

2.1 Summary of the hydraulic and solute tracer test results. 34

2.2 *E. coli* RS2-GFP recovery from tracer experiments. 46

3.1 List of parameters used to develop the Pi groups. 61

3.2 Base units of all parameters listed in Table 3.1. 61

3.3 List of the Pi groups employed in the statistical analysis, together with their physical interpretations. 62

3.4 Range of conditions under which this model is applicable. 64

3.5 Parameter estimate diagnostics for the model shown in Equation (3.3). . . . 64

4.1 Characterization results from hydraulic and solute tracer experiments for F and RF. 85

7.1 *E. coli* RS2-GFP recoveries from experiments conducted in the natural fractures. 105

8.1 Table of all the dimensionless numbers used in the multiple linear regression analysis. Each row represents values corresponding to one tracer experiment. 112

8.1 (cont.) Table of all the dimensionless numbers used in the multiple linear regression analysis. Each row represents values corresponding to one particulate tracer experiment. 113

8.2 Table of all the dimensionless numbers used to verify the predictive model. Each row represents values corresponding to one particulate tracer experiment. 114

9.1 *E. coli* RS2-GFP recoveries from experiments conducted in the replica fracture. 116

List of Abbreviations and Symbols

A	Areal extents of the fracture
A_P	Surface area of particulate
b_c	Equivalent hydraulic aperture
b_f	Equivalent frictional-loss aperture
b_m	Equivalent mass balance aperture
BTC	Breakthrough curve
C_{eff}	Concentration of tracer exiting fracture
$\bar{C}_{eff}$	Average concentration of tracer exiting fracture
C_{meas}	Measured tracer concentration
CFSTR	Continous flow stirred tank reactor
CFT	Colloid filtration theory
CFU	Colony-forming units
COV	Coefficient of variation
COV_S	Surrogate measure of COV
CWA	Clean Water Act
D	Diffusion coefficient
DDW	Deionized, degassed water
DLVO	Derjaguin, Landau, Verway, and Overbeek
EDL	Electric double layer
E. coli	*Escherichia coli*
EPA	Environmental Protection Agency
EPS	Extrapolymeric substances
F	Natural Fracture
f_r	Fraction of particles retained within fracture
FV	Fracture volume
g	Gravitational constant
HPLC	High-performance liquid chromatography

I	Ionic strength of solution
L	Length of fracture (parallel to flow)
LPS	Lipopolysaccharides
N_{AV}	Avogadro's number
N_{IS}	Dimensionless number 1
N_{Pe}	Dimensionless number 9
N_Q	Dimensionless number 2
OWRA	Ontario Water Resources Act
PBS	Phosphate buffered saline
q	Specific discharge
Q	Flow rate
Q_M	Matrix charge
Qn	Quartile n (where n = 1, 2, 3, 4)
Q_P	Particulate charge
RF	Replicate Fracture
$R_{\%}$	Percent Recovery
SDWA	Safe Drinking Water Act
t_m	Mean residence time of tracer
$\bar{t}$	Average time between consecutive samples
T	Absolute temperature
W	Width of fracture (perpendicular to flow)
USGS	United States Geological Survey
vDW	van der Waals
V_{recirc}	Volume of the recirculation system
β_i	Regression model parameter estimates (i = 1, 2, 3...)
ΔH	Hydraulic headloss
η	Viscosity of solution
γ	Fluid weight density
κ	Regression constant
μ	Dynamic viscosity
Φ_P	Diameter of particle
ρ_P	Particle density
ρ_S	Density of solution
σ	Standard deviation of the equivalent apertures

Declaration of Academic Achievement

This thesis was prepared in accordance with the guidelines set forth by the McMaster School of Graduate Studies for theses consisting of work prepared for publication in peer-reviewed journals. Chapters 2, 3, and 4 have been prepared and/or submitted for publication. As such, these chapters have been co-authored. The original contributions of the thesis author to each paper and the reasons for including them in the main body of this thesis are outlined below:

Chapter 2: Colloid Retention Mechanisms in Single, Saturated, Variable-Aperture Fractures *by: S.N. Rodrigues, S.E. Dickson & J. Qu*

The idea for these experiments came from S.E. Dickson. All authors contributed to the design of the experiments discussed in this paper. S.N. Rodrigues and J. Qu conducted the experiments from 2007-2009. S.N. Rodrigues analyzed the data under the guidance of S.E. Dickson. S.N. Rodrigues prepared the manuscript, and S.E. Dickson edited it. This work should be included in the main body of the thesis because it resulted in a novel understanding of the behaviour of *E. coli* RS2-GFP in fractured rocks.

Chapter 3: A Statistical Model for Particulate Retention Mechanisms in Single, Saturated, Variable-Aperture Fractures *by: S.N. Rodrigues & S.E. Dickson*

The data used in developing this model was obtained from experiments conducted by S.N. Rodrigues and others in the Dickson Laboratory. S.N. Rodrigues performed the statistical analysis from 2011-2012 under the guidance of S.E. Dickson. S.N. Rodrigues prepared the manuscript, and S.E. Dickson edited it. The results of this research, namely the development

of a statistical model that identifies and reasonably predicts the transport of particulates in fractures warrants its inclusion in the main body of this thesis.

Chapter 4: The Influence of Matrix Properties on Particulate Transport in Single, Saturated, Variable-Aperture Fractures and Visually Capturing the Preferential Transport of *E. coli* RS2-GFP *by: S.N. Rodrigues & S.E. Dickson*

The idea for the visualization experiments came from S.N. Rodrigues and S.E. Dickson. S.N. Rodrigues designed and conducted the *E. coli* RS2-GFP visualization experiments from 2008-2012. S.N. Rodrigues analyzed the data under the guidance of S.E. Dickson. S.N. Rodrigues prepared the manuscript, and S.E. Dickson edited it. The images of *E. coli* RS2-GFP transport through a fracture visually confirm, for the first time, the existence of the preferential transport of biocolloids within fractures. In addition, this research isolates the influence of matrix properties on the transport of biocolloids in fractures, and therefore, should be included in the main body of this thesis.

Chapter 1

Introduction

This chapter summarizes the motivation and scope of this thesis, and provides some background knowledge including a description of fractured aquifers, the legislation pertaining to groundwater, and the relevant theoretical concepts which are fundamental to the research presented in this thesis. Following the McMaster School of Graduate Studies Guide for the Preparation of Master's and Doctoral Theses, each scholarly work that is prepared for publication (i.e. Chapters 2, 3, and 4) are preceded by a summary of that paper that sets the context and highlights the overall implications of that work. Each paper is then incorporated as published (or as prepared for publication). The overall conclusions and implications from all three papers are summarized in Chapter 5. Suggestions for future work are presented in Chapter 6. To minimize the repetition of information, the methodologies and calculations discussed in Chapters 3 and 4 refer the reader to Rodrigues et al. (2012) which is Chapter 2.

1.1 Impetus and Scope of Research

The Geological Survey of Canada identifies the characterization of fractured aquifers as one of the most relevant groundwater knowledge gaps in Canada (Rivera, 2005). Owing to

the lack of knowledge pertaining to the transport of microorganisms in fractured aquifers and the large uncertainties that are currently introduced upon characterizing fractured aquifers using the techniques designed for porous media, this research aims to improve the mechanistic understanding of particulate transport in fractured aquifers. An improved understanding of the mechanisms that contribute to the fate and transport of particulates in fractures could feed into the development of much needed, fracture-specific characterization techniques.

Thesis Scope and Objectives

The transport of particulates in laboratory-scale, single, saturated, variable-aperture fractures was investigated under a range of flow conditions. The degree of particulate retention was analyzed and related to the aperture field characteristics of each fracture in order to identify the most influential particulate retention mechanisms. The following objectives were designed as part of this investigation.

The first research objective is to improve the mechanistic understanding of particulate transport in fractured aquifers through physical, laboratory-scale experiments. In these experiments, the behaviour of *E. coli* RS2-GFP in single, fully saturated, approximately planar, variable-aperture fractures, obtained from the natural environment, was investigated. The relationship between retention mechanisms, aperture field characteristics, and specific discharge is explored through a series of experiments consisting of fractures with different aperture field characteristics under a range of flow conditions.

The second objective of this research is to use an extensive data set to develop a model that describes the retention of particulates in single, saturated, variable-aperture fractures based on: the fracture matrix material properties, fracture aperture field characteristics, particulate surface properties, particulate sizes, and flow conditions.

The third objective of this research is to explore the effects of fracture matrix properties on the fate and transport of *E. coli* RS2-GFP. To accomplish this task, the results of *E. coli* RS2-GFP tracer experiments conducted in a natural fracture are compared to those

conducted in an epoxy replica of that same fracture. In addition, a secondary objective is to capture novel images of *E. coli* RS2-GFP transport through a fracture and observe the effects of specific discharge on this transport.

Each objective, presented in Chapter 2, 3, and 4, respectively, forms the basis of a paper that has been accepted or submitted for publication prior to the defense of this Ph.D. thesis.

1.2 Background

1.2.1 Groundwater and Fractured Rock Aquifers

Groundwater quality is a serious issue in Canada. Nearly 11 million Canadians depend on groundwater for their potable water; that is approximately a third of all Canadians, and this proportion rises to approximately 80% for rural residents (Nowlan, 2007). In May 2000, the town of Walkerton, Ontario unknowingly consumed groundwater contaminated with *E. coli* O157:H7. Thousands of people suffered from serious gastrointestinal illnesses and seven people died. The contaminated groundwater was drawn from an area of the aquifer consisting of very shallow overburden overlying highly fractured rock (O'Connor, 2002). Seventy percent of Canada's regional aquifers exist within fractured media (Rivera, 2005). Fractured aquifers are amongst the most poorly understood natural environments, despite posing very high risks to the protection of potable water sources. The Walkerton Tragedy serves as a jarring reminder of the importance of understanding the vulnerabilities of different sources of potable water and of appropriately managing each source.

Unlike porous media, fractured aquifers have very irregular groundwater flow pathways making it difficult to predict the dispersion and immobilization (or retention), of contaminants within the aquifer. Fractures in rock or clay aquifers are commonly thought to act as contaminant highways resulting in quick and significant contamination of groundwater.

The presence of fractured rocks or channelized sedimentary deposits in the subsurface can tremendously enhance the transport of pathogens due to the presence of pathways that are orders of magnitude larger than those typically found in porous media. Groundwater flow velocities in fractured rocks can range from 0.3 to 8000 m·day^{-1}, and up to 26000 m·day^{-1} in karstic aquifers (Pekdeger and Matthess, 1983). The magnitude of the flow can cause detachment of deposited contaminants reducing the immobilization or retention of contaminants. Consequently, it is believed that fractured rock aquifers are far less capable of retaining bacteria, viruses and protozoa from suspension than their porous media counterparts (Crane and Moore, 1984). An improved understanding of the fate and transport of contaminants in fractured aquifers could be helpful in informing policy and/or decision-makers in the future.

1.2.2 Groundwater Legislation in Ontario

In Ontario, there are no acts that apply solely to groundwater; however, the Statutes of Ontario have many regulations that pertain to waters, which by definition, include groundwater (OWRA, 1990). The Ontario Water Resources Act (OWRA), the Environmental Protection Act (EPA), the Fisheries Act, the Clean Water Act (CWA) and the Safe Drinking Water Act (SDWA) are some of the Provincial and Federal laws that exist to protect Canada's water resources. The OWRA is concerned with protecting the quality and quantity of Ontario's water resources at present and for the future (OWRA, 1990). The EPA focuses on contamination prevention, spills prevention and contingency plans (EPA, 2007). The CWA focuses on preserving and protecting Canada's natural water resources that also serve as sources of drinking water (CWA, 2006). The CWA is founded on a risk-based approach, striving to continuously identify, quantify, and mitigate new, existing, and potential risks to drinking water sources (CWA, 2006). The CWA uses a 'belt-and-suspenders principle', employing multiple barriers to protect the public. As part of this multi-barrier approach, it is essential to understand all activities on land posing a threat to drinking water resources and use this knowledge to develop safe land-use practices. The objective of the SDWA is

to protect the public from drinking water health hazards by establishing and regulating the use of drinking water sources, drinking water distribution systems, and the various drinking water laboratories and operators (SDWA, 2002). The SDWA was created to ensure the safety of public drinking water and many of its regulations emerged from post-Walkerton recommendations.

Current source water protection legislation is based on the 'time of travel' approach which is the amount of time it takes for water to travel through an aquifer before reaching a well. Longer travel times are associated with cleaner water. The presence of fractures within an aquifer can make it extremely difficult to predict an appropriate time of travel; therefore, a more thorough understanding of pathogen transport in fractured aquifers could be used to modify the existing legislation, making it more relevant to fractured aquifers. There are many questions the science has yet to fully answer. For instance, is the 'time of travel' approach acceptable in all aquifers, particularly those with larger travel pathways such as fractures? When performing vulnerability assessments, is it reliable to treat solute contaminants and particulate contaminants identically? Do all pathogens (e.g., *Cryptosporidium parvum*, *Giardia*, *E. coli*) travel through an aquifer in the same manner? Is there any merit in the evidence-based approach (i.e.: if an aquifer has been used as a drinking water source for a long time, is it still a safe source)? Overall, Ontario's water management initiatives are based on the best science available; however, in the realm of fractured aquifers, the science is relatively sparse. Some of the questions mentioned above were used as triggers in the design of the research presented herein.

1.2.3 Fracture Characterization

Over the last century, the science has focused on porous media aquifers, with relatively few studies being conducted on fractured aquifers. Consequently, when it comes to the characterization of fractured aquifers, the same approach as that for porous media is com-

monly employed (Rivera, 2005). Due to the inherent physical differences between the two types of aquifers, it is difficult to estimate the uncertainties that result from using a porous media approach to characterize fractured aquifers. The importance of characterizing the aquifers lays in understanding flow processes, contamination processes, and interconnectivity between aquifers. Fractured aquifers are characterized by their orientation (assumption is usually planar), density (number of fractures per length or per volume of aquifer), aperture size (distance between the fracture walls), channeling (existence of preferential flow paths), fracture connectivity and fracture skins (temporal alterations in fracture surface from flow which may change permeability and transport characteristics) (Krasny and Sharp, 2007). Characterizing a fractured aquifer is useful in understanding particulate and solute transport within the fracture, perhaps posing a threat to a nearby well.

1.2.4 Concept of 'Equivalent Aperture'

To apply known equations of fluid flow researchers often simplify an approximately planar, variable aperture fracture to an equivalent distance between two parallel plates, called an 'equivalent aperture'. This concept is depicted in Figure 1.1. The different shades of gray

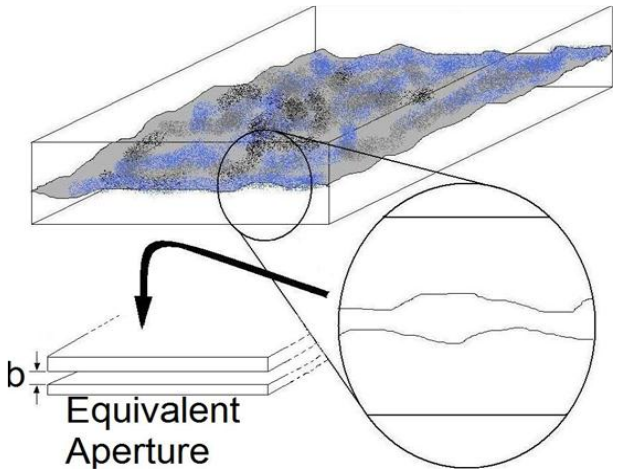

Figure 1.1: Concept of equivalent aperture

depict how a typical, approximately planar, aperture may vary spatially. In a colour copy of this document, the blue areas represent fluid flowing through the aperture. The assumption of equivalent aperture simplifies a three-dimensional problem into a two-dimensional one which is acceptable since the fluid flow is along the fracture plane (and not into the rock matrix).

Due to the developing nature of this research area in the 1970's and 1980's, there was a lack of a common vocabulary for equivalent apertures; this was addressed in a technical note in the early 1990s such that three equations to calculate equivalent apertures are now generally accepted in the literature: mass balance, frictional loss, and cubic law apertures (Tsang, 1992). Details of the calculation of each equivalent aperture can be found in Chapter 2 Section 2.3.1; however, a brief theoretical understanding of each equivalent aperture follows. The equivalent frictional loss aperture is inversely proportional to the hydraulic headloss that occurs across the length of a fracture. Since the smallest pore spaces cause the largest headloss, this equivalent aperture is most sensitive to the smallest aperture regions.

The equivalent hydraulic aperture, or cubic law equivalent aperture, is the only equivalent aperture of the three that can be determined without conducting a solute tracer experiment. This equivalent aperture describes the transmissivity of the fracture aperture since it depends on the volumetric flow and hydraulic headloss.

The equivalent mass balance aperture is directly proportional to the mean residence time of a conservative solute tracer. The largest pore spaces in the fracture transport the largest volumes of a solute tracer, therefore this equivalent aperture is most sensitive to the largest aperture regions. Additionally, the mass balance equivalent aperture has been identified as the best estimate of the arithmetic mean aperture (Tsang, 1992).

1.2.5 Definition of 'Specific Discharge'

All of the fractures discussed throughout this research varied in aperture size and areal extents. A flow rate applied to a very wide fracture would cause different flow conditions in that fracture than the same flow rate applied to a very narrow fracture. Consider for example, placing an object (like a thumb) over the opening of a flowing garden hose without adjusting the flow controls. A narrower opening in the hose causes the water to travel at a much higher velocity despite no other change in the system. Likewise, using the same flow rate in different fractures would result in extremely variable average linear flow velocities in each fracture, corresponding to very different flow conditions. For this reason, specific discharge was used to measure the flow conditions in each fracture. The specific discharge is a measure of the volumetric flux through the fracture, and is therefore comparable between fractures. The specific discharge is calculated as follows:

$$q = \frac{Q}{w \cdot b_m} \tag{1.1}$$

where q $[L \cdot T^{-1}]$ is the specific discharge, Q $[L^3 \cdot T^{[} - 1]$ is the flow rate, w $[L]$ is the width of the fracture and b_m $[L]$ is the equivalent mass-balance aperture. Using Equation (1.1) the required flow rates were determined such that the desired specific discharge was achieved for each combination of fracture and desired flow condition.

1.2.6 Colloid Filtration Theory

Aquifers are comprised of a matrix that is fixed in space, consisting of soils, rocks or clays, and having pore spaces through which water and small particles, together known as the bulk fluid, may travel. Upon contact, some of these particles, which may include particulate contaminants, can become attached to the collector thereby being removed, or filtered from the bulk flow. Colloid-sized particles range from about 1nm to just over 1μm in length or

diameter and are strongly influenced by surface properties. The size of colloidal particles subjects them to forces typically associated with molecules (e.g., van der Waals; Brownian), in addition to body forces (like gravity) (Reimus, 1995).

Colloid Filtration Theory (CFT) was developed (Yao et al., 1971) to describe the deposition mechanisms of colloidal particles onto collector surfaces taking into account the advection (or convection), dispersion and sorption of the particles (de Marsily, 1986). Although the paper focused on the filtration of water and wastewater contaminants in a packed-bed sand filter where each grain of sand is considered a collector, the theory it introduced has been adopted by many to adequately describe colloid filtration in groundwater environments.

According to CFT, colloids make contact with a surface in one of three ways: interception (due to the physical size of the colloid it comes into contact with the collector), sedimentation (due to a colloidal density greater than the density of water it deposits onto a surface) and diffusion (due to Brownian motion it randomly comes into contact with a collector)(Yao et al., 1971). These mechanisms are shown in Figure 1.2. There are several processes that

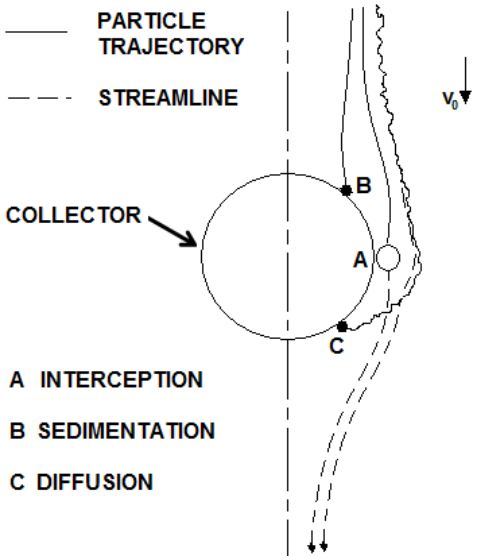

Figure 1.2: Mechansisms of colloid attachment (Yao et al, 1971)

act together to cause the retention of particles within an aquifer. Fluid mechanics of the

solution will influence the transport of colloidal contaminants (like *E. coli*) to a surface for deposition; however, irreversible attachment to that surface will be dictated by mechanical entrapment, the interaction of colloidal forces, and biological adhesion. The mechanisms of mechanical entrapment are attachment, filtration and straining (Yao et al., 1971; An et al., 2000). Attachment mechanisms for colloids and *E. coli* will be discussed in detail in Sections 1.2.8 and 1.2.9, respectively. Filtration and straining are two mechanisms of mechanical entrapment. They differ only in the depth into the aquifer that a particle is able to travel. When particles are larger than the pore spaces (in this case, the fracture aperture), the particles are incapable of entering the fracture; this is called mechanical filtration. Straining, on the other hand, occurs when particles are able to enter the fracture and travel some distance before being immobilized due to size.

1.2.7 Pore, Charge, and Size Exclusion

There are some minor discrepancies on some of the technical jargon used in fracture research due to its developing nature. For the purposes of this thesis, the following definitions were employed. Pore exclusion refers to mechanical filtration. That is, due to the size of a particle, it is unable to sample the full areal extents of the fracture. This is because some of the pore spaces leading to areas of the fracture are smaller than the dimensions of the particle. Charge exclusion occurs when the repulsive forces between similarly charged particles and fracture walls prevent the particle from entering the regions nearest to the fracture walls (Zheng et al., 2009). Therefore, due to like charges, the particles are unable to access certain regions of the fractures.

Size exclusion is a phenomenon whereby larger particles are unable to sample the smallest velocities from the velocity profile and will therefore travel faster than smaller particles. Since the fracture matrix is fixed in space, the velocity of the particles closest to the walls is the same as the velocity of the walls, that is, zero. The velocity profile between two fracture walls

in an ideal parallel plate fracture follows a parabolic distribution with zero velocity at each fracture wall and a maximum velocity at the centerline (de Marsily, 1986). Larger particles will have center of masses farther away from the fracture walls than smaller particles and are therefore unable to sample the smallest velocities.

1.2.8 Colloid Attachment Mechanisms

Attachment is included in CFT and typically results when a net attractive colloidal force exists between colloid and collector. The DLVO theory, named after Derjaguin, Landau, Verway, and Overbeek, describes the net interaction forces between a charged colloidal particle and a collector surface (Roy and Dzombak, 1996; Gu, 2004). DLVO theory accounts for two-types of colloidal forces: attractive long-range van der Waals (vdW) forces and repulsive electric double layer (EDL) forces, which are both dependent on the separation distance between the colloid and the collector surface (Gu, 2004). Van der Waals forces occur when molecules making up the colloidal particle interact with molecules on the collector surface to induce a dipole. EDL forces are a function of overlapping counter-ion clouds in the vicinity of a charged surface, as well as the differences in free energy experienced when the two components move closer together or farther apart from each other (An et al., 2000). It is important to note that the assumptions for the DLVO theory, namely, homogeneity, uniformly-charged, molecularly-flat surfaces, are strongly violated by real bacteria and fracture surfaces; however, the theory still provides a useful conceptual framework for bacterial deposition onto surfaces (An et al., 2000).

1.2.9 *E. coli*-Specific Attachment Mechanisms

E. coli, compared to other colloids, have several biological advantages that act to increase successful attachment to a surface. In particular, an *E. coli* bacterium typically has about 5-10 appendages called flagellar filaments which perform hydrodynamic work on the

fluid suspension allowing the bacteria to move rapidly and change their direction of motion abruptly (Macnab, 1996). Motile bacteria have an increased probability of making contact with groundwater surfaces, resulting in higher rates of collision and attachment, and are therefore more likely to be filtered out of the bulk flow (Becker et al., 2003). In comparison to other colloids, *E. coli* which typically have 100-1000 fimbriae (or pili) acting as adhesin units, have an increased binding ability to attach to surfaces (Low et al., 1996).

As prokaryotes, *E. coli* have no true nucleus and very simple cellular structures. The cell membrane contains the insides of the cell including the cytoplasm, genetic information in the form of a single (close-looped) DNA molecule, several plasmids (coding for enzymes and proteins) and ribosomes (protein assembly structures). The cell membrane, which separates the interior of the bacterial cell from the environment, is made up of protein (60%) and phospholipids (40%) arranged such that the external surface of this cell membrane is hydrophobic (Chapelle, 2001).

Surrounding the cell membrane is the cell wall, which consists of peptidoglycan, a three-dimensional polymer consisting of sugars and amino acids which are cross-linked with short peptide bridges, and functions to structurally support the cell (Chapelle, 2001). The cell wall of most bacteria falls into one of two categories: Gram negative and Gram positive, referring to the ability of the cell wall to retain Grams stain when washed with ethyl alcohol. *E. coli* O157:H7 is a gram negative bacteria (meaning it does not retain Grams stain); as such, the peptidoglycan layer of a bacterial cell is thinner and is surrounded by a layer of phospholipids, lipoproteins, and lipopolysaccharides (Chapelle, 2001).

In addition to size, charge, hydrophobicity, fimbriae and flagella, the presence of lipopolysaccharides (LPSs), on the surface of the *E. coli* significantly influences the attachment of this bacteria to mineral surfaces (like fractured rock aquifers) (Foppen and Schijven, 2006). A review on the literature concluded that *E. coli* is a relatively hydrophilic and strongly negatively charged organism (Foppen and Schijven, 2006). Two studies included in the review concluded that adhesion of hydrophilic microorganisms to aquifer surfaces is heavily influ-

enced by zeta potential and only marginally by hydrophobicity (Foppen and Schijven, 2006). The sticking efficiency of *E. coli* which is proportional to irreversible deposition is affected by the zeta potential of *E. coli*, solution chemistry, geochemical heterogeneity, bacteria population heterogeneity, and the LPS bacterial wall composition (Foppen and Schijven, 2006). Experimental results in porous media studies show that as the ionic strength of solution increases, so too does *E. coli* deposition as a result of the change in zeta potential (Nocito-Gobel and Tobiason, 1995).

1.2.10 Biofilm Formation in Fractures

In groundwater environments, biofilms consist of a microbial community as well as the extrapolymeric substances (EPS) that the bacteria release during growth and reproduction. These films have a porous, 'sponge-like' structure (Charbonneau et al., 2006). Ross et al. (2001) injected molasses as a carbon source to stimulate the growth of indigenous bacteria in a single fracture and found that bioclogging accelerated with time and at 22 days the hydraulic conductivity of the single, limestone fracture was two orders of magnitude lower than it was at the start of the study. Hill and Sleep (2002) also observed a decreased hydraulic conductivity in the range of two orders of magnitude with biofilm formation. The formation of biofilms causes hydraulic changes in the apparatus and the presence and effect of biofilms can be determined by monitoring hydraulic changes in the apparatus over the course of the experiments.

1.2.11 Surrogates for *E. coli* O157:H7

Some of the most common tracers for understanding contaminant transport in aquifers include non-pathogenic bacteria, microspheres, bacteriophages, conservative chemical tracers (like bromide, or iodide) as well as dyes (relatively infrequently). Polystyrene (latex) microspheres are a common surrogate of bacteria and oocysts in pathogen transport studies espe-

cially when non-pathogenic microorganisms are inappropriate for use. Although comparable to *E. coli* in size, most microspheres poorly mimic the surface properties and biological appendages of *E. coli*; these discrepancies may significantly affect the transport and attachment of the bacteria to aquifer and food surfaces, limiting the utility of microspheres as a surrogate for *E. coli*. Despite these discrepancies, microspheres are still useful tools because they are generally hydrophobic, convenient to purchase, consistently almost perfectly spherical, stable at temperatures commonly found in groundwater aquifers, resistant to biodegradation, and have a density almost identical to that of water (Becker et al., 1999).

Non-pathogenic bacteria are often used as an indicator for potential risk to public health in groundwater, (Edberg et al., 2000; Dai and Hozalski, 2006) and as an indicator for the efficiency of decontamination processes within the food industry (Eblen et al., 2005; Keeling et al., 2009; Kim and Harrison, 2009). The World Health Organization regards the presence of fecal bacteria as a very sensitive method of quality assessment (as quoted in Edberg et al. (2000)). To improve model predictions of bacterial behaviour in fractured aquifers, a better understanding of the interaction of cell characteristics with fractured media is necessary (Becker et al., 2003). Bacterial tracers are often chosen based on two criteria: (1) the existence of behavioural data for that particular strain, and (2) some degree of antibiotic resistance to facilitate contamination-free laboratory tests (Sherwood et al., 2003). *E. coli* RS2-GFP was the strain of *E. coli* employed in these experiments because they are nonpathogenic, easily innumerable, and resistant to several antibiotics which were used to minimize the risk of contamination in the laboratory.

References

An, Y. H., Dickinson, R. B., Doyle, R. J., 2000. Mechanisms of Bacterial Adhesion and Pathogenesis of Implant and Tissue Infections. Totowa, New Jersey: Humana Press Inc.

Becker, M., Metge, D., Collins, S., Shapiro, A., Harvey, R., 2003. Bacterial Transport Experiments in Fractured Crystalline Bedrock. Ground Water 41 (5), 682–689.

Becker, M. W., Reimus, P. W., Vilks, P., 1999. Transport and Attenuation of Carboxylate-Modified Latex Microspheres in Fractured Rock Laboratory and Field Tracer Tests. Ground Water 37 (3), 387–395.

Chapelle, F. H., 2001. Ground-Water Microbiology and Geochemistry. John Wiley & Sons Inc.

Charbonneau, A., Novakowski, K., Ross, N., 2006. The Effect of a Biofilm on Solute Diffusion in Fractured Porous Media. Journal of Contaminant Hydrology 85, 212–228.

Crane, S., Moore, J., 1984. Bacterial Pollution of Groundwater: A Review. Water, Air and Soil Pollution, 67–83.

CWA, 2006. Clean Water Act Chapter 22.

Dai, Z., Hozalski, R. M., 2006. Evaluation of Microspheres as Surrogates for Cryptosporidium parvum Oocysts in Filtration Experiments. Environ. Sci. Technol. (37), 1037–1042.

de Marsily, G., 1986. Quantitative Hydrology: Groundwater Hydrology for Engineers. San Diego: Academic Press.

Eblen, D., Bassam, A., Sapers, G., 2005. Studies to Select Appropriate Nonpathogenic Surrogate Escherichia coli Strains for Potential Use in Place of Escherichia coli O157:H7 and Salmonella in Pilot Plant Studies. Journal of Food Protection 68, 282–291.

Edberg, S. C., Rice, E. W., Karlin, R. J., Allen, M. J., 2000. Escherichia coli: The Best Biological Drinking Water Indicator for Public Health Protection. Journal of Applied Microbiology 88, 106S–116S.

EPA, 2007. Environmental Protection Agency, Ontario Regulation 224.

Foppen, J., Schijven, J., 2006. Evaluation of Data from the Literature on the Transport and Survival of Escherichia coli and Thermotolerant Coliforms in Aquifers Under Saturated Conditions. Water Research 40, 401–426.

Gu, Y., 2004. Deposition of Liquid Drops onto Solid Surfaces.

Hill, D. D., Sleep, B. E., 2002. Effects of Biofilm Growth on Flow and Transport Through a Glass Parallel Plate Fracture. Journal of Contaminant Hydrology 56, 227–246.

Keeling, C., Niebuhr, S. E., Acuff, G. R., Dickson, J. S., 2009. Evaluation of Escherichia coli Biotype 1 as a surrogate for Escherichia coli O157:H7 for Cooking, Fermentation, Freezing and Refrigerated Storage in Meat Processes. Journal of Food Protection 72, 728–732.

Kim, J., Harrison, M., 2009. Surrogate Selection of Escherichia coli O157:H7 Based on Cryotolerance and Attachment to Romaine Lettuce. Journal of Food Protection 72, 1385–1389.

Krasny, J., Sharp, J. J., 2007. Groundwater in Fractured Rocks. In: Groundwater in Fractured Rocks International Conference. Prague: Taylor and Francis Group, London, UK.

Low, D., Braaten, B., van der Woude, M., 1996. Escherichia coli and Salmonella: Cellular and Molecular Biology. ASM Press, Washington D.C., Ch. Fimbriae, pp. 146–157.

Macnab, R. M., 1996. Escherichia coli and Salmonella: Cellular and Molecular Biology. Vol. 44. Ch. Flagella and Motility, pp. 123–145.

Nocito-Gobel, J., Tobiason, J. E., 1995. Effects of Ionic Strength on Colloid Deposition and Release. Colloids and Surfaces A.

Nowlan, L., 2007. Eau Canada The Future of Canada's Water. Vancouver: UBC Press, Ch. Out of Sight, Out of Mind? Taking Canada's Groundwater for Granted, pp. 55–83.

O'Connor, M. J., 2002. Part One A Summary Report of the Walkerton Inquiry. Toronto: Queen's Printer for Ontario.

OWRA, 1990. Ontario Water Resources Act, R.S.O c. O. 40.

Pekdeger, A., Matthess, G., 1983. Factors of Bacteria and Virus Transport in Groundwater. Environmental Geology 5 (2), 49–52.

Reimus, P. W., 1995. The Use of Synthetic Colloids in Tracer Transport Experiments in Saturated Rock Fractures. Los Alamos National Laboratories, Los Alamos, New Mexico.

Rivera, A., 2005. How well do we understand groundwater in Canada? A Science Case Study. Natural Resources Canada and Geologic Survey of Canada.

Ross, N., Villemur, R., Deschenes, L., Samson, R., 2001. Clogging of a Limestone Fracture By Stimulating Groundwater Microbes. Water Resources 35 (8), 2029–2037.

Roy, S., Dzombak, D., 1996. Colloid Release and Transport Processes in Natural and Model Media. Colloids and Surfaces A: Physicochemical and Engineering Aspects, 245–262.

SDWA, 2002. Safe Drinking Water Act, Chapter 32, Section 1.

Sherwood, J. L., Sung, J. C., Ford, R. M., Maneval, J. E., Smith, J. A., 2003. Analysis of Bacterial Random Motility in a Porous Medium Using Magnetic Resonance Imaging and Immunomagnetic Labeling. Environmental Science & Technology 37, 781–785.

Tsang, Y., 1992. Usage of 'Equivalent Apertures' for Rock Fractures as Derived from Hydraulic and Tracer Tests. Water Resources Research 28 (5), 1451–1455.

Yao, K.-M., Habibian, M. T., O'Melia, C., November 1971. Water and Waste Water Filtration: Concepts and Applications. Environmental Science & Technology 5 (11), 1105–1112.

Zheng, Q., Dickson, S., Guo, Y., 2009. Differential Transport and Dispersion of Colloids Relative to Solutes in Single Fractures. Journal of Colloid and Interface Science 339 (1), 140–151.

Chapter 2

Colloid Retention Mechanisms in Single, Saturated, Variable-Aperture Fractures

Summary of Paper I: Colloid Retention Mechanisms in Single, Saturated, Variable-Aperture Fractures *(Accepted, Water Research, August 2012)*

The research presented in this paper was designed to identify the retention mechanisms that have a large influence on the transport of biocolloids, namely, *E. coli* RS2-GFP, in fractured groundwater environments. This paper discusses the results, conclusions, and implications derived from over 40 tracer experiments that were conducted in three natural fractures, employing a conservative solute tracer, and *E. coli* RS2-GFP. Hydraulic and solute tracer experiments were conducted to characterize the aperture field of each of the three natural fractures. Three flow conditions, ranging over three orders of magnitude, were selected such that they represented a variety of groundwater flow rates. Solute and particulate tracer experiments were conducted in triplicate for each fracture, under each flow condition. A mass-balance equation was used to calculate the percentage of the mass of solute or number of particulates that was retained within the fracture. The overall implications of this work are as follows:

- It is typically believed that flow rate is the most significant factor in determining retention. However, the transport of particulates in fractures is heavily dependent on the ability of the particulate to attach to the fracture walls, the coefficient of variation of the aperture field, and the flow conditions.
- This study showed the high utility of the surrogate measure of the coefficient of variation of the aperture field in understanding particulate transport in fractures. Employing this technique at the field scale should be investigated as it could improve the characterization of fractured aquifers.
- In this study, particulate transport depended on the number of fracture volumes flushed through the fracture and not the rate at which those flushes occurred.

Please note that data collected or analyzed in this segment of the research, but not presented within this paper, can be found in Appendix A.

ABSTRACT

The characterization of fractured aquifers is commonly limited to the methodologies developed for unconsolidated porous media aquifers, which results in many uncertainties. Recent work indicates that fractured rocks remove more particulates than they are conventionally been credited for. This research was designed to quantify the number of *E. coli* RS2-GFP retained in single, saturated, variable-aperture fractures extracted from the natural environment. Conservative solute and *E. coli* RS2-GFP tracer experiments were used to elucidate the relationships between dominant retention mechanisms, aperture field characteristics, and flow rate. A non-destructive method of determining a coefficient of variation (COV) for each fracture was used to better understand the transport behaviour of *E. coli* RS2-GFP. The results from this research all point to the importance of aperture field characterization in understanding the fate and transport of contaminants in fractured aquifers. The mean aperture was a very important characteristic in determining particulate recovery, so were matrix properties, COV_S, and flow rate. It was also determined that attachment is a much more significant retention mechanism than straining under the conditions employed in this research. Finally, it was demonstrated that the dominant retention mechanism in a fracture varies depending on the specific discharge. An improved understanding of the mechanisms that influence the fate and transport of contaminants through fractures will lead to the development of better tools and methodologies for the characterization of fractured aquifers, as well as the ability to manipulate the relevant mechanisms to increase or decrease retention, depending on the application.

Key words:

fracture; particulate transport; *Escherichia coli*; aperture field characterization; particulate retention mechanism; breakthrough curve; tracer test; equivalent aperture; retention mechanism

Contributors

The idea for these experiments came from S.E. Dickson. All authors contributed to the

design of the experiments discussed in this paper. S.N. Rodrigues and J. Qu conducted the experiments. S.N. Rodrigues analyzed the data under the guidance of S.E. Dickson. S.N. Rodrigues prepared the manuscript, and S.E. Dickson edited it.

Role of the Funding Source

This research was funded by the Canadian Water Network, NSERC Discovery Grant (S.E. Dickson) and Consulting Engineers of Ontario Water Quality Research Award (S.N. Rodrigues). The funding sources had no involvement in the study design, in the collection, analysis and interpretation of data, in the writing of the report, or in the decision to submit the article for publication.

2.1 Introduction

Groundwater is one of the most important natural resources in North America. In 2005, the US was withdrawing almost 83 billion gallons of groundwater per day (Barber, 2009). Approximately 51% of Americans rely on groundwater for domestic purposes (USGS, 1999), and 98% of Americans who supply their own water depend on groundwater (USGS, 2011). In Canada, approximately 30% of the population depends on groundwater for their potable water; this proportion rises to about 80% for rural residents (Nowlan, 2007). Seventy percent of the regional aquifers in Canada exist within fractured media (Rivera, 2005). More than half of all the waterborne illnesses recorded from 1971 through 2006 in the United States resulted from contaminated groundwater (Craun et al., 2010). As a result of increased demand for water, extracting groundwater from fractured aquifers is becoming a reality, and perhaps a necessity. In particular, areas of the US experiencing population growth (the Northeast and Southeast) as well as the Western mountainous regions, are likely to turn to fractured aquifers to meet demand (USGS, 2002). With the increasingly large number of North Americans dependent on this natural resource, groundwater quality is a serious public health issue, and its contamination has the potential to jeopardize the health of many.

In two of the largest groundwater contamination episodes in North America, fractured aquifers contributed to the quick and extensive transport of pathogens into local drinking-water wells. In May 2000, the town of Walkerton, Ontario, Canada unknowingly consumed groundwater contaminated with *E. coli* O157:H7. Thousands of people suffered from serious gastrointestinal illnesses and seven people died. The contaminated groundwater was drawn from an area of the aquifer consisting of very shallow overburden and highly fractured rock (O'Connor, 2002). Similarly, Put-In-Bay, Ohio, USA suffered a groundwater-associated outbreak of *E. coli* and other pathogens in 2004 where approximately 1450 people became ill (Fong et al., 2007). The porous aquifer, which provided minimal filtration, was located above a fractured limestone aquifer which facilitated pathogen transport through the aquifer and into local wells (Fong et al., 2007). Pathogens may cause acute illness, particularly in the

very young, elderly, and immunocompromised. Therefore, a good understanding of the fate and transport of particulates in fractured aquifers is necessary for the protection of public health.

2.1.1 Background

Unlike unconsolidated porous media, fractured aquifers have very irregular groundwater flow patterns making it difficult to predict the travel pathways of contaminants. The presence of fractured rocks or channelized sedimentary deposits in the subsurface can tremendously enhance the distance and/or speed at which pathogens travel due to the presence of pathways that are orders of magnitude larger than those typically found in unconsolidated porous media. Groundwater flow velocities in fractured rocks can range from 0.3 to 8 000 $m \cdot d^{-1}$, and up to 26 000 $m \cdot d^{-1}$ in karstic aquifers (Pekdeger and Matthess, 1983). The magnitude of the flow can mobilize attached particulates reducing the retention of particulate contaminants due to shear forces. Consequently, it is believed that fractured rock aquifers have a much lower capacity to retain bacteria, viruses and protozoa compared to unconsolidated porous media aquifers (Crane and Moore, 1984).

There are several processes that act together to cause the retention of particles in subsurface environments. Hydrodynamics influence the transport of colloidal contaminants (e.g., *E. coli*) to a surface; however, attachment to that surface is dictated by mechanical entrapment, the interaction of colloidal forces (e.g., electric double layer and van der Waals), and biological adhesion. The mechanisms of mechanical entrapment are attachment, filtration and straining (Yao et al., 1971; An et al., 2000). Filtration and straining differ only by the depth into the aquifer that a particle is able to travel prior to becoming trapped. Mechanical filtration occurs when particles are larger than the pore spaces, or fracture apertures in the aquifer through which it is traveling, and are therefore incapable of entering the aquifer. Straining occurs when a particle is able to enter the pores or fractures in an aquifer and

travel some distance before becoming immobilized due to its size.

Researchers have conducted many experiments involving fractured rocks at the laboratory and field scales. Scholl et al. (1990) studied the effect of different subsurface minerals on bacterial attachment. In this study, mineral 'chips' (approximately 1.5 cm×2 cm×<3mm thick) of quartz, muscovite, and limestone were characterized by a surface area index, which describes the different amount of surface area available for bacterial attachment between quartz and limestone. Due to a rougher surface texture, the limestone chips had more than twice the surface area available for bacterial attachment compared to the quartz chips. Not surprisingly, a significant difference in bacterial attachment was observed between the limestone and the quartz with approximately three to four times more bacterial attachment observed on the limestone chips. This highlighted the fact that different materials have different affinities for bacterial attachment (Scholl et al., 1990).

Vilks and Bachinski (1996) conducted tracer experiments in a fractured laboratory-scale granite block using bromide and uranine as conservative solute tracers and microspheres of various sizes and materials as particulate tracers. The colloids typically eluted before solutes. However, the groundwater velocity had a larger effect on the colloids than the solutes. At low groundwater velocities (32 and 240 $m \cdot year^{-1}$), colloid transport was significantly slower, and recovery was significantly lower, than at higher groundwater velocities. In contrast, groundwater velocity had much less effect on the transport and recovery of conservative solutes.

In bacterial tracer experiments conducted at the field scale, Becker et al. (2003) observed that over 90% of the solute tracer mass was recovered compared to under 4% for each of the four strains of bacteria and two types of microspheres employed. In field-scale experiments conducted in a granite fracture, Vilks et al. (1997) found that the flow velocity did not have a significant effect on the recovery of colloidal silica at groundwater velocities of 1.6 and 2.9 $m \cdot h^{-1}$. Lapcevic et al. (1999) conducted one of the few field-scale studies under natural gradient conditions using a fluorescent dye tracer experiment in a single fracture. The tracer

data were subsequently interpreted using finite element transport models to investigate the effects of variable-aperture fractures on solute transport. With reasonable model parameter approximations, the authors were able to simulate tracer plumes that closely resembled the observed field plume.

Several research groups have developed models to describe and predict contaminant transport in fractured aquifers. In conceptual and mathematical models for tracer breakthrough curve tailing, Becker and Shapiro (2003) found that advective forces were a significant contributor to breakthrough tailing. However, hydrodynamic dispersion and flow field geometry can not be ignored in the design of tracer experiments in highly heterogeneous fractured media. Chrysikopoulos and Abdel-Salem (1997) developed a model to describe the transport of colloids in saturated fractures and found that it predicted the presence of preferential transport pathways. In addition, the model shows that large-sized particles have earlier breakthroughs due to size exclusion which increases the dispersion of colloids. Developing models that incorporate the findings of laboratory and field scale research is an important task, as it bridges the gap between science and practice.

Despite the growing literature on contaminant transport in fractured aquifers, the characterization of fractured aquifers is still an issue that needs to be addressed. Owing to a lack of fracture-specific methodologies, the assessment methods for porous media aquifers are often employed on fractured aquifers leading to many uncertainties (Nowlan, 2007). In contrast to unconsolidated porous media, fractured aquifers tend to have large pore spaces in which groundwater and contaminants may travel preferentially. These preferential flow pathways consist of features like fractures, vugs and conduits. The presence of these features causes the hydraulic conductivity of fractured rock aquifers to vary considerably over relatively short distances making it difficult to characterize contaminant transport in fractured rocks using stochastic methods (Shapiro et al., 2008).

The goal of this research is to improve the mechanistic understanding of particulate transport in fractured aquifers through physical, laboratory-scale experiments. In these experi-

ments, the behaviour of *E. coli* RS2-GFP in single, horizontal, saturated fractures, obtained from the natural environment, was investigated. The relationship between retention mechanisms, aperture field characteristics, and flow rate was explored by conducting a series of experiments in fractures with different aperture field characteristics under a range of flow rates.

2.2 Materials and Methods

These experiments employed a total of three laboratory-scale rock samples, which were collected from outcrops and fractured upon return to the laboratory. The aperture field characteristics were measured through hydraulic and solute tracer experiments. Known concentrations of *E. coli* RS2-GFP were released at the upstream end of the fracture under a range of specific discharges, and the effluent breakthrough curves (BTC) were measured.

2.2.1 Fracture Plane Preparation

Two of the fractures employed in these experiments, hereafter referred to as F1 and F2, are dolomitic limestone fractures that were collected from an outcrop in Kingston, Ontario, Canada and prepared for experimentation by Dickson and Thomson (2003). The third fracture (F3) was obtained from a granite outcrop just west of Carnarvon, Ontario, Canada and was prepared for experimentation by Sekerak (2004). The samples were extracted using a Quick Cut saw equipped with a diamond-tipped blade, and were chosen due to the presence of a visible plane of weakness (i.e. stylolite or bedding plane). Upon return to the laboratory, a uniaxial force was applied to each sample to induce a tension fracture through the plane of weakness mimicking the formation of fractures in the natural environment due to weathering or stress relief.

The photographs in Figure 2.1 show the surfaces of a dolomitic limestone and a granite

sample after being fractured in the laboratory. Dolomitic limestone is a type of carbonate rock (composed of calcium carbonate); however, the calcium ions are partially replaced by magnesium ions in the carbonate molecule. Granite is an igneous rock consisting largely of quartz and feldspar. The porosity of the dolomitic limestone was determined to be 0.23%

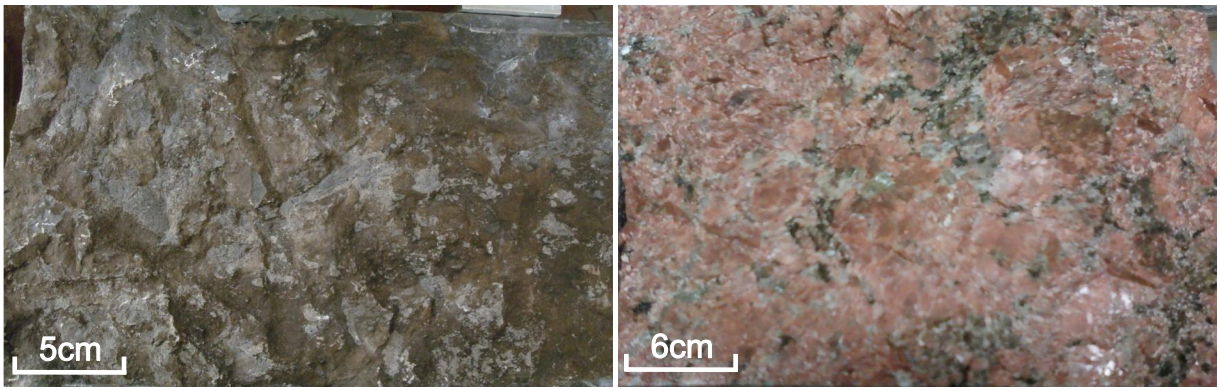

(a) Dolomitic limestone (b) Granite

Figure 2.1: Photographs of the top view of the two types of fractures employed in these experiments.

(Dickson and Thomson, 2003). The porosity of the granite sample could not be determined directly without destroying the fracture, however it is reasonable to assume that it is in the range of 0.05 to 1% (Freeze and Cherry, 1979). Since each rock contains a single fracture, and since the hydraulic conductivity of dolomite and granite typically range from 10^{-7} - 10^{-8} and 10^{-9} - 10^{-10} cm·s^{-1} respectively (Bear, 1972), matrix flow and diffusion are negligible compared to flow through the fracture over the duration of these experiments.

2.2.2 Experimental Setup

Figure 2.2 shows a schematic diagram of the experimental apparatus. Flow was parallel to the longitudinal edges of the fracture which were sealed (GE Silicone Window and Door) as no-flow boundaries. The upstream and downstream ends of the fracture were capped with flow cells (shaded in gray), which were constructed out of plexiglass. Six ports, each

with a five-millimeter diameter, were drilled into each flow cell and equipped with Swagelock fittings. These ports were used to pump water into the system, to measure the hydraulic head, and to enable the mixing of the contents of the flow cell. To achieve continuous mixing in the flow cells, a recirculation system (Figure 2.2) was constructed from Teflon tubing (Nalgene, 0.3175 cm) perforated at 2 mm intervals along its length and threaded diagonally through the flow cell. Pump tubing was attached to each end of the Teflon tubing to form a closed loop and an injection/withdrawal cell was inserted into the recirculation loop. A peristaltic pump recirculated the contents of the flow cell. Small volumes of concentrated

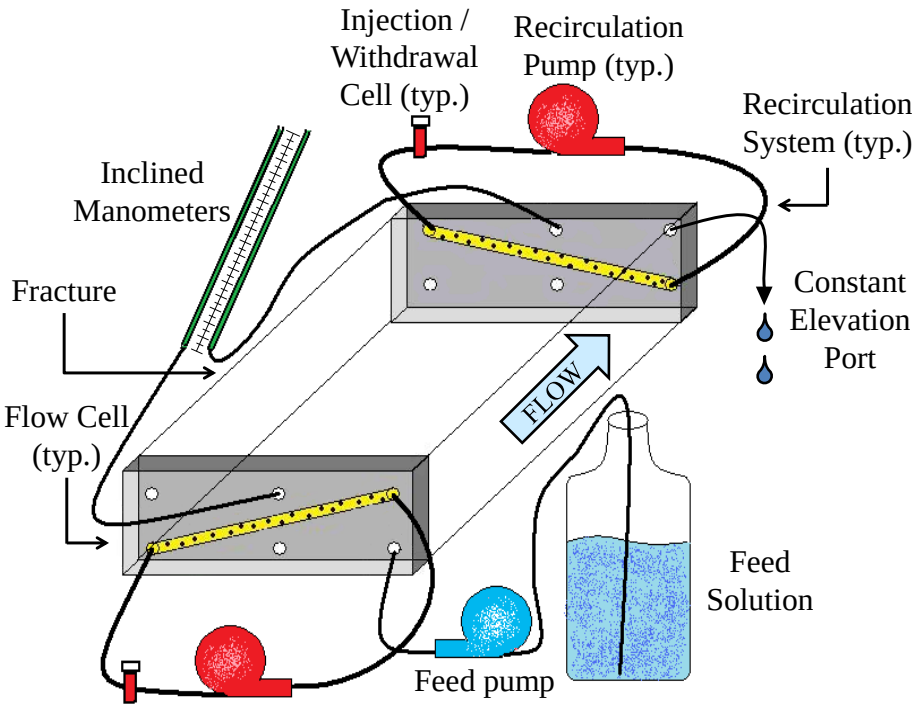

Figure 2.2: Schematic diagram of the experimental apparatus.

solute tracer and bacteria were injected into the upstream injection/withdrawal cell and mixed with the volume of the flow cell to achieve the desired influent concentration. Samples were withdrawn from the downstream injection/withdrawal cell. A dye test was performed on each recirculation system to determine the time required for the volume of fluid in the flow cell to become a uniform solution. The time recorded was used as the minimum mixing time after a tracer was released into the upstream injection/withdrawal cell and before the

feed pump was initiated to ensure that a uniform mixture would be entering the fracture at the start of each experiment. A variable speed drive peristaltic feed pump (MasterFlex L/S 7523-70) injected water into the upstream flow cell to create a hydraulic gradient that induced flow through the fracture. The effluent port, on the downstream end of the fracture, was maintained at a constant elevation.

One port on each of the upstream and downstream flow cells was connected to an inclined piezometer to enable the measurement of head loss across the length of the fracture. Calipers were employed to accurately measure the difference in water level between the upstream and downstream piezometers.

2.2.3 Fracture Plane Saturation

Each fracture was saturated with carbon dioxide gas prior to injecting any aqueous solution. Carbon dioxide is much more soluble in water than air is, and therefore it completely dissolved in the aqueous solution upon saturation ensuring no pockets of air remained in the fracture. The feed water was specially prepared for these experiments by adjusting the pH of MilliQ water and adding a buffer to prevent the dissolution of carbonate compounds in the rock. The feed water was also degassed by bubbling helium through it to prevent the possibility of gases coming out of solution during experiments due temperature changes in the laboratory. The buffered, deionized, degassed water (DDW), with pH = 8, and negligible ionic strength, was pumped through the fracture for approximately 16-18 hours prior to the start of any experiments.

2.2.4 Aperture Field Characterization

Hydraulic tests were conducted to determine the equivalent hydraulic aperture. Each hydraulic test was conducted by pumping buffered DDW through the fracture at a constant

flow rate and measuring the resulting head loss across the fracture. Hydraulic tests were conducted under a range of flow rates on each fracture to ensure that the experiments were conducted within the linear range of the specific discharge versus head loss relationship, indicating that the cubic law is likely valid (Brush and Thomson, 2003). Hydraulic tests were also repeated at least thrice for each specific discharge in each fracture to ensure repeatability.

Solute tracer tests were conducted to investigate solute transport and to measure the mass balance and frictional loss apertures. Bromide was selected as the solute tracer because it is conservative and relatively easy to quantify. The fractures were fully saturated as described in Section 2.2.3 prior to each solute tracer experiment. A low volume, high concentration (0.3 mL of 10 g/L Br^- as NaBr with molar concentration = 0.125 M and pH = 9.8) slug of tracer was injected into the upstream injection/withdrawal cell, and the recirculation system was turned on for the pre-determined mixing time to ensure a uniform concentration of tracer in the upstream flow cell. The feed pump was then turned on to pump buffered DDW through the fracture. Due to the relatively large volume of the influent flow cell relative to the volume of the fracture (Table 2.1), this procedure did not result in a true pulse input. The solution in the influent flow cell was diluted by feed water over the course of each experiment, resulting in an exponentially decaying input. The decreasing bromide concentration in the upstream recirculation system can be described as follows (Zheng et al., 2008):

$$C_{in}(t) = \frac{M_{Br}}{V_{recirc}} \cdot EXP\left(\frac{-Q \cdot t}{V_{recirc}}\right) \tag{2.1}$$

where C_{in} $[M \cdot L^{-3}]$ is the concentration of bromide in the upstream flow cell, t $[T]$ is the time, M_{Br} $[M]$ is the mass of bromide, V_{recirc} $[L^3]$ is the recirculation volume and Q $[L^3 \cdot T^{-1}]$ is the flow rate.

A background sample was collected prior to the start of each experiment and subsequent samples were withdrawn periodically from the downstream injection/withdrawal cell throughout each experiment. High-performance liquid chromatography (HPLC) (Varian ProStar

330) was used to quantify the bromide in the samples retrieved during the solute tracer tests according to the method described by Hautman et al. (1997). Samples of approximately two milliliters were extracted during each sampling event using a disposable plastic syringe and injected into an HPLC analysis vial. Standard concentrations of bromide were prepared according to Standard Method 1020B (APHA et al., 2006). To ensure repeatability, each tracer test was repeated a minimum of twice and mass balance calculations were conducted on the bromide in each experiment for quality assurance purposes.

2.2.5 *E. coli* RS2-GFP Tracer Tests

E. coli RS2-GFP was selected as a non-pathogenic strain of *E. coli* for use in these experiments. This strain of *E. coli* is rod-shaped with zeta potential of approximately -12 mV and approximate dimensions of 2.5 μm in length and 0.8 μm in diameter (Passmore et al., 2010). Previously used in experiments conducted by Saini et al. (2003), *E. coli* RS2-GFP is a derivant of RS-1. It fluoresces due to the presence of a green fluorescent protein and is resistant to two antibiotics (kanamycin and rifampicin) significantly reducing the risk of contamination during experiments. The green fluorescent protein excites at 365 nm (or optimally at 488 nm) and emits at 510 nm. The *E. coli* RS2-GFP was obtained from the Emelko Laboratory (Department of Civil Engineering, University of Waterloo, Ontario, Canada). The Waterloo culture was obtained through Dr. Larry Halverson from the Department of Agriculture and Biosystems Engineering at Iowa State University, Ames, IA, USA. Pure cultures were maintained and prepared for experimentation according to the method described by Passmore et al. (2010).

The *E. coli* RS2-GFP tracer tests were conducted at 1.4, 14, and 140 m·day^{-1}. The specific discharges were chosen such that they range over three orders of magnitude to represent a variety of groundwater flow rates observed in fractured aquifers. Prior to running an *E. coli* RS2-GFP experiment, the fractured rock setup was saturated as described in Section

2.2.3; however, a phosphate buffered saline (PBS) solution was used in place of the buffered DDW. The PBS solution had a pH of approximately 8 and an ionic strength of 0.64 M. As with the solute tracer tests, the feed pump was stopped during the injection and mixing of the *E. coli* RS2-GFP in the upstream injection/withdrawal cell. Three millilitres of approximately 3×10^8 CFU $\cdot$ mL^{-1} *E. coli* RS2-GFP suspension was released into the upstream injection/withdrawal cell and allotted the appropriate mixing time as determined by the dye tests such that an exponentially decaying input of *E. coli* RS2-GFP entered the fracture upon the start of each experiment. The feed pump was then turned on and periodic sampling of the downstream recirculation system commenced. Sampling was most frequent immediately after the feed pump was turned on (to capture a well-defined rising limb and peak concentration) and less frequent as time elapsed and the effluent concentration started tailing. A background sample was also extracted prior to each experiment to ensure that no bacteria remained in the fracture from previous experiments. Serial dilutions were plated and *E. coli* RS2-GFP was enumerated according to the methods described by Passmore et al. (2010). Each experiment was conducted thrice under identical conditions to ensure repeatability.

2.3 Results and Discussion

2.3.1 Aperture Field Characterization

The equivalent hydraulic aperture, b_c [L], was calculated using:

$$b_c = \left(\frac{12\ \mu\ Q\ L}{\gamma\ W\ |\Delta H|} \right)^{1/3} \tag{2.2}$$

where γ [M $\cdot$ L^{-3}] is the fluid weight density, and μ [M $\cdot$ T^{-2} $\cdot$ L^{-2}] is the dynamic viscosity of the fluid, L [L] is the length of the fracture in the direction of flow, W [L] is the width of the fracture perpendicular to the direction of flow and ΔH is the hydraulic headloss [L] over

the length of the fracture.

Table 2.1 summarizes the results obtained from the hydraulic and tracer tests. Figure 2.3

Table 2.1: Summary of the hydraulic and solute tracer test results.

Fracture	Rock Type[b]	Length	Width	Recirculation Volume[c] Upstream	Recirculation Volume[c] Downstr.	Bromide Recovery	Equivalent Aperture[d, e] b_c	Equivalent Aperture[d, e] b_m	Equivalent Aperture[d, e] b_f	COV_S[f] σ/b_m	Reynold's Number
		[m]	[m]	[m^3]	[m^3]	[%]	[mm]	[mm]	[mm]	[-]	[-]
F1	DL	0.245	0.160	1.06E-04	7.98E-05	73	0.170 ± 0.006	2.620 ± 0.046	0.040 ± 0.011	0.555	0.030
F2	DL	0.295	0.220	1.27E-04	1.07E-04	101	0.170 ± 0.005	4.370 ± 0.107	0.030 ± 0.011	0.564	<0.001
F3	G	0.370	0.230	7.51E-05	7.25E-05	94	0.305 ± 0.006	3.780 ± 0.059	0.090 ± 0.009	0.548	0.570

a. All experiments were conducted at 25 ± 2 °C, and the values of the parameters used in these calculations correspond to those at 25 °C (i.e., ρ = 997 kg/m^3, η = 0.00089 N·s/m^2).

b. "DL" indicates dolomitic limstones and "G" indicates granite.

c. Recirculation volume includes the volume of the flow cell, injection/withdrawal cell, and tubing external to the flow cell.

d. Equivalent apertures show the standard deviation determined from experiments conducted in triplicate.

e. b_c, b_m, and b_f are the equivalent cubic law, mass balance, and frictional loss apertures, respectively.

f. σ is the standard deviation of the three equivalent apertures and COV_S is a surrogate measure of the aperture field coefficient of variation.

shows a graph of specific discharge versus head loss for F1 and is typical of all fractures. Figure 2.3 clearly shows a linear relationship between head loss and specific discharge indicating

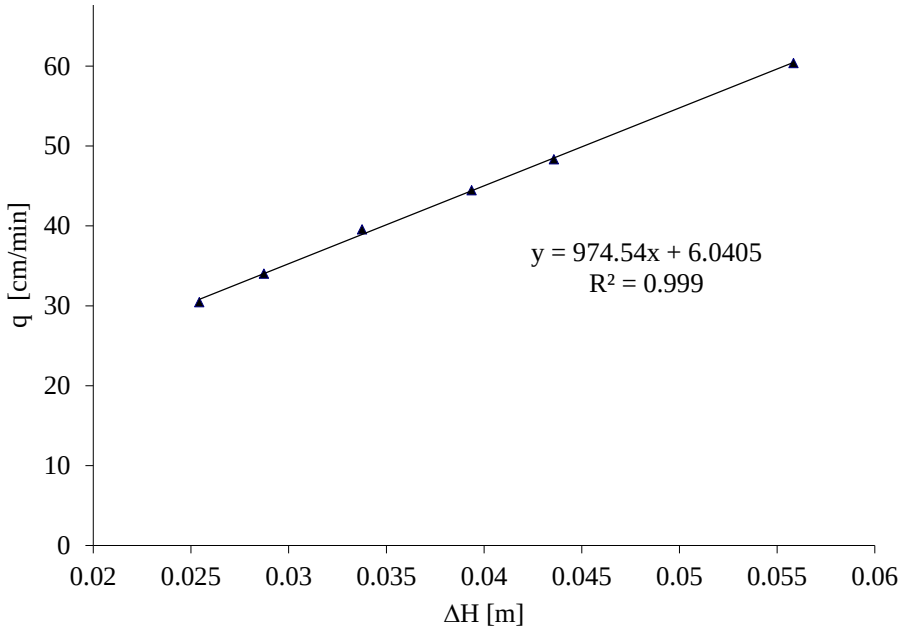

Figure 2.3: Specific discharge (q) versus ΔH for F1. The least squares simple linear regression trend line is shown. Error bars representing the standard deviation of known concentrations determined in triplicate can not be seen because they are smaller than the symbols.

that these experiments were conducted within the laminar flow range, and therefore, the use of Equation (2.2) is reasonable. This is further supported by the fact that the Reynold's numbers reported for each experiment in Table 2.1 are less than one.

All samples collected during the tracer experiments are representative of the effluent concentration in the recirculation system (ie. flow cell) at the time of collection, not of that exiting the fracture. The concentration exiting the fracture becomes diluted upon entering the flow cell due to its large volume, $V_{recirc}[L^3]$ (Table 2.1). Therefore, the measured concentration, $C_{meas}[M \cdot L^{-3}]$, must be adjusted to determine the bromide concentration actually exiting the fracture, $C_{eff-frac}[M \cdot L^{-3}]$, at the time the sample was collected. The measured concentration was adjusted using a mass balance on a continuous flow stirred-tank reactor (CSTR):

$$C_{eff-frac}(t) = \frac{V_{recirc}}{Q} \cdot \frac{dC_{meas}(t)}{dt} + C_{meas}(t) \tag{2.3}$$

Equation (2.3) was approximated as follows:

$$C_{eff-frac}(t) = \frac{V_{recirc}}{Q} \cdot \frac{C_{meas}(t) - C_{meas}(t - \Delta t)}{\Delta t} + C_{meas}(t) \tag{2.4}$$

The variance of the back-calculated break-through curve was determined as follows (Fahim and Wakao, 1982):

$$Var = \frac{C_{eff-avg}(t) \cdot (t^n_{avg} - t_m) \cdot \Delta t_n}{C^n_{eff-avg}(t) \cdot \Delta t} \tag{2.5}$$

where the mean bromide residence time (t_m) was calculated as follows (Fahim and Wakao, 1982):

$$t_m = \frac{\sum C_{eff-avg}(t) \cdot t_{avg}(t) \cdot \Delta t(t)}{\sum C_{eff-avg}(t) \cdot \Delta t} \tag{2.6}$$

Figure 2.4 shows a measured and back-calculated bromide BTC from a solute tracer test conducted in Fracture F1 and is typical of the solute BTCs measured in all experiments. The variance of the back-calculated bromide BTC is also included in Figure 2.4.

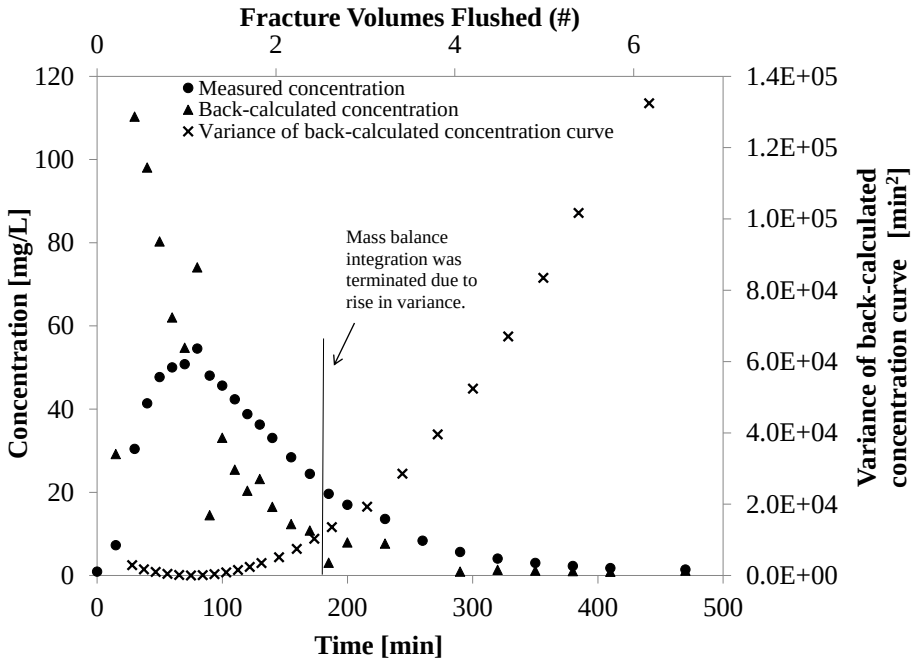

Figure 2.4: Bromide BTC from Fracture F1. Error bars representing the standard deviation of concentrations determined in triplicate can not be seen because they are smaller than the symbols.

The back-calculated peaks occurred sooner and were higher than the measured ones, which demonstrates that the bromide is being diluted upon exiting the fracture. The total mass of bromide exiting the fracture was determined by integrating the measured bromide BTC and is reported in Table 2.1. The integration was terminated at the point on the tail of the BTC at which the variance started to rise (the vertical line shown in Figure 2.4), as this indicates

the point in time where the error on the reported concentrations became unacceptable.

The mass balance aperture, b_m [L], relates the flow rate, Q $[L^3 \cdot T^{-1}]$, the mean residence time of tracer transport, $t_m[T]$, and the areal extents of the fracture, A $[L^2]$, according to Tsang (1992):

$$b_m = \frac{Q \cdot t_m}{A} \tag{2.7}$$

The frictional loss aperture, b_f [L], is given by Tsang (1992):

$$b_f = L \left(\frac{12\ \mu}{\gamma\ |\Delta H|\ t_m} \right)^{1/2} \tag{2.8}$$

where ΔH $[L]$ is the headloss, $L[L]$ is the length of the fracture, γ is the fluid weight density $[M \cdot L^{-3}]$, μ $[M \cdot T^{-2} \cdot L^{-2}]$ is the viscosity of the fluid, and t_m is the mean residence time.

The equivalent apertures reported in Table 2.1 exhibit the following relationship:

$$b_f < \ b_c < \ b_m \tag{2.9}$$

This relationship is expected, as the frictional loss aperture is dependent on the headloss across the fracture which is sensitive to the smallest aperture regions, while the mass balance aperture is dependent on the storage of mass across the fracture, which occurs in the largest aperture regions. The observed relationship is consistent with others' observations (e.g., Piggot and Elsworth (1993); Rasmussen (1995); Dickson and Thomson (2003); Zheng et al. (2008)).

Bromide recoveries ranged from 73% to 101% as reported in Table 2.1. The data for F2 falsely indicates that more bromide was recovered than was injected into the fracture, which

is clearly not possible. This is likely due to the summation of error in using the trapezoid method of integration and the fact that the flow rates were not perfectly steady throughout each experiment.

The variability of fracture apertures is typically described by the coefficient of variation (COV), which is defined as the ratio of the standard deviation to the arithmetic mean aperture. Variability is an extremely important aperture field characteristic in terms of transport mechanisms. Although the COV can not be calculated directly without a detailed map of the aperture field, the three equivalent apertures do provide sufficient information on the range of extreme aperture regions to determine a surrogate measure of the COV. Since the mass balance aperture is the closest approximation to the arithmetic mean aperture (Tsang, 1992; Zheng et al., 2008), a surrogate measure of the COV, COV_S was approximated as follows:

$$COV_S = \frac{\sigma(b_f, b_c, b_m)}{b_m} \tag{2.10}$$

where σ represents the standard deviation of the equivalent frictional loss, hydraulic, and mass balance apertures. A small COV_S indicates that the fracture has few extreme aperture regions and a large COV_S indicates that the fracture is extremely variable. A COV_S equal to zero would be found in a parallel plate aperture with no extreme aperture regions.

2.3.2 Repeatability of the *E. coli* RS2-GFP Tracer Tests

Table 2.2 summarizes the observations from each *E. coli* RS2-GFP tracer test conducted. Each BTC was integrated to determine the cumulative number of *E. coli* RS2-GFP exiting the fracture and a corresponding percent recovery was calculated. Similar to the measured bromide BTCs, the concentration of the *E. coli* RS2-GFP exiting the fracture was diluted by the volume of the effluent flow cell and therefore the actual *E. coli* RS2-GFP concentrations exiting the fracture were determined by adjusting the measured values using Equation 2.3.

Only the back-calculated (actual) concentrations are presented.

Figure 2.5 shows the *E. coli* RS2-GFP BTC from triplicate experiments conducted in F1 at 140m $\cdot$ day^{-1}. The error bars on the data points represent the range of maximum and minimum concentrations calculated by:

$$1.5(\text{Q3-Q1}) + \text{Q3 and } \text{Q1-1.5(Q3-Q1)} \tag{2.11}$$

where Q1 and Q3 represent the first and third quartiles respectively. The BTCs shown in Figure 2.5 are typical of the results obtained from the experiments conducted in all three experimental fractures, at all three specific discharges. Typically, the *E. coli* RS2-GFP BTCs peaked quickly and remained steady over a long period of time before gradually tailing off.

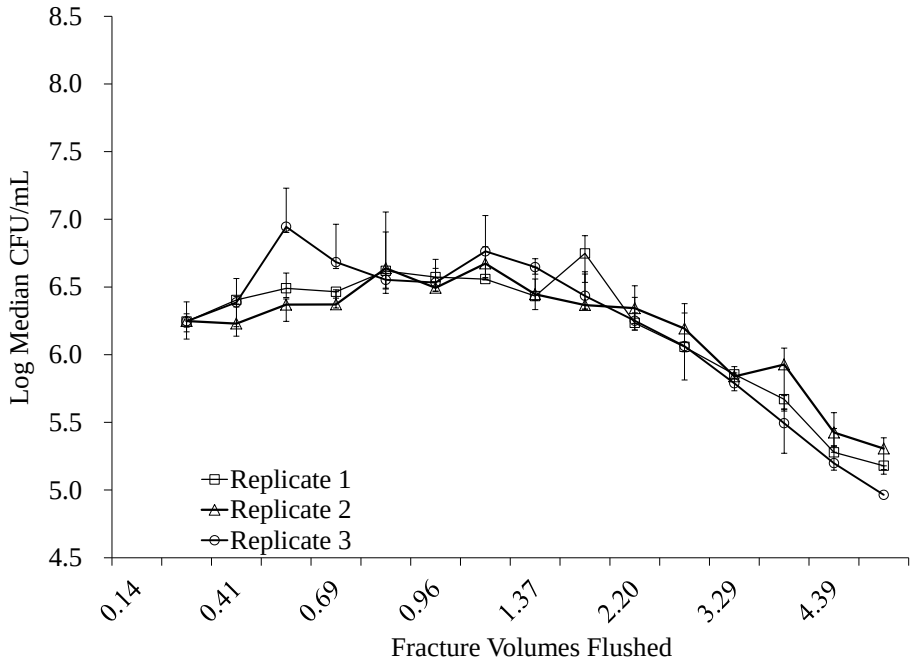

Figure 2.5: *E. coli* RS2-GFP BTCs for F1 (dolomitic limestone) at 140 m·day^{-1} (in triplicate). The symbols represent the back-calculated concentration of *E. coli* determined from serial dilutions and standard bacteria plating methods. Error bars were determined using Equation 4.8.

Figure 2.5 shows that the replicated BTCs matched each other well in terms of duration, magnitude, and shape. The results from all other *E. coli* RS2-GFP experiments were similarly repeatable. This indicates that the experiments are scientifically reliable despite the inherent challenges of working with microorganisms, which include susceptibilities to inoculum preparation, bacterial survival, and enumeration methods.

Figure 2.6 shows the BTCs of bromide and *E. coli* RS2-GFP in F1 at 140 m·day^{-1}. The solute and particulate BTCs were very different in terms of duration, magnitude, and shape. Although earlier breakthrough of the particulates is expected as a result of size exclusion (Keller and Sirivithayapakorn, 2004; Zheng et al., 2009), the peak arrival time between the two tracers can not be differentiated; however, the peak concentration of the two tracers differs by 2.5 orders of magnitude. In addition, the tail of the *E. coli* RS2-GFP BTCs is significantly longer than that of the bromide BTC. Finally, the total recovery was 73% for

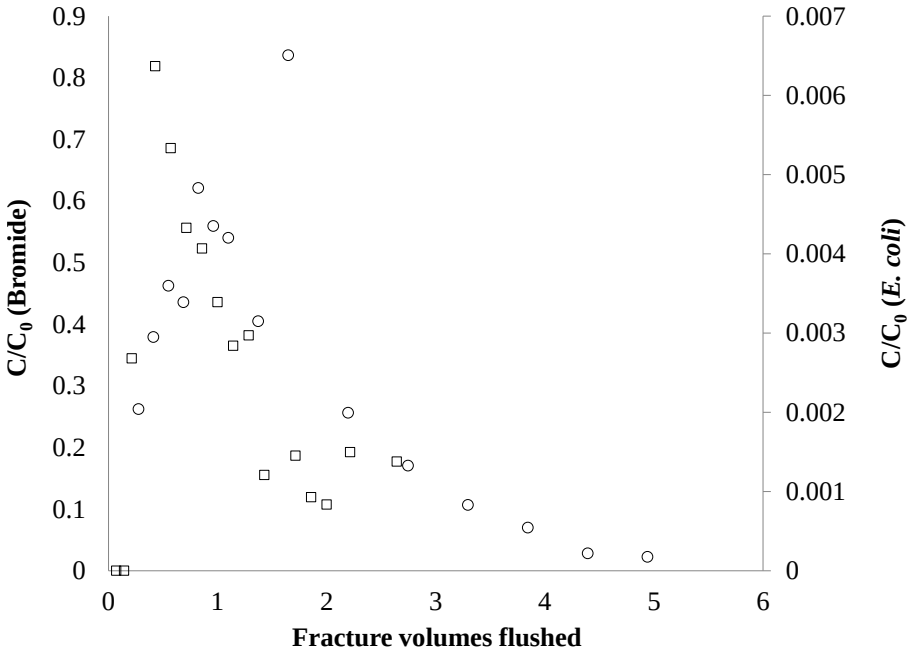

Figure 2.6: BTCs of □ Bromide and ◯ *E. coli* RS2-GFP for F1 at 140 m·day^{-1}.

bromide and 43% for *E. coli* RS2-GFP. The differences observed between the solute and particulate BTCs are likely due to the reversible attachment of the *E. coli* RS2-GFP to

the fracture wall. The trends of earlier peaks, longer tails, and lower overall recovery for particulates compared to solutes is consistent with the literature (e.g., Vilks and Bachinski (1996); Becker and Shapiro (2003); Sinreich and Flynn (2009)).

Influence of Aperture Field Characteristics on *E. coli* RS2-GFP Recoveries

Figure 2.7 shows the percent recovery of *E. coli* RS2-GFP for each fracture at different specific discharges. At the lowest specific discharge, *E. coli* RS2-GFP recovery decreases with increasing equivalent mass balance aperture. However, at specific discharges of 14 and 140 m·day^{-1}, no clear relationship between specific discharge and aperture size seems to exist. This indicates that the dominant retention mechanism is not consistent within a fracture; it is dependent on flow rate to some degree. Shear forces are likely to contribute to detachment at

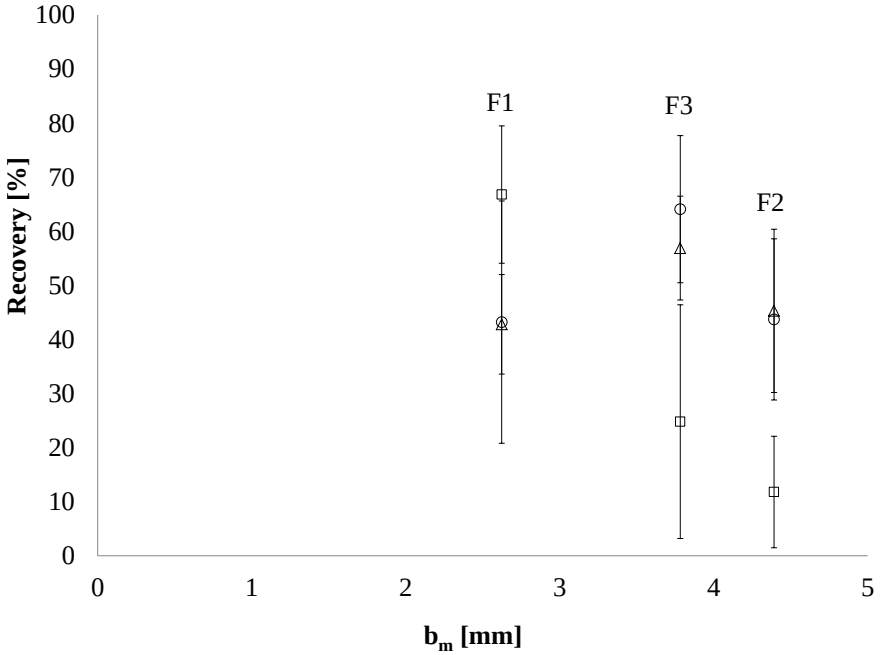

Figure 2.7: *E. coli* RS2-GFP recovery versus mass-balance aperture for each fracture at □ 1.4, ◯ 14, and △ 140 m·day^{-1}. Error bars represent the standard deviation of *E. coli* RS2-GFP recovery from experiments conducted in triplicate.

high specific discharges, which would act to increase the observed *E. coli* RS2-GFP recovery in F2 and F3 at the higher specific discharges. Additionally, larger apertures coupled with

low specific discharges may provide more time for Brownian motion to facilitate collisions, and subsequent attachment, between the *E. coli* RS2-GFP and the fracture wall. In addition, low specific discharges result in smaller shear forces, which means less detachment is likely occurring. The exception to this observation is F1, in which the two highest specific discharges resulted in lower recoveries than they did in F2 and F3. Figure 2.7 indicates that overall, the recovery decreases as the mean aperture increases.

Figure 2.8 shows the COV_S, which is a surrogate measure for aperture field variability (calculated according to Eq. (2.10)), plotted against the bacteria recoveries. For F2 and F3, a larger COV_S results in less *E. coli* RS2-GFP recovery at identical specific discharges. However, this trend is not observed with F1. Large COV_S values indicate the presence of

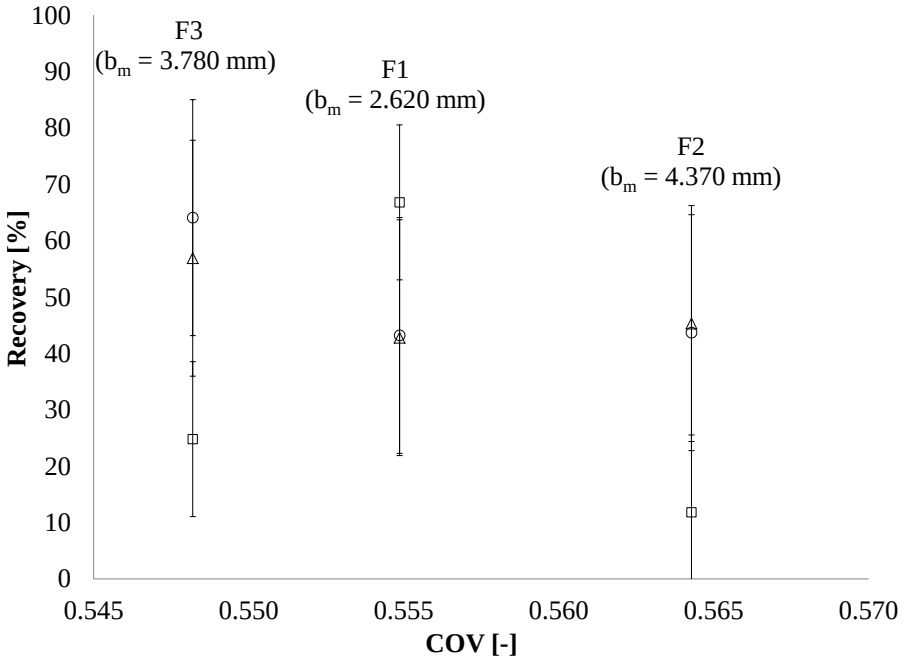

Figure 2.8: *E. coli* RS2-GFP recovery versus COV_S of the aperture field for each fracture at specific discharges of □ 1.4, ◯ 14, and △ 140 m·day^{-1}. Error bars represent the standard deviation of *E. coli* RS2-GFP recovery from experiments conducted in triplicate.

the extreme aperture regions (very small and/or very large). These extreme aperture regions could invoke different retention mechanisms resulting in reduced *E. coli* RS2-GFP recoveries, specifically: the presence of large extreme aperture regions could cause the *E. coli* RS2-GFP

to slow down allowing more time for collisions through Brownian motion; the presence of small extreme apertures could cause straining of the *E. coli* RS2-GFP; and sudden changes from an extremely small aperture region to a large one could result in the formation of micro-turbulence which would promote collisions between the *E. coli* RS2-GFP and the fracture walls, and subsequent attachment. Therefore, it is expected that larger COV_Ss result in lower recoveries. Figure 2.8 shows that F2 has the largest COV_S of all the fractures employed in these experiments, and thus it is not surprising that F2 typically has lower *E. coli* RS2-GFP recoveries than F1 and F3 at similar specific discharges. The exception to this observation is that the recoveries in F2 do not differ significantly from those of F1 at the two highest specific discharges. This may be due to the fact that although all the COV_Ss of F1, F2, and F3 are statistically different, the magnitudes of the COV_Ss of F1 and F2 may not be different enough to alter the retention mechanisms. The general trend of lower recoveries with increasing COV_Ss indicates that attachment, and not straining, is the dominant retention mechanism.

Figure 2.8 shows that F3 has the smallest COV_S of all the experimental fractures. It is therefore likely that it also has fewer extreme aperture regions compared to F1 and F2, resulting in less dispersion and fewer stagnant regions than F1 and F2. F1 and F2 typically experienced very long *E. coli* RS2-GFP tails relative to F3. This acts to reduce the peak concentration exiting the fracture and lengthen the tail of the BTC. This demonstrates the significant effect that aperture field characteristics have on particulate transport, and the importance of developing improved characterization techniques.

Figure 2.9 compares the log-normalized BTCs from all three fractures at 140 $m \cdot d^{-1}$. The corresponding data at 1.4 and 14 $m \cdot d^{-1}$ are not shown; however, the trends are the same but less pronounced at the lower specific discharges. Different fractures had the highest peak concentrations at different specific discharges; however, F3 typically had the earliest peak concentrations and shortest tails. The exception to this observation is that the peaks in F1 and F3 occurred simultaneously at the lowest specific discharge. F3 is a granitic rock,

whereas F1 and F2 are both dolomitic limestone. Scholl et al. (1990) observed that limestone surfaces were much rougher than quartz surfaces and demonstrated that three to four times the number of bacteria attached to the limestone compared to quartz. Similarly, in porous media micromodels employed by Auset and Keller (2006), rougher grain surfaces resulted in higher particulate collision efficiencies which were attributed to the postulation that grain roughness alters the hydrodynamics of the groundwater fluid, which effectively alters the streamlines. Since granite (F3) is composed mainly of feldspar and quartz, the very different transport behaviour observed in F3 could be explained by less attachment in F3 due to its

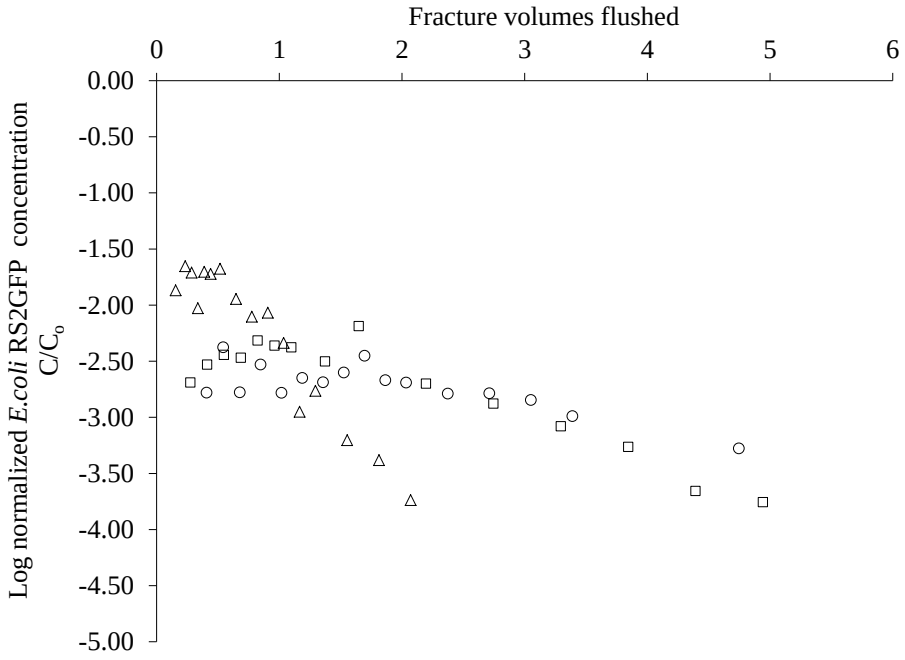

Figure 2.9: Log normalized median *E. coli* RS2-GFP BTCs for □ F1 (dolomitic limestone), ◯ F2 (dolomitic limestone), and △ F3 (granite) at 140 m·day^{-1}.

high quartz content and smoother surfaces than the dolomitic limestone surfaces of F1 and F2. This demonstrates the large role that matrix properties play on bacterial transport through fractures.

Influence of Specific Discharge on *E. coli* RS2-GFP Recoveries

Figure 2.10 and Table 2.2 show the average *E. coli* RS2-GFP recovery at each specific discharge for all three fractures. As shown in Figure 2.10, for F1, the lowest specific discharge results in the largest *E. coli* RS2-GFP recovery; whereas, for F2 and F3 the lowest specific discharge corresponds to the lowest *E. coli* RS2-GFP recovery. Since the observed recoveries for each fracture vary with specific discharge, these results suggest that *E. coli* RS2-GFP retention is not due to straining in these experiments but that different retention mechanisms dominate in different fractures due to the variability of the aperture fields employed (i.e., aperture field and/or matrix properties). Typically, it is postulated that larger specific discharges result in larger shear forces, which may cause detachment and result in less retention due to attachment (i.e. larger recoveries). However, this postulation only seems to

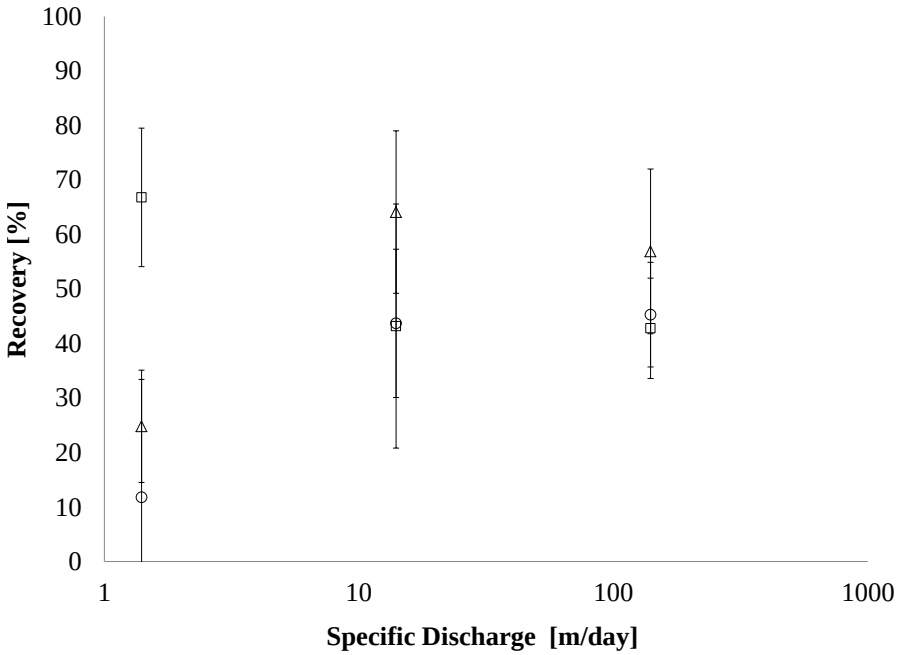

Figure 2.10: Specific discharge versus average *E. coli* RS2-GFP recovery for □ F1 (dolomitic limestone), ◯ F2 (dolomitic limestone), and △ F3 (granite). Error bars represent the standard deviation of *E. coli* RS2-GFP recovery from experiments conducted in triplicate.

hold true for F2 and F3, both of which have larger mean apertures (b_m) than F1. In F1, the largest recovery was observed at the lowest specific discharge. It is not clear what transport

mechanism or characteristic of F1 is responsible for this behavior, which is inconsistent with the observations from F2 and F3. It should be emphasized that this is not an anomalous result; these experiments were repeated in triplicate. Therefore, it can be concluded with confidence that the seemingly conflicting results between F1 and the other two fractures are due to factors not considered in this study (e.g., biological appendages, bacteria-specific propulsion) and not experimental error. These data suggest that flow rate alone cannot predict retention in fractures, and that the aperture field characteristics also have a significant effect on biocolloid retention.

Table 2.2: *E. coli* RS2-GFP recovery from tracer experiments.

Fracture ID	Rock Type[a]	Length [m]	Width [m]	b_m[b] [mm]	COV_S[c] [-]	Specific Discharge [m/day]	Replicates [#]	Recovery [%]	Standard deviation [%]
F1	DL	0.245	0.160	2.63	0.55	1.4	3	66.8	12.7
						14	3	43.2	22.4
						140	3	42.8	9.2
F2	DL	0.295	0.220	4.37	0.564	1.4	3	11.8	10.3
						14	3	43.7	14.9
						140	3	45.3	15.1
F3	G	0.370	0.230	3.78	0.548	1.4	3	24.8	21.6
						14	3	64.1	13.6
						140	3	56.9	9.6

a. "DL" indicates dolomitic limstones and "G" indicates granite.
b. b_m represents the equivalent mass balance aperture.
c. COV_S is a surrogate measure of the coefficient of variation of the aperture field (Eq. 10).

Figure 2.10 and Table 2.2 show that at the lowest specific discharge, the range of recoveries between fractures is quite large. In contrast, at the highest specific discharge, the range of recoveries between fractures is much narrower. This trend likely occurs because at lower specific discharges, the bacteria have more time in which to experience more collisions with the fracture surface due to Brownian motion. At higher specific discharges, the biocolloids likely remain in a more uniform suspension across the flow profile, as hydrodynamic forces likely dominate over Brownian motion under these conditions. It can then be deduced that the narrower recoveries observed between fractures at higher specific discharges are a result of less variable retention mechanisms, since the number of mechanisms invoking attachment

and detachment have decreased.

Figure 2.11 shows the log normalized median *E. coli* RS2-GFP BTCs for F1 at three

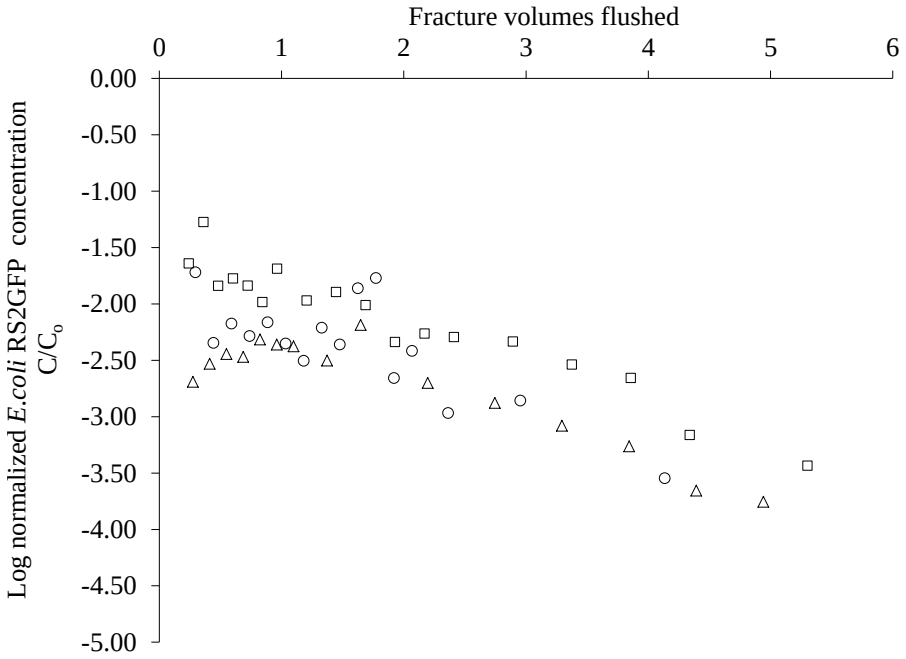

Figure 2.11: Log normalized median *E. coli* RS2-GFP BTCs for F1 at □ 1.4, ◯ 14, and △ 140 m·day^{-1}.

different specific discharges and shows that the maximum percent recovery is dependent on the number of fracture volumes flushed, not the specific discharge. The data for F2 and F3 are not shown, but reveal the same trend. This indicates the importance of the travel pathways, which is an artifact of the aperture field, on the transport of particulates. F1 typically requires approximately four to five fracture volume flushes to achieve a two-log decrease in *E. coli* RS2-GFP concentrations regardless of the flow rate, whereas F2 and F3 require approximately three and two fracture volume flushes respectively, in order to achieve the same decrease in *E. coli* RS2-GFP concentration. It is interesting that F1 has the smallest areal extent and the smallest mean aperture of all three fractures, as shown in Table 2.1. In addition, F2 and F3 have similar areal extents and mean apertures, which are significantly larger than those of F1. It took a larger number of fracture volume flushes to transport the *E. coli* RS2-GFP through a fracture with a smaller areal extent *and* a smaller

mean aperture, indicating the presence of a more tortuous flow pathway in F1, compared to F2 and F3. Tortuosity is a characteristic of the aperture field and significantly influences *E. coli* RS2-GFP transport in these experiments. This finding is consistent with that of Vilks and Bachinski (1996), who conducted a laboratory-scale study on the transport of colloids through a fractured granite block. They observed that colloid transport was very sensitive to flow path, and in some cases, more sensitive to flow path than groundwater velocity. Lapcevic et al. (1999) conducted a field-scale study in a single fracture and found that tortuous flow pathways increased the transverse dispersion of a fluorescent conservative solute tracer. Furthermore, the transport model developed by Chrysikopoulos and Abdel-Salem (1997) also predicted the presence of preferential flow paths in fractures. This finding demonstrates the importance of aperture field characterization in addition to knowledge of the flow conditions when interpreting particulate transport.

2.4 Conclusions

Laboratory-scale experiments are a useful way to study contaminant transport because of the ability to control experimental conditions and conduct mass balances. An improved understanding of the mechanisms that influence the fate and transport of contaminants in fractured aquifers will be invaluable in the quest to develop characterization methodologies that are specific to fractured aquifers. This study sheds light on the mechanistic understanding of solute and biocolloid transport in single, saturated, laboratory-scale fractures. In particular:

- The successful characterization of the fractures in this study was imperative to better understanding the mechanisms of particulate retention in fractures.The matrix surface properties, the COV_S, and the flow pathways significantly influenced the transport of *E. coli* RS2-GFP. The implication of this finding is that each of these factors plays a role in particulate transport, and therefore the characterization techniques employed in

this research should be investigated at the field scale to determine if they are suitable for the characterization of fractured aquifers at the field scale.

- Under the range of conditions employed in this research, it was found that higher specific discharges and/or smaller apertures do not always facilitate particulate transport. In this study, the attachment mechanism played a significant role in determining the degree of particulate retention observed. In addition, it is likely that factors not investigated in this study played a role in the anomalous behaviour observed in F1 at the lowest specific discharge. This finding challenges conventional assumptions that particulate transport in fractures is predominantly dependent on aperture field characteristics and specific discharge.

- The number of fracture volumes required to achieve a 2-3 log decrease in BTC concentration is approximately constant for each fracture and depended on aperture field characteristics and matrix properties, not specific discharge. This implies that the tortuosity of the flow path within the fracture has a larger influence than the specific discharge on the volume of fluid required to achieve a specific decrease in effluent concentration.

References

An, Y. H., Dickinson, R. B., Doyle, R. J., 2000. Mechanisms of Bacterial Adhesion and Pathogenesis of Implant and Tissue Infections. Totowa, New Jersey: Humana Press Inc.

APHA, AWWA, WEF, 2006. Standard Methods for the Examination of Water and Wastewater.
URL http://standardmethods.org/Store/index.cfm[Accessed:Jan.21,2010]

Auset, M., Keller, A., 2006. Pore-scale Visualization of Colloid Straining and Filtration in Saturated Porous Media Using Micromodels. Water Resources Resarch 42.

Barber, N., 2009. Summary of Estimated Water Use in the United States in 2005. U.S. Geological Survey Fact Sheet, 3098.

Bear, J., 1972. Dynamics of Fluids in Porous Media. Dover Publications.

Becker, M., Metge, D., Collins, S., Shapiro, A., Harvey, R., 2003. Bacterial Transport Experiments in Fractured Crystalline Bedrock. Ground Water 41 (5), 682–689.

Becker, M., Shapiro, A., 2003. Interpreting Tracer Breakthrough Tailing from Different Forced-Gradient Tracer Experiment Configurations in Fractured Bedrock. Water Resources Research 39 (1).

Brush, D., Thomson, N., 2003. Fluid Flow in Synthetic Rough-Walled Fractures: Navier-Stokes, Stokes and Local Cubic Law Simulations. Water Resources Research 39 (4).

Chrysikopoulos, C., Abdel-Salem, A., 1997. Modeling olloid ransport and eposition in at-urated ractures. Colloids and Surfaces A: Physicochemical and Engineering Aspects 121, 189–202.

Crane, S., Moore, J., 1984. Bacterial Pollution of Groundwater: A Review. Water, Air and Soil Pollution, 67–83.

Craun, G., Brunkard, J., Yoder, J., Roberts, V., Carpenter, J., Wade, T., Calderon, R., Roberts, J., Beach, M., Roy, S., July 2010. Causes of Outbreaks Associated with Drinking Water in the United States from 1971 to 2006. Clinical Microbiology Reviews 23 (3), 507–528.

Dickson, S., Thomson, N., 2003. Dissolution of Entrapped DNAPLs in Variable Aperture Fractures: Experimental Data and Empirical Model. Environmental Science & Technology 37, 4128–4137.

Fong, T., Mansfield, L., Wilson, D., Schwab, D., Molloy, S., Rose, J., June 2007. Massive Microbiological Groundwater Contamination Associated with a Waterborne Outbreak in Lake Erie, South Bass Island, Ohio. Environmental Health Perspectives 115 (6), 856–864.

Freeze, R., Cherry, J., 1979. Groundwater. Prentice-Hall, Inc., Ch. 9, p. 412.

Hautman, D., Munch, D., Pfaff, J., 1997. Method 300.1, Determination of Inorganic Anions in Drinking Water by Ion Chromatography, Revision 1.0.

Keller, A., Sirivithayapakorn, S., 2004. Early Breakthrough of Colloids and Bacteriophage MS2 in a Water-Saturated Sand Column. Water Resources Research 40.

Lapcevic, P., Novakowski, K., Sudicky, E., August 1999. The Interpretation of a Tracer Experiment Conducted in a Single Fracture Under Conditions of Natural Groundwater Flow. Water Resources Research 35 (8), 2301–2312.

Nowlan, L., 2007. Eau Canada The Future of Canada's Water. Vancouver: UBC Press, Ch. Out of Sight, Out of Mind? Taking Canada's Groundwater for Granted, pp. 55–83.

O'Connor, M. J., 2002. Part One A Summary Report of the Walkerton Inquiry. Toronto: Queen's Printer for Ontario.

Passmore, J., Rudolph, D., Mesquita, M., Cey, E., Emelko, M., 2010. The Utility of Microspheres as Surrogates for the Transport of E. coli RS2g in Partially Saturated Agricultural Soil. Water Research 44, 1235–1245.

Pekdeger, A., Matthess, G., 1983. Factors of Bacteria and Virus Transport in Groundwater. Environmental Geology 5 (2), 49–52.

Piggot, A., Elsworth, D., 1993. Laboratory Assessment of the Equivalent Apertures of a Rock Fracture. Geophysical Research Letters 20 (13), 1387–1390.

Rasmussen, T., June 1995. Laboratory Characterization of Fluid Flow Parameters in a Porous Rock Containing a Discrete Fracture. Geophysical Research Letters 22 (11), 1401–1404.

Rivera, A., 2005. How well do we understand groundwater in Canada? A Science Case Study. Natural Resources Canada and Geologic Survey of Canada.

Saini, R., Halverson, L., Lorimor, J., 2003. Rainfall Timing and Frequency Influence on Leaching of Escherichia coli RS2G through Soil Following Manure Application. Journal of Environmental Quality 32, 1865–1872.

Scholl, M., Mills, A., Herman, J., Hornberger, G., 1990. The Influence of Mineralogy and Solution Chemistry on the Attachment of Bacteria to Representative Aquifer Materials. Journal of Contaminant Hydrology 6, 321–336.

Sekerak, B., 2004. Development of an Interfacial Tracer Test for DNAPL Entrapped in Discrete Fractured Rock. Master's thesis, McMaster University.

Shapiro, A., Renken, R., Harvey, R., Zygnerski, M., Metge, D., 2008. Pathogen and Chemical Transport in the Karst Limestone of the Biscayne Aquifer: 2. Chemical Retention from Diffusion and Slow Advection. Water Resources Research 44.

Sinreich, M., Flynn, R., 2009. Use of Particulate Surrogates for Assessing Microbial Mobility in Subsurface Ecosystems. Hydrogeology Journal 17, 49–59.

Tsang, Y., 1992. Usage of 'Equivalent Apertures' for Rock Fractures as Derived from Hydraulic and Tracer Tests. Water Resources Research 28 (5), 1451–1455.

USGS, 1999. Ground water (general interest publication).
URL http://pubs.usgs.gov/gip/gw/[Accessed:July2011]

USGS, October 2002. Fractured-Rock Aquifers Understanding an Increasingly Important Source of Water. Fact Sheet FS-112-02.

USGS, 2011. Ground Water Use in the United States.
URL http://ga.water.usgs.gov/edu/wugw.html[Accessed:July2011]

Vilks, P., Bachinski, D., 1996. Colloid and Suspended Particle Migration Experiments in a Granite Fracture. Journal of Contaminant Hydrology 21, 269–279.

Vilks, P., Frosh, L., Bachinski, D., 1997. Field-Scale Colloid Migration Experiments in a Granite Fracture. Journal of Contaminant Hydrology 26, 203–314.

Yao, K.-M., Habibian, M. T., O'Melia, C., November 1971. Water and Waste Water Filtration: Concepts and Applications. Environmental Science & Technology 5 (11), 1105–1112.

Zheng, Q., Dickson, S., Guo, Y., 2008. On the Appropriate 'Equivalent Aperture' for the Description of Solute Transport in Single Fractures: Laboratory-Scale Experiments. Water Resources Research 44.

Zheng, Q., Dickson, S., Guo, Y., 2009. Differential Transport and Dispersion of Colloids Relative to Solutes in Single Fractures. Journal of Colloid and Interface Science 339 (1), 140–151.

Chapter 3

A Statistical Model for Particulate Retention Mechanisms in Single, Saturated, Variable-Aperture Fractures

Summary of Paper II: A Statistical Model for Particulate Retention Mechanisms in Single, Saturated, Variable-Aperture Fractures *(Submitted to Ground Water, July 2012)*

A novel, step-wise, multiple linear regression model was developed using extensive historical tracer data to identify the key factors contributing to particulate retention in fractures. The model employs data from over 70 particulate tracer tests conducted in laboratory-scale fractures to successfully identify the most influential particulate retention mechanisms. Ten factors were included in the statistical analysis, of which the three that were found to be significant in predicting particulate retention in fractures are, the ratio of the ionic strength of solution to the matrix surface charge, the ratio of the particle charge to the matrix charge, and the Peclet number. This finding is consistent with the findings of the first paper which concluded that attachment plays a determining role in the degree of retention observed. Attachment is heavily affected by the electrostatic conditions present in the fracture. Aside from the three significant factors, the following were deemed less important in predicting particulate retention: the geometry of the tracer, the variability of the aperture field, the equivalent aperture, the density of the particulate, and the ratio of inertial forces to viscous forces acting on the particulate. In addition, the model is able to adequately predict retention using some of the data that was intentionally omitted during model development. No other predictive model based on the statistics of tracer experiments conducted in laboratory-scale fractures has previously been reported in the literature.

Please note that data collected or analyzed in this segment of the research, but not presented within this paper, can be found in Appendix B.

ABSTRACT

Fractured aquifers are some of the most poorly understood subsurface environments despite posing one of the highest risks to the protection of potable groundwater. In order to develop improved groundwater remediation strategies, a better understanding of the fate and transport of particulates in fractures needs to be established. This research aimed at improving the understanding of the factors affecting particulate transport through the development of an empirical model based on laboratory-scale transport data. The model presented in this research employed data from over 70 particulate tracer tests conducted in single, saturated, variable-aperture fractures. The model revealed that the most important mechanisms influencing colloid and biocolloid retention in fractures, are the ratio of the ionic strength of solution to collector charge, the ratio of particle to collector charge, and the ratio of advective to diffusive forces as described by the Peclet number. The predictive abilities of the model were verified using data that were omitted from the model. The model was able to reasonably predict the fraction of particles retained. This research presents, for the first time, a statistical model for particulate retention in groundwater environments and takes an important step towards an improved understanding of particulate transport in fractures.

Key words:

fracture; particulate retention mechanism; statistics; predictive equation; multiple linear regression; *Escherichia coli*; microsphere; particulate transport

Contributors

The data used in developing this model was obtained from experiments conducted by S.N. Rodrigues and others in the Dickson Laboratory. S.N. Rodrigues performed the statistical analysis under the guidance of S.E. Dickson. The manuscript was prepared by S.N. Rodrigues and edited by S.E. Dickson.

Role of the Funding Source

This research was funded by the Canadian Water Network, NSERC Discovery Grant (S.E. Dickson) and Consulting Engineers of Ontario Water Quality Research Award (S.N. Ro-

drigues). The funding sources had no involvement in the study design, collection, analysis, and interpretation of data, writing of this paper, or in the decision to submit this article for publication.

Highlights

The ratio of fluid ionic strength to collector charge is the most important predictor of retention.

The ratio of particle to collector charge, along with the Peclet number, also influences retention.

The model presented reasonably predicts particulate retention in single, saturated fractures.

3.1 Background

Despite the abundance of groundwater research that exists today, scientists and policy makers are seeking a better understanding of particulate transport through fractured aquifers. In fact, due to a lack of fracture-specific characterization techniques, the methods developed for porous media aquifers are often employed on fractured aquifers (Nowlan, 2007). This leads to many uncertainties due to the stark physical differences between the two types of aquifers which affect hydrodynamics and transport mechanisms and therefore the behaviour of particulates within an aquifer. Knowledge of the mechanisms that influence the fate and transport of particulates in fractured aquifers will help improve existing characterization techniques, could feed into the development of new fracture-specific characterization techniques, and is required to improve management and remedial strategies for fractured aquifers.

Classic filtration theory, as it is now known, was introduced by Yao et al. (1971). Since then, many studies have found that some particulates and collectors (filter beds) behave in a manner that deviates from the classic filtration theory. In porous media studies, researchers observed deviations between theoretical expectations and empirical observations and proposed mechanistic modifications to the the classic filtration theory, (e.g., Tufenkji and Elimelech, 2004; Tufenkji and Elimelech, 2005; Tong and Johnson, 2007; Bradford et al., 2011). In addition to empirical models in porous media, several stochastic models have also been presented which consider filtration theory in conjunction with interaction energies, colloid and collector sizes, and other factors known to cause deviations from the classic filtration theory (e.g., Shapiro and Bedrikovetsky, 2010; Bradford and Toride, 2007). Classic filtration theory was developed for porous media and does not translate well to particulate filtration in fractures. As such, an increasing number of studies are focusing on the filtration of particulates in fractures (e.g., Berkowitz and Scher, 1997; Cumbie and McKay, 1999; Masciopinto et al., 2008). All of the studies mentioned above are aimed at improving the mechanistic understanding and prediction of filtration theory. However, despite the growing literature in the area of particulate transport in fractures, to the best of the authors' knowledge, this

is the first time a statistical model has been developed to help identify and understand the mechanisms that influence particulate transport through fractures at the pore scale.

The model presented in this paper represents a statistical analysis of the data collected from physical model experiments conducted to investigate particulate transport through single, saturated fractures. Specifically, these experiments were designed to examine the effects of the fracture matrix material properties, fracture aperture field characteristics, particulate surface properties, particulate sizes, and flow conditions on particulate retention in variable aperture fractures. The statistical model developed in this work is useful for determining the most influential particulate retention mechanisms, and can therefore guide further work in this field.

3.2 Model Development

The data used for the regression model was collected from over 70 particulate tracer experiments which employed a total of ten single, saturated, laboratory-scale fractures and two types of particulates (bacteria and polystyrene microspheres). Five of the fractures were extracted from the natural environment and five were synthetic epoxy casts of each of the natural fractures. Three of the natural rock fractures were collected from outcrops near Kingston, Ontario and the other two were retrieved near Guelph, Ontario. All of the natural rock samples were fractured in the laboratory and prepared for experimentation as described in Rodrigues et al. (2012). It was assumed that diffusion into the fracture matrix was negligible over the short duration of these experiments because the porosities are so small (and zero for epoxy). However, Brownian motion can cause the particles to behave in a diffusion-like manner moving in directions other than the direction of flow. Each fracture was characterized through hydraulic and solute tracer tests, which were employed to determine the equivalent hydraulic, mass balance, and frictional loss apertures. Known concentrations of *E. coli* RS2-GFP or carboxylated polystyrene microspheres were released at the upstream

end of each fracture under a range of specific discharges, and the effluent breakthrough curves (BTC) were measured. Details regarding the methodology employed to conduct these experiments are included in Rodrigues et al. (2012). The particulate retention from each experiment, as derived from the BTC, was used to develop an empirical model to identify the relative importance of aperture field characteristics, surface properties, particle sizes, and flow rate on particulate retention mechanisms under the range of conditions employed in these experiments.

Over 70 particulate tracer tests were conducted and approximately four-fifths of the data was used for model development, reserving the last one-fifth of the data for verifying the predictive ability of the model. Statistical analysis software (SAS Version 9.3) was used to perform a step-wise multiple linear regression. Stepwise multiple linear regression is an iterative technique in which different combinations of variables are included and omitted based on the value each variable adds to the model and its significance. The overall significance of the added variable to the model is assessed by the coefficient of multiple determination. The process terminates when the most parsimonious (fewest variables with good prediction) equation is obtained. In developing this model, a significance level $\alpha = 0.05$ was used to determine the significance of each variable.

In addition, it was assumed that the predictors, or independent variables, follow a normal distribution and the errors of the predictors and the predicted values are normally distributed with both, the standard variance and the mean, about zero. The verification of these assumptions is discussed in Section 3.3.1.

3.2.1 Dimensionless Numbers

An examination of the system revealed 16 parameters, including variables and constants, representing physical quantities that may affect particulate retention in fractures (Table 3.1), composed of six base units (Table 3.2). These variables include the bulk flow rate, the ionic

strength and temperature of the bulk fluid, the collector and particle surface charges, the size and density of the particle, and the mass balance, frictional loss, and hydraulic equivalent apertures.

Table 3.1: List of parameters used to develop the Pi groups.

#	Variable	Physical Representation	#	Variable	Physical Representation
1	Q_P	Particle charge	9	ϕ_P	Particle diameter
2	Q_M	Matrix charge	10	T	Absolute temperature
3	I	Ionic strength of solution	11	ρ_s	Density of solution
4	b_f	Frictional loss equivalent aperture	12	η	Viscosity of water
5	b_c	Hydraulic equivalent aperture	13	N_{Av}	Avogadro's number
6	b_m	Mass balance equivalent aperture	14	g	Gravitational constant
7	ρ_P	Particle density	15	D	Diffusion coefficient
8	q	Specific discharge	16	$R_{\%}$	Percent recovery

The constants include: Avogadro's number, fluid density, dynamic viscosity of the fluid, the gravitational constant, and the Boltzmann constant. Therefore, the Buckingham-Pi theorem states that this system can be adequately represented by ten dimensionless numbers, subsequently referred to as 'Pi groups'.

Table 3.2: Base units of all parameters listed in Table 3.1.

#	Base unit
1	Length (meters)
2	Mass (kilograms)
3	Time (seconds)
4	Number of electrons
5	Number of moles
6	Number of particles

Ten independent dimensionless groups, representing the different mechanisms that influence retention, were formed from the 16 parameters listed in Table 3.1. The Pi groups considered

Table 3.3: List of the Pi groups employed in the statistical analysis, together with their physical interpretations.

#	Definition	Physical Representation	#	Definition	Physical Representation
1	$N_Q = \frac{Q_P}{Q_M}$	Ratio of particle surface charge to matrix surface charge.	6	$N_{b_f} = \frac{\phi_P}{b_f}$	Particle straining as a function of the frictional loss equivalent aperture.
2	$N_{IS} = \frac{N_{Av} \cdot I \cdot A_P^{1.5}}{Q_M}$	Ionic strength of solution, surface area of particle, matrix charge.	7	$N_{b_c} = \frac{\phi_P}{b_c}$	Particle straining as a function of the cubic law equivalent aperture.
3	$N_{geo} = \frac{6 \cdot b_f}{\phi_P}$	Surface area to volume of the particle in relation to the smallest aperture regions.	8	$N_{Re} = \frac{\rho_s q b_c}{\eta}$	Reynold's number, characterizing inertial to viscous forces on the particle.
4	$N_{Gr \cdot Ad} = \frac{\rho_P \cdot g \cdot b_m}{\rho_s q^2}$	Gravitational forces to advective forces acting on the particle.	9	$N_{Pe} = \frac{b_m q}{D}$	Peclet number, characterizing advective to diffusive forces on the particle.
5	$N_{COV} = \frac{\sigma(b_f, b_c, b_m)}{b_m}$	Aperture variability over the areal extents of the fracture.	10	$f_r = 1 - R_{\%}$	Fraction of the particulates retained within the fracture after tracer tests.

in the stepwise regression model are listed in Table 3.3, together with a physical interpretation of their significance.

3.3 Results and Discussion

The walls of fractures tend to have rough surfaces, which reduce the near-surface shear forces that hinder the initial phase of bacterial attachment. In addition, uneven surfaces usually have molecular grooves or canyons that act to increase the cell-to-surface contact for colloids (Young, 2006). These two factors have been considered, respectively, in the regression model by: 1) taking into account the different surface areas of the bacteria and the microspheres and 2) using a surrogate measure of the COV (coefficient of variation) to describe aperture field variability for each fracture. Additionally, the rod shape of *E. coli* RS2-GFP may positively influence its ability to withstand detachment due to shear forces because it has a larger surface area available for long-term attachment (Young, 2006). Some

biological features of the *E. coli* RS2-GFP, such as any appendages used in attachment and/or propelling motions, were not considered through the Pi groups, as the determination of their existence and size was beyond the scope of this research.

Equation (3.1) shows the power function employed in this stepwise multiple regression analysis, which is intrinsically linear as shown in Equation (3.2).

$$Y = \kappa \cdot N_1^{\beta_1} \cdot N_2^{\beta_2} \cdot N_3^{\beta_3} ... \cdot N_{10}^{\beta_{10}} \tag{3.1}$$

$$\ln(Y) = \kappa^* + \beta_1 \ln N_1 + \beta_2 \ln N_2 + \beta_3 \ln N_3 + ... + \beta_{10} \ln N_{10} \tag{3.2}$$

where Y is the regressor, κ^* is the natural logarithm of the constant κ, N_i represents the Pi groups, also known as predictor variables, and β_i is the parameter estimate for each N_i, as determined through the regression analysis.

Equation (3.3) was developed by regressing the natural logarithm of the fraction of particles retained in the fracture against the natural logarithms all 10 Pi groups in a stepwise manner to estimate the values of β_i.

$$f_r = N_Q^{-0.0072} N_{IS}^{0.065} N_{Pe}^{-0.090} \tag{3.3}$$

where f_r is the fraction retained, and the three most significant predictors of retention are N_Q (ratio of the particle surface charge to the surface charge of fracture wall), N_{IS} (relation between the particle surface area and the ionic strength of solution), and N_{Pe} (Peclet number characterizing the ratio of advective to diffusive forces acting on the particle).

As shown in Equation (3.3), Pi groups 1, 2, and 9 were the three most significant predictors of particulate retention. This is not surprising as the surface properties of the collector particle have been shown to influence particulate retention in porous media systems (e.g., Low et al., 1996; Roy and Dzombak, 1996; An et al., 2000; Gu, 2004). Pi group 1 is a ratio

of the surface charges of the particle to the rock matrix. Pi group 2 represents the ratio of the ionic strength of solution to the charge of the particulate. The ninth Pi group, which is also commonly known as the Peclet number, is a ratio of the rate of advection to the rate of diffusion. Equation (3.3) is applicable under the range of conditions used in the experimental phase of this research which are summarized in Table 3.4.

Table 3.4: Range of conditions under which this model is applicable.

Parameter	Range	Units
Matrix charge	0.2-24	mV
Particle zeta potential	-12 to -18	mV
Particle surface are	0.8-4	mm^2
Ionic strength	1E-4 - 0.64	M
Specific discharge	1.4-140	m/day
Diffusion coefficient	4.2E-13 - 9.7E-12	m^2/s

3.3.1 Regression Diagnostics

The model developed through this research (Equation (3.3)) has a coefficient of multiple determination of 0.64. It is evident that one or more additional mechanisms influencing particulate retention in fractures is not accounted for in this model. However, it is still a useful model, as it provides insight towards some of the relevant mechanisms. Table 3.5 summarizes the regression diagnostics for the parameter estimates from the model, including

Table 3.5: Parameter estimate diagnostics for the model shown in Equation (3.3).

Variable	Parameter Estimate	Variance	t-Value	Pr > |t|	VIF	95% Confidence Limits	
Intercept	0.040	0.45422	0.06	0.95	0	-1.309	1.388
Ln(N_Q)	-0.072	0.00081	-2.52	0.01	2.02	-0.129	-0.015
Ln(N_{IS})	0.065	0.00014	5.53	<0.0001	1.55	0.042	0.088
Ln(N_{Pe})	-0.090	0.00140	-2.40	0.02	1.43	-0.164	-0.015

the variances, t-values, variance inflation factors and 95% confidence intervals. The regression

diagnostics indicate that the intercept is not statistically different from zero (based on a high variance, a t-value close to zero associated with a high probability of equalling zero, and confidence intervals centred about zero). Therefore the intercept was omitted from the model. N_{IS}, N_Q, and N_{Pe} all had low variances, t-values not equal to zero associated with very low probabilities of equalling zero, and relatively narrow confidence intervals that are not centred about zero, indicating that the parameters are non-zero. In addition, each of the three Pi groups have a low variance inflation factor (below 2.1) indicating there there is no significant correlation between the predictor variables.

A residual analysis was conducted to verify the assumption that the predictor variables and the residuals are normally distributed. As shown in Figure 3.1, the standardized residuals fall approximately on a straight line, and 95% of the standardized residuals fall in the interval (-2, +2), indicating that the errors are normally distributed.

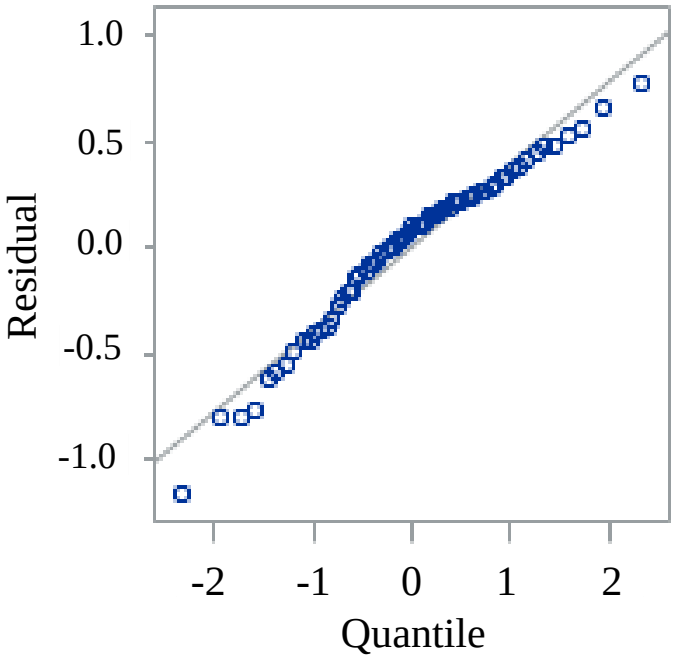

Figure 3.1: Normal probability plot for observed values.

In addition, Figures 3.2 a, b, and c illustrate the standardized residuals versus N_{IS}, N_Q, and N_{Pe}, respectively, and show that they are are distributed about zero, and no trends exist.

This indicates the normality of the Pi groups employed in this analysis.

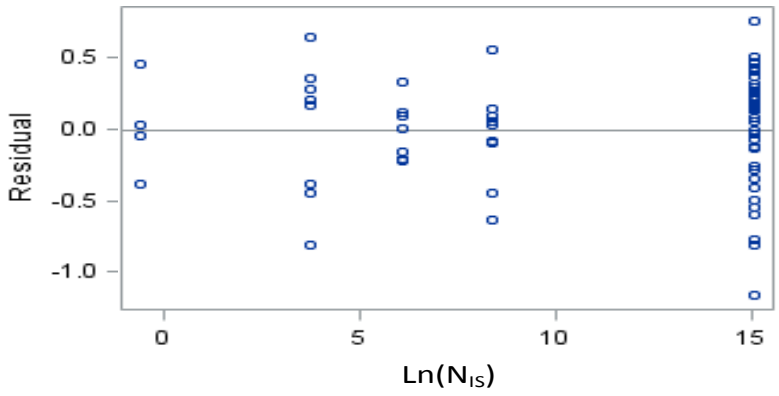

(a)

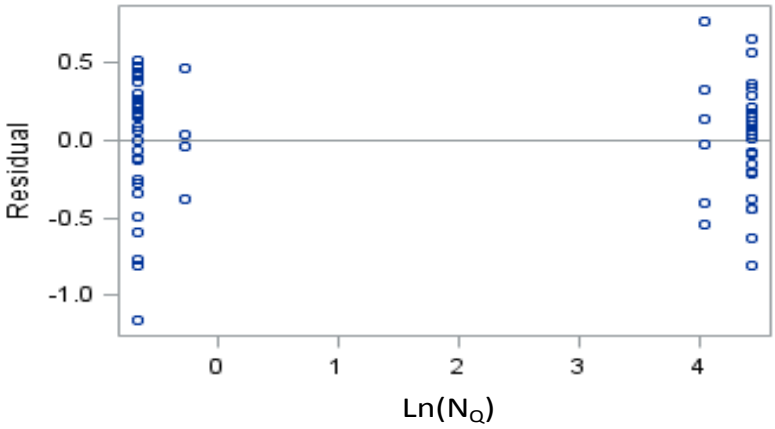

(b)

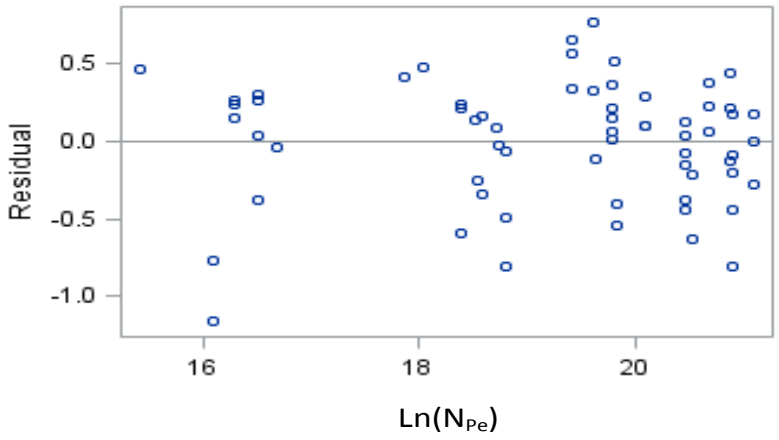

(c)

Figure 3.2: Residual versus a) $\ln N_{IS}$, b) $\ln N_Q$, and c) $\ln N_{Pe}$ for the natural logarithm of fraction retained.

3.3.2 Model Verification

Equation (3.3) was used to predict particulate retention using data that were intentionally left out of the model during the development phase of this research. Figure 3.3 shows the predicted values of the natural logarithm of retention plotted against the corresponding observed values.

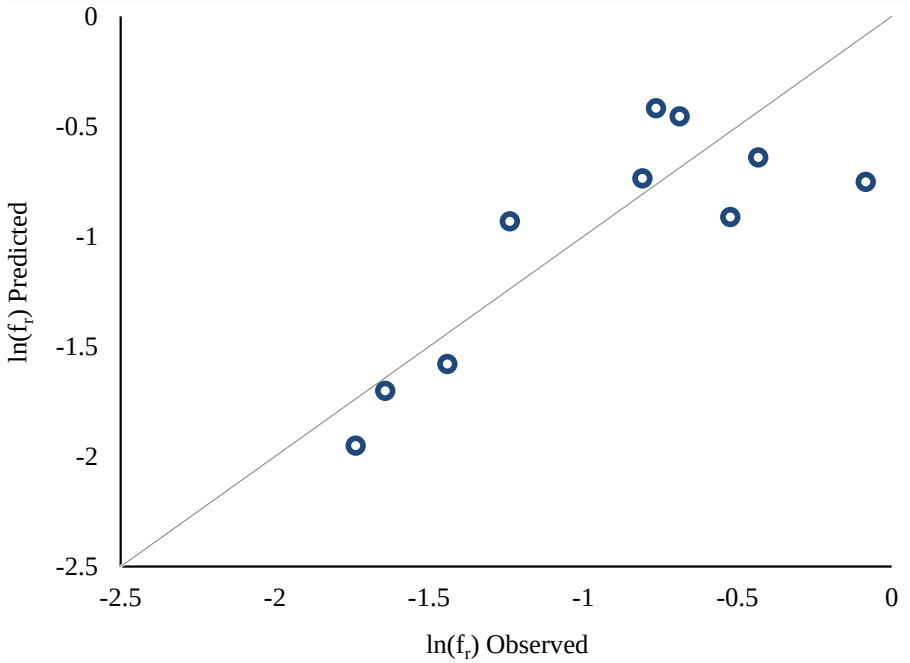

Figure 3.3: Log-normalized values of predicted versus observed retention.

The coefficient of determination for the plot of predicted versus observed values (Figure 3.3) is 0.68, indicating that 68% of the deviation about the mean is explained by the model, and 32% can be attributed to mechanisms not accounted for, and error.

3.4 Conclusions

In this research, a predictive model for the retention of colloids and biocolloids was obtained by regressing data from over 70 particulate tracer experiments. From the model, it is

evident that the most important factors affecting particulate retention in fractures are the ratio of the ionic strength of solution to the collector surface charge, the surface charges of the particle and the collector, and the flow characteristics as described by the Peclet number. Under the conditions tested during the experimental phase of this research, the less significant factors influencing particle retention are the surface area to volume ratio of the particle, the aperture variability, the equivalent aperture, the density of the particle, and the Reynold's number. This research broadened the mechanistic understanding of particulate transport in single, saturated fractures by statistically analyzing the results from scientifically sound particulate tracer experiments. In doing so, this research took an important step in developing much needed fracture-specific characterization techniques and could guide future research.

References

An, Y. H., Dickinson, R. B., Doyle, R. J., 2000. Mechanisms of Bacterial Adhesion and Pathogenesis of Implant and Tissue Infections. Totowa, New Jersey: Humana Press Inc.

Berkowitz, B., Scher, H., 1997. Theory of Anomalous Chemical Transort in Random Fracture Networks. The American Physical Society: Physical Review E 57 (5).

Bradford, S. A., Toride, N., 2007. A Stochastic Model for Colloid Transport and Deposition. J. Environ. Qual. 36 (1346-1356).

Bradford, S. A., Torkzaban, S., Simunek, J., 2011. Modeling Colloid Transport and Retention in Saturated Porous Media Under Unfavorable Attachment Conditions. Water Resources Research 47.

Cumbie, D. H., McKay, L. D., 1999. Influence of Diameter on Particle Transport in a Fractured Shale Saprolite. Journal of Contaminant Hydrology 37, 139–157.

Gu, Y., 2004. Deposition of Liquid Drops onto Solid Surfaces.

Low, D., Braaten, B., van der Woude, M., 1996. Escherichia coli and Salmonella: Cellular and Molecular Biology. ASM Press, Washington D.C., Ch. Fimbriae, pp. 146–157.

Masciopinto, C., La Mantia, R., Chrysikopoulos, C. V., 2008. Fate and Transport of Pathogens in a Fractured Aquifer in the Salento Area, Italy. Water Resources Research 44 (1).

Nowlan, L., 2007. Eau Canada The Future of Canada's Water. Vancouver: UBC Press, Ch. Out of Sight, Out of Mind? Taking Canada's Groundwater for Granted, pp. 55–83.

Rodrigues, S., Dickson, S., Qu, J., 2012. Colloid Retention Mechanisms in Single, Saturated, Variable-Aperture Fractures. Water Research, accepted, DOI: 10.1016/j.watres.2012.08.033.

Roy, S., Dzombak, D., 1996. Colloid Release and Transport Processes in Natural and Model Media. Colloids and Surfaces A: Physicochemical and Engineering Aspects, 245–262.

Shapiro, A., Bedrikovetsky, P. G., 2010. A Stochastic Theory for Deep Bed Filtration Accounting for Dispersion and Size Distributions. Physica A 389, 2473–2494.

Tong, M., Johnson, P., 2007. Colloid Population Heterogeneity Drives Hyperexponential Deviation from Classic Filtration Theory. Environmental Science & Technology 41 (2), 493–499.

Tufenkji, N., Elimelech, M., 2004. Deviation from the Classical Colloid Filtration Theory in the Presence of Repulsive DLVO Interactions. Langmuir 20 (25), 10818–10828.

Tufenkji, N., Elimelech, M., 2005. Breakdown of Colloid Filtration Theory: Role of the Secondary Energy Minimum and Surface Charge Heterogeneities. Langmuir 21 (3), 841–852.

Yao, K.-M., Habibian, M. T., O'Melia, C., November 1971. Water and Waste Water Filtration: Concepts and Applications. Environmental Science & Technology 5 (11), 1105–1112.

Young, K., 09 2006. The Selective Value of Bacterial Shape. Microbiology and Molecular Biology Reviews 70 (3), 660–703.

Chapter 4

The Effect of Matrix Properties and Specific Discharge on *E. coli* RS2-GFP Transport in Single, Saturated, Variable-Aperture Fractures

Summary of Paper III: The Effect of Matrix Properties and Specific Discharge on *E. coli* RS2-GFP Transport in Single, Saturated, Variable-Aperture Fractures

(Submitted to Water Research, September 2012)

In order to isolate the effects of matrix properties on the transport of *E. coli* RS2-GFP through fractures, tracer experiments were conducted in a natural fracture and a transparent, epoxy replica of that same fracture. The objectives of this research were to: 1) Identify the effect of matrix properties on the degree of particulate retention observed in a fracture, and 2) Visually capture the preferential transport of biocolloids in fractures. The aperture field characteristics of the replica closely matched those of the natural fracture, therefore the differences in *E. coli* RS2-GFP transport and retention between the fractures can be explained by matrix properties. The transparent nature of the replica was exploited to capture images of the *E. coli* RS2-GFP traveling through the replica fracture. These images confirmed the existence of preferential pathways in the fracture and revealed important transport characteristics of the *E. coli* RS2-GFP. In particular:

- Below specific discharges of approximately 30 $m \cdot day^{-1}$ *E. coli* RS2-GFP recoveries increased with increasing specific discharge. There exists a critical specific discharge somewhere between 30 and 150 $m \cdot day^{-1}$ at which increasing specific discharge does not result in further increases in recovery.

- The transport of *E. coli* RS2-GFP in the replica fracture was very different from transport in the natural fracture. Much higher *E. coli* RS2-GFP recoveries were observed from experiments conducted in the replica fracture and this observation is expected due to the more negative surface charge of the replica fracture (compared to the natural fracture) coupled with the negative zeta potential of the *E. coli* RS2-GFP. As a result of these like surface charges, larger repulsive forces (less favourable conditions for attachment) are present in the replica fracture.

- The images of the *E. coli* RS2-GFP traveling through the transparent epoxy replica

revealed that higher specific discharges caused the dominant preferential pathway of the *E. coli* RS2-GFP to broaden slightly. It is believed that this is a result of overcoming the higher critical pore entry pressures with larger specific discharges.

- Under identical specific discharges, the transport of *E. coli* RS2-GFP varied with different matrix properties. This result confirms the importance of both physical *and* chemical properties of the matrix together with those of the particulate in influencing the degree of retention that is observed in fractures.

Please note that the natural fracture discussed in this paper is the same fracture identified as F3 in Paper 1. Data collected or analyzed in this segment of the research, but not presented within this paper, can be found in Appendix A (F3 data) and Appendix C (replica data).

ABSTRACT

Fractured aquifers are a relatively under-studied area of groundwater science particularly because of the heterogeneities present in fractures which make it difficult to understand and predict the transport and retention of contaminants in these groundwater systems. This research was designed to elucidate some of the factors that contribute to particulate transport and retention in fractures, such as surface charge of the matrix and specific discharge. Solute and particulate tracer experiments were conducted in a fracture induced in a natural rock sample at the laboratory and an epoxy replica of that same fracture. A concerted effort to replicate the natural fracture resulted in very similar aperture field characteristics between the two fractures, such as equivalent apertures and matrix porosities. Therefore, the major difference between these two fractures is found in the matrix charge, essentially isolating the effects of fracture matrix charge on the transport and retention of *E. coli* RS2-GFP. Significantly less attachment was observed from the tracer experiments conducted in the in the replica fracture illustrating the large effect that matrix charge has on transport and retention of particulates in fractures. The *E. coli* RS2-GFP tracer results from experiments conducted in the replica fracture indicate that increasing specific discharge results in increasing recovery; however, there is a critical specific discharge at which particulate recovery does not increase with further increases of specific discharge. Since the replica fracture was cast out of transparent epoxy, images of the *E. coli* RS2-GFP transport through the fracture were collected. These images capture for the first time the preferential pathways of *E. coli* in fractures, and also demonstrate a slight broadening of the dominant preferential pathway under increasing flow conditions. These results are instructive to the development and improvement of predictive models for particulate transport in fractured aquifers.

Key words:
fracture; particulate retention mechanism; preferential pathway; matrix properties; Escherichia coli; transport visualization; particulate transport

Contributors

The idea for these experiments came from S.N. Rodrigues. Both authors contributed to the design of the experiments discussed in this paper. The experiments were conducted by S.N. Rodrigues. S.N. Rodrigues analyzed the data under the guidance of S.E. Dickson. S.N. Rodrigues prepared the manuscript, and S.E. Dickson edited it.

Role of the Funding Source

This research was funded by the Canadian Water Network, NSERC Discovery Grant (S.E. Dickson) and Consulting Engineers of Ontario Water Quality Research Award (S.N. Rodrigues). The funding sources had no involvement in the study design, collection, analysis, and interpretation of data, writing of this paper, or in the decision to submit this article for publication.

Highlights

Matrix properties have a significant influence on the degree of retention observed in fractures.
Increasing flow broadened, but did not reroute the dominant preferential pathway route.
At high specific discharges, attachment is determined by hydrodynamic, not electrostatic, forces.

4.1 Background

Fractured aquifers are amongst the most poorly understood natural environments due to the heterogeneous nature of fractures and fracture networks. The fractures in these aquifers act as 'contaminant highways', allowing dissolved and particulate contaminants to quickly and easily migrate large distances within the aquifer. Fracture heterogeneity makes it difficult to predict and characterize the fate and transport of contaminants within these subsurface environments. Despite the inherent differences between fractured and porous media aquifers, the characterization techniques developed for porous media aquifers are often employed on fractured aquifers, leading to many uncertainties (Nowlan, 2007). In order to safely use and manage fractured aquifers as sources of potable water, fracture-specific characterization techniques are required; an improved understanding of the fate and transport of contaminants in fractures could be used to develop these techniques.

Particulate retention within an aquifer is influenced by the interactions that occur between the particulate and the aquifer matrix. The mechanisms that cause a particle to collide with the fracture wall are sedimentation (due to the buoyant weight of the particle), Brownian motion (resulting from continuous bombardment of the particle from surrounding molecules), and interception (when a particle collides with a fracture wall while traveling along its natural trajectory) (Yao et al., 1971). After a collision occurs, particulate retention is governed by attachment.

Attachment is strongly influenced by the charge of the fracture walls, together with the charge of the particulate, due to the electrostatic and van der Waals interactions as described by classic DLVO (Derjaguin, Landau, Verway and Overbeek) theory. According to this theory, a reduction in the electrostatic repulsion between the particulate and the fracture walls promotes attachment. After considering traditional approaches and recent developments in the well-studied field of microbial transport in porous media, **?** suggests that improved microbial transport models should include the influence of aquifer matrix compositions on the fate

and transport of microorganisms in groundwater environments. To the best of the authors' knowledge no studies that isolate the effects of the surface charge of the fracture matrix on particulate transport in fractures have been reported in the literature, and this information could be used to improve the reliability of groundwater models.

In addition surface charge of the fracture wall, the existence of preferential flow paths in fractured aquifers, and their effect on contaminant transport, has been of much interest in the literature for some time now (e.g., McKay et al., 1993;Chrysikopoulos and Abdel-Salem, 1997; Zheng and Gorelick, 2003; Arnon et al., 2008; Zheng et al., 2009; Zheng et al., 2011). These studies agree that preferential flow paths consistently enhance contaminant transport through an aquifer. Due to the presence of fractures, McKay et al. (1993) found that bacteriophage traveled through a fractured clay aquifer more quickly than a conservative solute tracer, as the solute tracer experienced some diffusion into the matrix whereas the bacteriophage did not. Zheng and Gorelick (2003) and Zheng et al. (2011) found that the existence of connected networks of macropore preferential flow pathways had a dominant effect on the transport of solutes. Arnon et al. (2008) postulated that preferential pathways likely contributed to the extensive transport of steroidal hormones into an aquifer beneath a dairy farm after concluding that advection, dispersion and sorption alone were insufficient contributors to the extensive transport. Chrysikopoulos and Abdel-Salem (1997) developed a stochastic model for colloid transport and deposition in fractures and found that it predicted the presence of preferential colloid transport within the fracture. None of these studies, however, have actually visualized the preferential pathways of *E. coli*, or observed the effect of specific discharge on the transport pathways of *E. coli*. Understanding the shape and size of preferential flow paths, and how these characteristics are affected by varying flow conditions, will instruct the development of particulate transport models for fractured aquifers.

The objective of this research is to isolate the effects of matrix properties on particulate transport and attachment, and to determine the effect of specific discharge on preferential flow pathways. This was achieved by conducting laboratory-scale *E. coli* RS2-GFP tracer

experiments under a range of flow conditions, in two single, saturated, variable-aperture fractures: a natural dolomitic limestone fracture, and a transparent epoxy replica of the same fracture. In addition, the transport of *E. coli* RS2-GFP was visualized in the transparent epoxy cast under a range of specific discharges. This study demonstrates the importance of considering matrix surface charge and preferential flow pathways when developing predictive models for contaminant transport in groundwater environments.

4.2 Materials and Methods

The laboratory-scale, dolomitic limestone fracture used in this research was obtained from an outcrop near Kingston, Ontario, and will hereafter be referred to as 'F'. Dolomitic limestone is a carbonate rock consisting of calcium carbonate molecules with some of the calcium ions being replaced by magnesium ions. A transparent epoxy replica of F was cast in order to visualize the *E. coli* RS2-GFP traveling through the fracture during the tracer experiments, as well as to isolate the effect of matrix charge on the transport mechanisms, and will hereafter be referred to as 'RF'. Details of the casting method are included in Dickson (2001). Photographs of the fractures are shown in Figure 4.1. The natural and

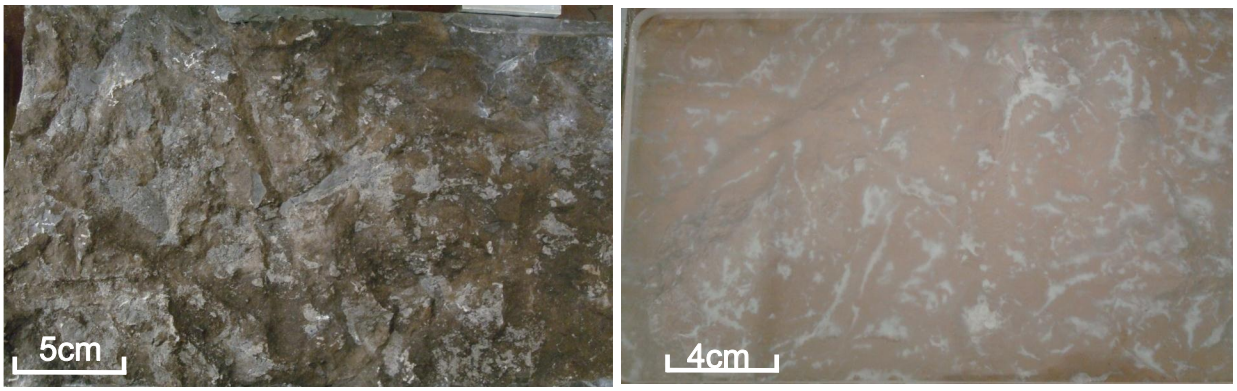

(a) Dolomitic limestone (b) Epoxy

Figure 4.1: Photographs of the top view of the two types of fractures employed in these experiments.

replicate fractures were prepared for experimentation by sealing the two longer edges as no-flow boundaries and affixing a volumetric flow cell on the upstream and downstream ends of the fracture.

The particulates used in these experiments were *E. coli* RS2-GFP, which were obtained from the Emelko Laboratory (Department of Civil Engineering, University of Waterloo, Waterloo, Canada). The Waterloo culture was obtained through Dr. Larry Halverson from the Department of Agriculture and Biosystems Engineering at Iowa State University, IA, USA, and the derivation of the strain is described in Saini et al. (2003). The cultures were maintained and prepared for experimentation following the methods described by Passmore et al. (2010). *E. coli* RS2-GFP is rod-shaped with semi-spherical caps. It has a zeta potential of approximately -12 mV and is approximately 2.5 μm in length, and 0.8 μm in diameter (Passmore et al., 2010). This strain of bacteria is resistant to two antibiotics which virtually eliminated any contamination issues during experimentation. It has been genetically tagged with a green fluorescent protein enabling it to fluoresce under UV light.

4.2.1 Experimental Setup

Figure 4.2 shows a schematic diagram of the experimental setup. The transparent rectangular prism in Figure 4.2 represents the fracture being used for experimentation. As shown in this figure, each volumetric flow cell consists of a perforated tube within the flow cell, which is joined at either end with pump tubing to form a closed recirculation loop. An injection/withdrawal cell and a peristaltic pump are located within the recirculation loop. When the recirculation pump is on, the contents of the flow cell and the injection/withdrawal cell are continuously mixed. The flow cells are used to inject fluid and introduce tracers at the upstream end of the fracture, and collect samples at the downstream end of the fracture. A second peristaltic pump connected to the upstream injection/withdrawal cell pumps the influent solution through the fracture. This pump is adjusted to achieve specific discharges

ranging over three orders of magnitude. An inclined piezometer, installed at each end of the fracture, is used to measure the headloss over the length of the fracture. Full details of the fracture setup are included in Rodrigues et al. (2012).

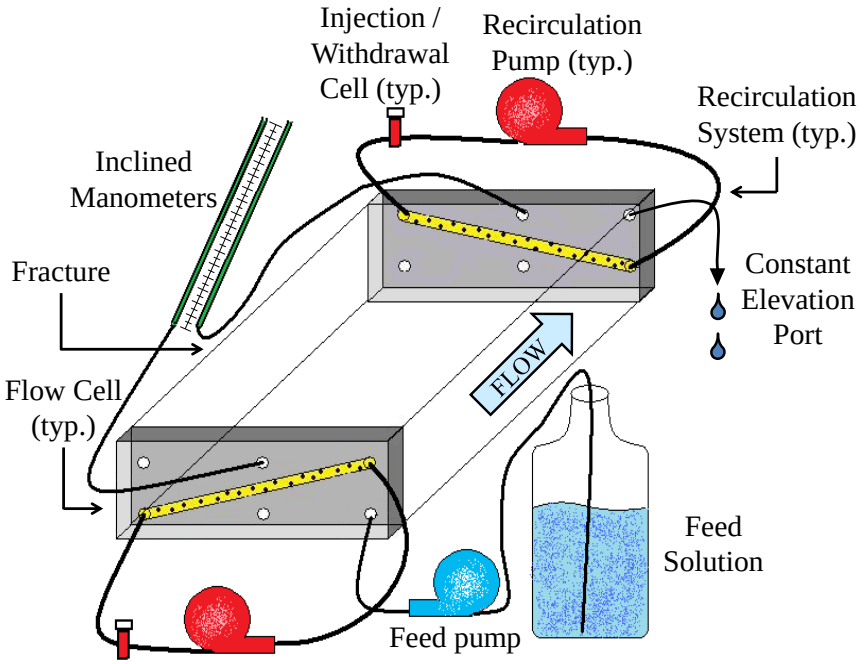

Figure 4.2: Schematic diagram of the experimental setup.

Dolomitic limestone has a much higher density than the epoxy employed for casting the fracture replica. This higher density results in the top-half of the natural fracture sitting snugly on the bottom half due to its own weight. The epoxy replica, however, required a compression system to achieve an aperture that was comparable to that of the natural fracture. Figure 4.3 shows a schematic diagram of the compression system, which consisted of a half-inch thick sheet of transparent plexiglass placed above and below the epoxy fracture (the fracture is represented by the rectangular prism drawn with dashed lines). The sheets of plexiglass were connected with 10 screw rods and twenty nuts and washers. The aperture size was changed by adjusting the nuts on the vertical screw rods, effectively adjusting the distance between the two pieces of plexiglass. Each nut was adjusted in a uniform manner every time an adjustment was made. Adjustments were made until the hydraulic apertures

of the replica and the natural fracture were equivalent.

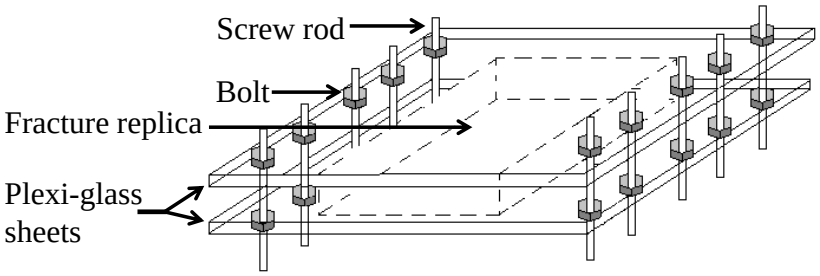

Figure 4.3: Schematic diagram of the epoxy replica compression system.

Figure 4.4 shows a schematic diagram of the fracture along with the image-capturing setup prepared for the visualization experiments. Using a transparent epoxy material to cast the replica enabled the visualization of the *E. coli* RS2-GFP traveling through the fracture.

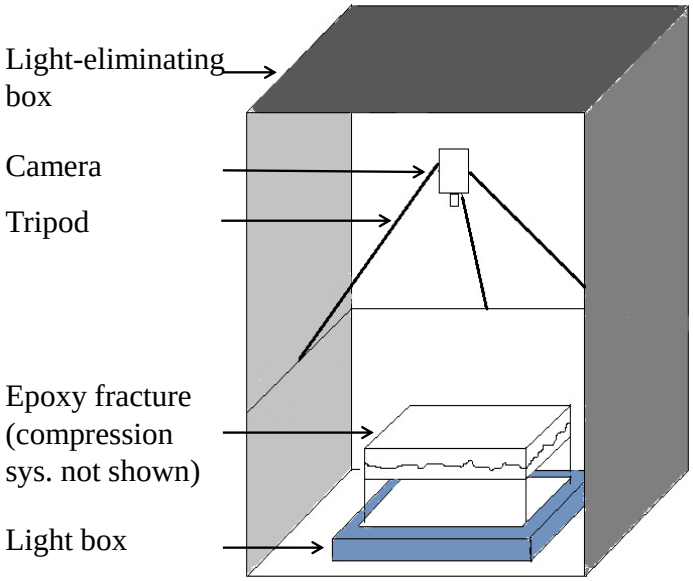

Figure 4.4: Schematic diagram of the fracture placed inside the image-capturing setup.

A scientific-grade charge-coupled device (CCD) camera ($CoolSNAP_{ES}$, Photometrics) was used to capture images of the *E. coli* RS2-GFP being transported through the fracture. The camera was able to detect the decrease in light penetration through the fracture as a result of

the increased turbidity due to the presence of the *E. coli* RS2-GFP. The images were processed and enhanced using Matlab. To reduce the noise from ambient light in the laboratory, the entire setup (light source, fracture, and camera) was arranged inside a light-eliminating box.

4.2.2 Fracture Plane Saturation

Carbon dioxide was used to saturate each fracture prior to injecting any aqueous solution. Compared to air, carbon dioxide is much more soluble in water, and therefore it completely dissolved in the aqueous solution upon saturation, ensuring no pockets of air remained in the fracture. The feed solution employed in the solute tracer experiments was deionized, degassed water (DDW), with pH = 8 and negligible ionic strength. Sodium hydroxide was used to buffer the DDW to prevent the dissolution of carbonate compounds in the rock. To prevent the possibility of gases coming out of solution during experimentation, the feed solution was degassed by bubbling helium through it. The specially prepared buffered DDW was pumped through the fracture for approximately 16-18 hours prior to the start of any experiments. Prior to running the *E. coli* RS2-GFP experiments, the fractured rock setup was saturated as described above, however, the DDW was replaced with a phosphate buffered saline (PBS) solution.

4.2.3 Fracture Plane Characterization

The natural and replicate fractures were fully characterized using hydraulic and solute tracer tests. The injection/withdrawal cell used to collect the BTC data is connected to the downstream recirculation loop. Hydraulic experiments were used to determine the equivalent hydraulic aperture, as well as to verify that all experiments were conducted under laminar flow conditions, (i.e. Reynold's number below one). A concerted effort was made to match the equivalent hydraulic aperture of RF to that of F.

The solute tracer experiments involved the release of a known mass of bromide (0.3 mL of 10 g/L, 0.125 M, pH = 9.8 Br^- as NaBr) into the upstream injection/withdrawal cell, and turning the recirculation system on full speed to mix the bromide with the contents of the upstream flow cell. Once the contents were fully mixed, the recirculation pump was turned down and the influent feed pump was turned on marking the beginning of the experiment. During the solute tracer experiments, the solution exiting the fracture is diluted upon entering the downstream flow cell, and therefore the measured concentration must be adjusted to determine the tracer concentration exiting the fracture. This adjustment was based on a mass balance of a continuous flow stirred tank reactor (CFSTR). The trapezoid rule was used to calculate the total mass of tracer that exited the fracture. Full details of these calculations are included in Rodrigues et al. (2012).

4.2.4 *E. coli* RS2-GFP Experiments

The particulate transport experiments were conducted after the fractures were fully characterized through the hydraulic and solute tracer experiments. Three milliliters of approximately 3×10^8CFU/mL *E. coli* RS2-GFP were released at the upstream end of the fully saturated fracture under a range of specific discharges, and the effluent BTC was measured. The BTCs were determined by plating serial dilutions of *E. coli* RS2-GFP according to the method described by Passmore et al. (2010). As with the solute tracer experiments, the number of *E. coli* RS2-GFP exiting the fracture was back-calculated using the same methods employed on the solute BTCs.

The BTCs report the solute or *E. coli* RS2-GFP concentration as a function of the number of 'fracture volume flushes', FVs, that have passed through the fracture. One FV physically represents the amount of fluid required to fill all the void space between the fracture walls and is often used in place of time as it enables the comparison of tracer BTCs from fractures according to the volume of fluid passing through the fracture instead of the amount of time

for which the experiment has been running. This is an important distinction when comparing flow conditions that range over three orders of magnitude. One fracture volume is calculated as follows:

$$FV = L \cdot W \cdot b_m \tag{4.1}$$

where FV [L^3] is the estimated volume of void space between the fracture walls, L [L] is the length of the fracture in the direction of flow, W [L] is the width of the fracture perpendicular to the flow, and b_m [L] is the equivalent mass balance aperture. The equivalent mass balance aperture is used in the calculation of FV because it has been shown to closely approximate the arithmetic mean aperture (Tsang, 1992; Zheng et al., 2008).

4.3 Results and Discussion

4.3.1 Fracture Aperture and Matrix Characterization

The three equivalent apertures reported in Table 4.1 represent the equivalent frictional loss, b_f, hydraulic, b_c, and mass balance, b_m, aperture. The equivalent frictional loss aperture, b_f [L], is given by Tsang (1992):

$$b_f = L \left(\frac{12\ \mu}{\gamma\ |\Delta H|\ t_m} \right)^{1/2} \tag{4.2}$$

where ΔH [L] is the hydraulic headloss over the length of the fracture, L[L] is the length of the fracture, γ [$M \cdot L^{-3}$] is the fluid weight density, μ [$M \cdot T^{-2} \cdot L^{-2}$] is the viscosity of the fluid, and t_m [T] is the mean residence time of the tracer. The mean bromide residence time (t_m) was calculated as follows (Fahim and Wakao, 1982):

$$t_m = \frac{\sum \bar{C}_{eff}(t) \cdot \bar{t} \cdot \Delta t}{\sum \bar{C}_{eff}(t) \cdot \Delta t} \tag{4.3}$$

where $\bar{C}_{eff}(t)[M \cdot L^{-3}]$ is the average bromide concentration exiting the fracture at the time the sample was taken. $\bar{t}[T]$ is the average time that has elapsed. The equivalent hydraulic aperture, b_c [L], was calculated using:

$$b_c = \left(\frac{12\ \mu\ Q\ L}{\gamma\ W\ |\Delta H|} \right)^{1/3} \tag{4.4}$$

where Q is the volumetric flow rate $[L^3 \cdot T^{-1}]$, L [L] is the length of the fracture in the direction of flow, and W [L] is the width of the fracture perpendicular to the direction of flow. The equivalent mass balance aperture, b_m [L], relates the flow rate, the mean residence time of tracer transport, and the areal extents of the fracture, A $[L^2]$, according to Tsang (1992):

$$b_m = \frac{Q \cdot t_m}{A} \tag{4.5}$$

Table 4.1: Characterization results from hydraulic and solute tracer experiments for F and RF.

Fracture ID	Length	Width	Recirc. Vol. (Upstr.)	Recirc. Vol. (Down.)	Surface Charge	Porosity	Bromide Recovery	Equivalent Aperture			COV	Reynold's Number
								b_f	b_c	b_m	σ/b_m	
	[m]	[m]	[m^3]	[m^3]	[mV]	[%]	[%]	[mm]	[mm]	[mm]	[-]	[-]
F	0.350	0.230	1.27E-04	1.07E-04	-7.5	0.23	94	0.10 ± 0.01	0.47 ± 0.02	3.78 ± 0.11	0.54	0.880
RF	0.349	0.230	4.90E-05	5.20E-05	-24.64	0	93	0.12 ± 0.04	0.45 ± 0.08	3.47 ± 0.04	0.53	0.630

a. All experiments were conducted at 25 ± 2 °C, and the values of the parameters used in these calculations correspond to those at 25 °C (i.e., ρ = 997 kg/m^3, η = 0.00089 N·s/m^2).
b. Recirculation volume includes the volume of the flow cell, injection/withdrawal cell, and tubing external to the flow cell.
c. Equivalent apertures for F3 show the standard deviation determined from experiments conducted in triplicate.
d. Equivalent apertures for RF3 show an estimated standard deviation determined from experiments conducted in duplicate. It was calculated as follows: s = SQRT[$\Sigma(x-\mu)^2/(N-1)$]
e. Reynold's Number = $(\rho \cdot q \cdot b_c) / \eta$
f. The porosity of the natural fracture is based on measurements conducted on dolomitic limestones from Dickson (2001).

The equivalent apertures reported in Table 4.1 exhibit the following relationship:

$$b_f < b_c < b_m \tag{4.6}$$

This relationship is consistent with others' observations (e.g., Piggot and Elsworth, 1993; Rasmussen, 1995; Dickson and Thomson, 2003; Zheng et al., 2008), and is expected since the

frictional loss aperture is sensitive to the smallest aperture regions which cause the largest headloss, while the mass balance aperture is sensitive to the larger aperture regions, which store more solute mass than their smaller counterparts.

Table 4.1 also shows a surrogate measure of the coefficient of variation (COV), which is an extremely important aperture field characteristic. The actual COV cannot be calculated without a detailed map of the aperture field; however, by definition, the COV is the ratio of the standard deviation of a sample to the arithmetic mean. Since the three equivalent apertures measured represent the range of extreme apertures, the standard deviation of these apertures is meaningful. Additionally, it has been demonstrated that the mass balance aperture is a good approximation of the arithmetic mean aperture (Tsang, 1992; Zheng et al., 2008). Therefore, with these values, a surrogate measure of the COV was determined as follows:

$$COV_S = \frac{\sigma(b_f, b_c, b_m)}{b_m} \tag{4.7}$$

where COV_S [-] is a surrogate measure of the coefficient of variation, and $\sigma(b_f, b_c, b_m)$ is the standard deviation of the three equivalent apertures measured in this work.

Table 4.1 also compares the equivalent apertures for F and RF. The hydraulic apertures of F and RF differ by approximately two percent (see Table 4.1). Moreover, the COVs for F and RF are very similar. The results shown in Table 4.1 indicate that the aperture field of RF replicates that of F quite well. Although F and RF have very comparable aperture fields, the material properties of dolomitic limestone are vastly different from those of epoxy. The most significant difference between the materials is the surface charge. As shown in Table 4.1, the surface charge of the epoxy fracture is more than three times as negative as that of the natural fracture. Table 4.1 also shows the porosities of each material are relatively comparable at < 1 percent for the natural fracture and zero for the epoxy fracture . Since the porosity of the dolomitic limestone is so low, and the duration of these experiments is relatively short, matrix diffusion is not a factor in these experiments.

The influence of the different matrix materials on particulate transport will be due to the surface charge, and not matrix diffusion. This is supported by the fact that the solute recoveries from the tracer tests are almost identical, indicating that: 1) there is negligible matrix diffusion in the natural fracture; and 2) since there is zero diffusion into the epoxy matrix (zero porosity as shown in Table 4.1), a solute recovery less than 100% is likely an artifact of the mass balance calculation performed on the downstream flow cell (details of which are included in Rodrigues et al. (2012)).

4.3.2 Quantitative *E. coli* RS2-GFP Tracer Test Results

Figure 4.5 shows the *E. coli* RS2-GFP BTCs from replicate experiments conducted in a) F at 14m·day^{-1} and b) RF at 15m·day^{-1}. These figures show that replicated *E. coli* RS2-GFP tracer experiments match each other well in terms of duration, magnitude, and shape, indicating that the experiments are repeatable despite the inherent challenges of working with

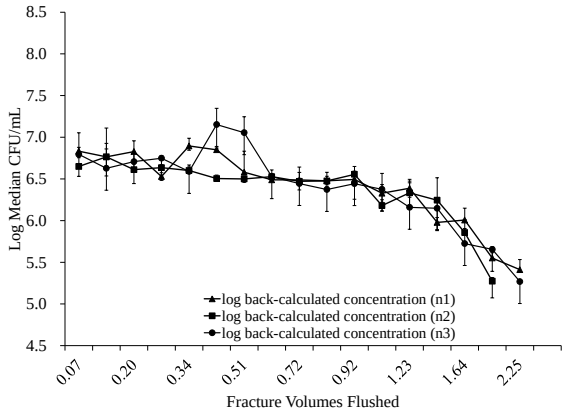

(a) F at 14 m·day^{-1} (in triplicate).

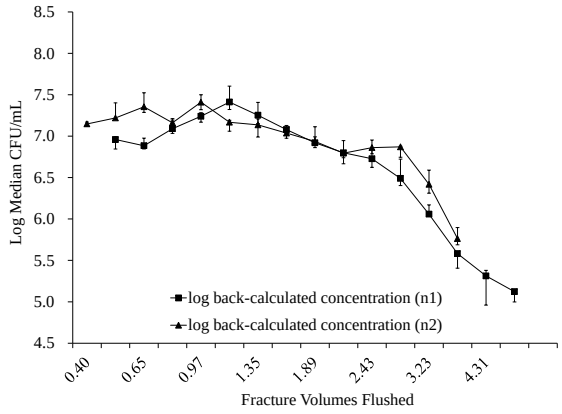

(b) RF at 15 m·day^{-1} (in duplicate).

Figure 4.5: *E. coli* RS2-GFP tracer tests in a) F at 14 m·day^{-1} (in triplicate) and in b) RF at 15 m·day^{-1} (in duplicate). Error bars represent the range of maximum and minimum concentrations and were determined using Equation 4.8.

microorganisms. The results shown in Figures 4.5a and 4.5b are typical of the results of all the experiments conducted in F and RF respectively, under all specific discharges. The error

bars on Figures 4.5 and 4.5b represent the range of maximum and minimum concentrations, and were calculated as follows:

$$1.5(Q3\text{-}Q1) + Q3 \text{ and } \quad Q1\text{-}1.5(Q3\text{-}Q1) \tag{4.8}$$

where Q1 and Q3 represent the first and third quartiles respectively. The recovery was calculated by integrating each BTC to determine the total number of *E. coli* RS2-GFP exiting the fracture, and comparing that to the number of *E. coli* RS2-GFP that was released upstream.

Figure 4.6 shows the average recovery of *E. coli* RS2-GFP for F and RF over a range of specific discharges. As shown in Figure 4.6, both the F and RF experiments display a trend of increasing recovery with increasing specific discharge at specific discharges at and below approximately 30 m·day^{-1}. However, there exists a critical specific discharge

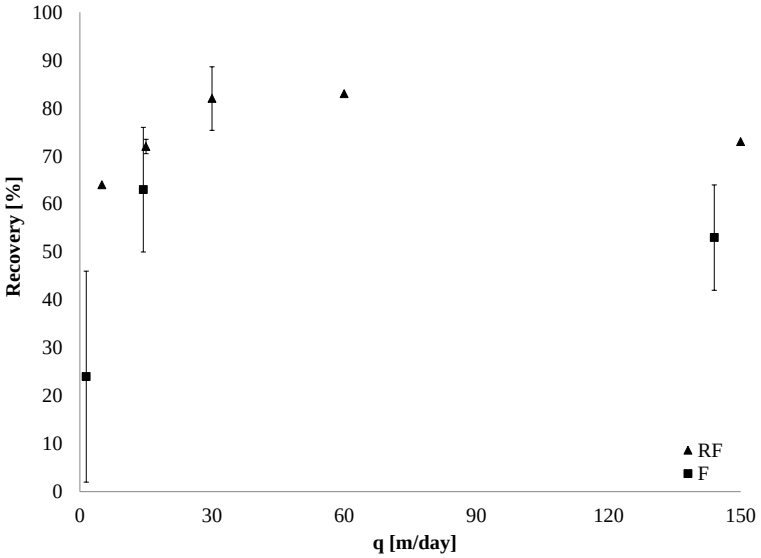

Figure 4.6: Average *E. coli* RS2-GFP recovery at different specific discharges for F and RF. Error bars represent the standard deviation of replicated experiments. The two data points without error bars were not replicated.

somewhere between 30 and 150 m·day^{-1} beyond which no increase in recovery is observed with increasing specific discharge. It is postulated that at the higher specific discharges,

hydrodynamic forces enable the *E. coli* RS2-GFP to overcome repulsive electrostatic forces resulting in more collisions between the particulates and the fracture wall, and therefore more attachment. Previous tracer studies conducted in F and other experimental fractures revealed a similar trend (Rodrigues et al., 2012).

Figure 4.7 shows the *E. coli* RS2-GFP BTCs for F and RF at specific discharges of 14 and 15 m·day^{-1}, respectively. As shown in Figure 4.7, the RF BTC has a larger peak concentration and a longer tail than the BTC for F. This finding is typical of all the BTCs obtained from F and RF. The higher effluent concentration from RF is likely an indication that relatively little attachment is occurring in RF compared to F. These results are consistent with Figure 4.6 which shows that F achieved a recovery of approximately 43% whereas RF had

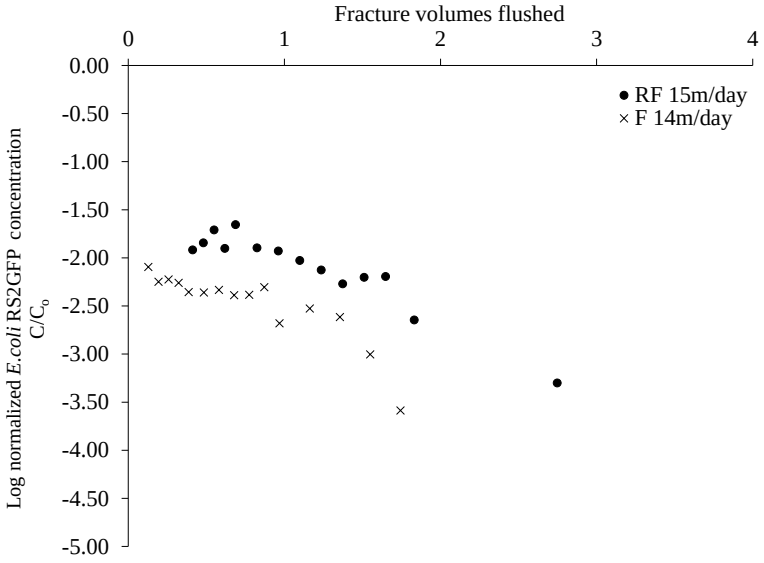

Figure 4.7: *E. coli* RS2-GFP BTCs for F and RF at 14 and 15 m·day^{-1}, respectively.

a recovery of approximately 72% under comparable flow conditions. These results confirm that the retention mechanisms occurring in F are more effective than those occurring in RF. Since F and RF have nearly identical aperture fields, with the exception of matrix surface properties, this observation is most likely attributable to the different surface charges of the fracture matrices.

Figure 4.8 shows the log normalized BTCs under a range of flow conditions for a) F and b) RF. This figure shows that each fracture, regardless of specific discharge, typically requires a constant number of fracture volume flushes to achieve a 1 to 2.5 log decrease in *E. coli* RS2-GFP concentration. Figure 4.8 shows that F typically requires between two and three fracture volume flushes, whereas RF typically requires between three and four fracture volume flushes, before the effluent *E. coli* RS2-GFP concentrations are below detectable limits. This indicates that, within the range of specific discharges investigated in this work, it is the retention mechanisms, and not the specific discharge, that plays the larger role in overall recovery of *E. coli* RS2-GFP in fractures.

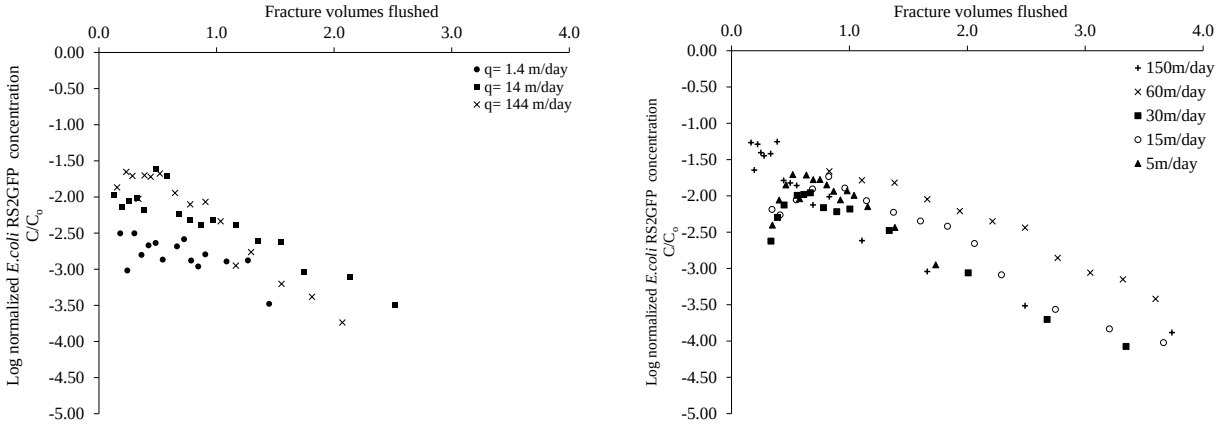

(a) *E. coli* RS2-GFP BTCs for F.

(b) *E. coli* RS2-GFP BTCs for RF.

Figure 4.8: Log normalized median *E. coli* RS2-GFP BTCs in a) F and b) RF at different specific discharges.

Typically, the observations from the *E. coli* RS2-GFP BTCs in Figure 4.8 demonstrate that: 1) the BTCs for RF are smoother than the BTCs for F, and 2) specific discharge has very little effect on the shape and magnitude of the *E. coli* RS2-GFP BTCs from RF compared to those from F. F and RF both have a negative surface charge (Table 4.1). However, since the *E. coli* RS2-GFP also have a negative surface charge, according to DLVO theory, the larger negative surface charge of RF results in larger repulsive electrostatic forces between the *E. coli* and RF than with the *E. coli* and F. Therefore, fewer collisions between the *E.*

coli RS2-GFP and the fracture wall will result in attachment in RF compared to the number of collisions in F that result in attachment. Since collisions are required for attachment to occur, attachment conditions are more favourable in F than in RF. It is also likely that the difference in retention observed between F and RF (43 % versus 72%, respectively) is due to attachment.

4.3.3 Qualitative *E. coli* RS2-GFP Tracer Test Results

Figure 4.9 shows the imaging results of the tracer experiments at different specific discharges (rows) and at different fracture volume flushes (columns). Consistent with the BTCs shown in Figure 4.8, these images reveal that at different specific discharges, but identical

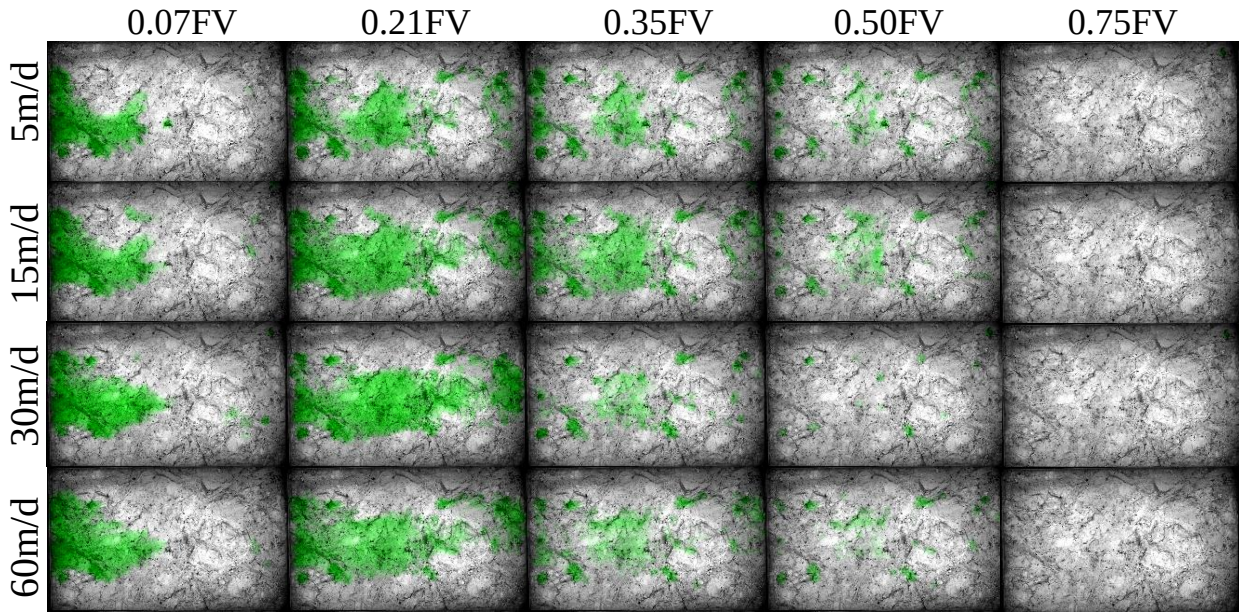

Figure 4.9: *E. coli* RS2-GFP traveling through RF at various specific discharges (rows) captured at different fracture volume flushes (columns). Bulk flow is from left to right.

fracture volume flushes, the *E. coli* RS2-GFP appear to be transported a similar distance through the fracture, indicating that the transport of *E. coli* RS2-GFP through the fracture is determined by the number of fracture volume flushes and not by specific discharge. Since larger specific discharges would be accompanied by larger shear forces that could cause the

detachment of microorganisms from a surface, the similarities of the images in Figure 4.9 at identical fracture volume flushes but different specific discharges, together with the similarities of the BTCs for RF shown in Figure 4.8 further suggest that little *E. coli* RS2-GFP attachment is occurring in RF.

As shown in Figure 4.9, there appears to be a dominant preferential pathway through which the *E. coli* RS2-GFP travel under all specific discharges. As the specific discharge increases, the *E. coli* RS2-GFP typically sample a wider area of the aperture field along the dominant preferential pathway. The most likely explanation for this is that the higher specific discharges result in enough pressure for the fluid, and thereby the particulates, to invade smaller aperture regions.

It must be noted that the detection limits of the camera were higher than the lowest concentrations of the *E. coli* RS2-GFP. That means that when the *E. coli* RS2-GFP concentration became too dilute, the camera could no longer detect the presence of *E. coli* RS2-GFP. Therefore, the images falsely indicate that after approximately 0.75 fracture volumes all of the *E. coli* RS2-GFP had exited the fracture. However, these images show valuable information regarding the transport of *E. coli* RS2-GFP under different specific discharges and the preferential travel pathways in fractures.

4.4 Conclusions

Due to the heterogeneous nature of fractures, fractured aquifers are amongst the most poorly understood natural environments despite the large threat they pose to groundwater sources. This research demonstrated the large influence of matrix properties on the transport of *E. coli* RS2-GFP. Moreover, this research visually demonstrated the presence of and behaviour of the preferential pathways of *E. coli* RS2-GFP under a variety of flow conditions, which has never been previously reported in the literature. In addition, through this

research an improved mechanistic understanding of particulate transport in fractures was developed, which is instructive to groundwater management and protection strategies, as well as modeling of particulate transport. In particular:

- Below specific discharges of approximately 30 m·day^{-1} the recovery of *E. coli* RS2-GFP increases with increasing specific discharge; however, there exists a critical specific discharge somewhere between 30 and 150m·day^{-1} beyond which the recovery remains relatively steady with increasing specific discharge. This is an important observation because under very large flow conditions, hydrodynamic forces are likely enabling the *E. coli* RS2-GFP to overcome the repulsive electrostatic forces, promoting collisions, and therefore attachment, between the like charged *E. coli* RS2-GFP and the matrix.

- To achieve a 2-3 log decrease in BTC concentration, F typically required between two and three fracture volume flushes, whereas RF typically required between three and four fracture volume flushes. The number of fracture volume flushes required to achieve these decreases in concentration was independent of specific discharge. Moreover, RF consistently had higher recoveries than F. Since the major difference between F and RF is in the surface charge of the matrix, this finding demonstrates the importance of surface charge in predicting the fate and transport of particulates in fractured ground water environments and highlights the importance of surface charge in characterizing and/or managing a fractured aquifer that could be used as a source of potable water.

- The visualization results demonstrated that at increasing specific discharges, the dominant preferential pathway of the *E. coli* RS2-GFP in RF remained the same, however, at higher specific discharges, the preferential pathway broadened slightly. It is postulated that the higher specific discharges are accompanied by higher pressures enabling the fluid, and thereby the particulates, to invade smaller aperture regions.

References

Arnon, S., Dahan, O., Elhanany, S., Cohen, K., Pankratov, I., Gross, A., R. Z., Baram, S., Shore, L., 2008. Transport of Testosterone and Estrogen from Dairy-Farm Waste Lagoons to Groundwater. Environmental Science & Technology 42.

Chrysikopoulos, C., Abdel-Salem, A., 1997. Modeling olloid ransport and eposition in at-urated ractures. Colloids and Surfaces A: Physicochemical and Engineering Aspects 121, 189–202.

Dickson, S., Thomson, N., 2003. Dissolution of Entrapped DNAPLs in Variable Aperture Fractures: Experimental Data and Empirical Model. Environmental Science & Technology 37, 4128–4137.

Dickson, S. E., 2001. Dissolution of Entrapped DNAPLs in Variable Aperture Fractures. Ph.D. thesis, University of Waterloo, Waterloo, Ontario, Canada.

Fahim, M., Wakao, N., 1982. Parameter Estimation from Tracer Response Measurements. The Chemical Engineering Journal 25, 1–8.

McKay, L. D., Cherry, J. A., Bales, R. C., Yahya, M. T., Gerba, C. P., 1993. A Field Example of Bacteriophage as Tracers of Fracture Flow. Environmental Science & Technology 27, 1075–1079.

Nowlan, L., 2007. Eau Canada The Future of Canada's Water. Vancouver: UBC Press, Ch. Out of Sight, Out of Mind? Taking Canada's Groundwater for Granted, pp. 55–83.

Passmore, J., Rudolph, D., Mesquita, M., Cey, E., Emelko, M., 2010. The Utility of Microspheres as Surrogates for the Transport of E. coli RS2g in Partially Saturated Agricultural Soil. Water Research 44, 1235–1245.

Piggot, A., Elsworth, D., 1993. Laboratory Assessment of the Equivalent Apertures of a Rock Fracture. Geophysical Research Letters 20 (13), 1387–1390.

Rasmussen, T., June 1995. Laboratory Characterization of Fluid Flow Parameters in a Porous Rock Containing a Discrete Fracture. Geophysical Research Letters 22 (11), 1401–1404.

Rodrigues, S., Dickson, S., Qu, J., 2012. Colloid Retention Mechanisms in Single, Saturated, Variable-Aperture Fractures. Water Research, accepted, DOI: 10.1016/j.watres.2012.08.033.

Saini, R., Halverson, L., Lorimor, J., 2003. Rainfall Timing and Frequency Influence on Leaching of Escherichia coli RS2G through Soil Following Manure Application. Journal of Environmental Quality 32, 1865–1872.

Tsang, Y., 1992. Usage of 'Equivalent Apertures' for Rock Fractures as Derived from Hydraulic and Tracer Tests. Water Resources Research 28 (5), 1451–1455.

Yao, K.-M., Habibian, M. T., O'Melia, C., November 1971. Water and Waste Water Filtration: Concepts and Applications. Environmental Science & Technology 5 (11), 1105–1112.

Zheng, C., Bianchi, M., Gorelick, S. M., 2011. Lessons Learned from 25 Years of Research at the MADE Site. Ground Water 49 (5), 649–662.

Zheng, C., Gorelick, S. M., 2003. Analysis of Solute Transport in Flow Fields Influenced by Preferential Flowpaths at the Decimeter Scale. Ground Water 41 (2), 142–155.

Zheng, Q., Dickson, S., Guo, Y., 2008. On the Appropriate 'Equivalent Aperture' for the Description of Solute Transport in Single Fractures: Laboratory-Scale Experiments. Water Resources Research 44.

Zheng, Q., Dickson, S., Guo, Y., 2009. Differential Transport and Dispersion of Colloids Relative to Solutes in Single Fractures. Journal of Colloid and Interface Science 339 (1), 140–151.

Chapter 5

Conclusions

One of the most exciting aspects of this work was that it focused on conducting a study of particulate transport in fractured environments, which are amongst the mostly poorly understood natural environments, despite the high risks they pose to the protection of drinking water sources. The experimental setup was designed to mimic natural groundwater conditions and a significant effort was made to characterize each of the fractures. Best practices were followed when conducting the *E. coli* RS2-GFP tracer experiments and this resulted in data that were repeatable and reliable. An extensive dataset (generated by myself and others in this laboratory) was used to identify the most important factors contributing to particulate retention and to develop a predictive model for the retention of (bio)colloids in fractures. The tracer experiments conducted in one of the natural fractures and an epoxy replica of that same fracture enabled the isolation of the effects of matrix properties on particulate transport. The following discussion draws out the overall implications of the research presented in this thesis.

5.1 Conclusions & Implications from Chapter 2

The analysis of the tracer experiments conducted in three natural fractures and presented in Paper 1 reveals the following:

- The mean aperture, the COV_S and the specific discharge are all important factors affecting particulate recovery in fractures due to the significant influence each has on attachment and detachment of *E. coli* RS2-GFP to the fracture surfaces.
- The COV_S helped explain the characteristic properties of the peak concentrations and the tails of the *E. coli* RS2-GFP BTCs. This could be a useful tool in developing improved characterization techniques for fractured aquifers at the field scale.
- Higher specific discharges and/or smaller apertures do not always facilitate particulate transport. In this study, the attachment mechanism played a significant role in determining retention. In fact, the number of fracture volumes required to achieve a 2-3 log decrease in BTC concentration is independent of specific discharge.

Appropriate fracture characterization is imperative to understanding and predicting the fate and transport of particulate contaminants in fractured groundwater environments. The mean aperture and COV_S can be determined at the field scale and their determination could result in improved fractured aquifer characterization.

5.2 Conclusions & Implications from Chapter 3

The statistical analysis performed on over 70 particulate tracer experiments discussed in Paper 2 revealed the following:

- The most important factors affecting particulate retention in fractures are the ratio of

the solution chemistry and particulate geometry to the zeta potential of the fracture surface, the ratio of the zeta potentials of the particle and the collector, and the flow characteristics as described by the Peclet number.

- Under the conditions tested during the experimental phase of this research, the less significant factors influencing particle retention are the surface area to volume ratio of the particle, the aperture variability, the equivalent aperture, the density of the particle, and the Reynold's number.

The identification and relation of the most important factors contributing to particulate retention in fractures based on extensive empirical data has never before been presented in the literature. The ionic strength of solution, and the surface charge of the collector act together to affect the degree of attachment that occurs. Therefore, the importance of ionic strength and collector surface properties in predicting retention is consistent with earlier findings within the research presented in this thesis, which indicate the significant role of attachment in particulate retention in these studies.

5.3 Conclusions & Implications from Chapter 4

The comparative analysis between the tracer experiments conducted in the natural fracture as well as a replica of that same fracture, in addition to the images which captured the transport of *E. coli* RS2-GFP through the replica fracture revealed the following:

- *E. coli* RS2-GFP recoveries were much higher in the tracer experiments conducted in the epoxy replica fracture than in experiments conducted in the natural fracture. The different surface properties of the two fractures was influential in determining attachment, and hence, recoveries.

- The *E. coli* RS2-GFP travel through the replica fracture primarily through a dominant preferential pathway. This pathway broadens under increasing flow conditions.
- Colloid/biocolloid transport and retention is dependent on the physical *and* chemical properties of the system, and play a significant role in determining the degree of retention achieved in a fractured aquifers.

Employing a transparent epoxy replica fracture enabled a direct comparison between fractures of nearly identical aperture field characteristics, but vastly different matrix properties. In effect, this study isolates the role that matrix properties play in *E. coli* RS2-GFP retention in fractures, and points to the significant effect of the matrix properties on retention. Since the work presented in earlier portions of this thesis indicated the significance of attachment as a retention mechanism for *E. coli* RS2-GFP, and knowing that attachment is affected by electrostatic forces, the finding that fracture matrix properties have a significant effect on attachment, and thus retention, is not surprising. In addition to isolating the effects of matrix properties on retention, the images capturing *E. coli* RS2-GFP transport through the fracture are not only novel, they also reveal relevant and important information on the transport of biocolloids in fractures. Of note is that increasing specific discharges, seem to be accompanied by larger critical pore entry pressures enabling the bulk fluid, and thereby the *E. coli* RS2-GFP, to sample smaller sections of the aperture field.

5.4 Concluding Remarks

The research presented in this thesis forms a coherent and substantial body of work that significantly advances the knowledge in this field. Relatively few studies have been conducted to improve the understanding and characterization of fractures in natural groundwater environments. The data presented herein represents novel findings and implications that have never before been published in this capacity. This information could be helpful in informing

and updating groundwater management policies and land-use practices so that they better reflect the science. In the groundwater field, there is so little fracture-specific information available that coupling the understanding of a critical environmental setting (fractures) with high-quality particulate tracer experiments and associated modeling represent significant contributions to the literature.

Chapter 6

Suggestions for Future Work

The research discussed in this thesis was designed to identify pore-scale retention mechanisms. However,s verifying these findings at the field-scale is a very relevant task. It is possible that the specific mechanisms identified through this research have a higher or lower significance under field-scale flow and aperture conditions which may vary by several orders of magnitude.

The mass balance aperture and the COV_S were identified as important measures when characterizing a fracture. It would be interesting to verify that these measures have a similar utility for characterizing fractured aquifers at the field-scale.

Collecting more particulate tracer data could be used to improve the predictive abilities of the statistical model developed in this research. Ideally, field-scale data from tracer experiments of similar quality to the ones presented in this thesis could be used to develop a statistical model that improves the mechanistic understanding of particulate retention at the field-scale.

The importance of the ionic strength of solution, together with the charges of the collector and the particulate were identified through the statistical model developed in this research.

Therefore, it would be interesting to conduct visualization tracer experiments employing the *E. coli* RS2-GFP under a range of ionic strengths of solution and flow conditions.

The *E. coli* RS2-GFP appear to sample smaller aperture regions within the fracture under larger specific discharges. It would be valuable to identify the effect of increasing specific discharge on the preferential flow paths of microspheres since microspheres are often used as surrogates for microorganisms. Therefore, conducting tracer experiments using microspheres of similar charge to the *E. coli* RS2-GFP without changing the ionic strength of the bulk solution or the flow conditions employed in these experiments could identify some of the similarities and differences in preferential transport between microspheres and microorganisms.

Chapter 7

Appendix A

Table 7.1: *E. coli* RS2-GFP recoveries from experiments conducted in the natural fractures.

Fracture ID	**b_c** [mm]	**b_m** [mm]	**b_f** [mm]	**σ / b_m** [-]	**Specific Discharge** [cm/min]	**Replicates** [#]	**Average recovery** [%]	**Standard deviation** [%]
F1	0.167	2.624	0.042	0.555	0.1	3	66.8	12.7
					1	3	43.2	22.4
					10	3	42.8	9.2
F2	0.169	4.392	0.033	0.564	0.1	3	11.8	10.3
					1	3	43.7	14.9
					10	3	45.3	15.1
F3	0.305	3.783	0.087	0.548	0.1	3	24.8	21.6
					1	3	64.1	13.6
					10	3	56.9	9.6

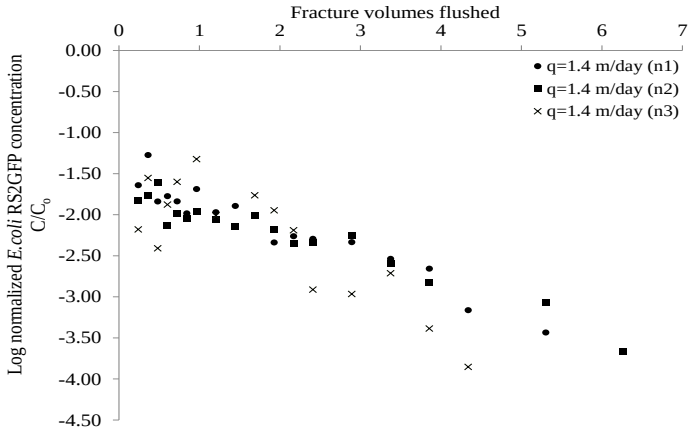

(a) q = 0.1cm·min^{-1}

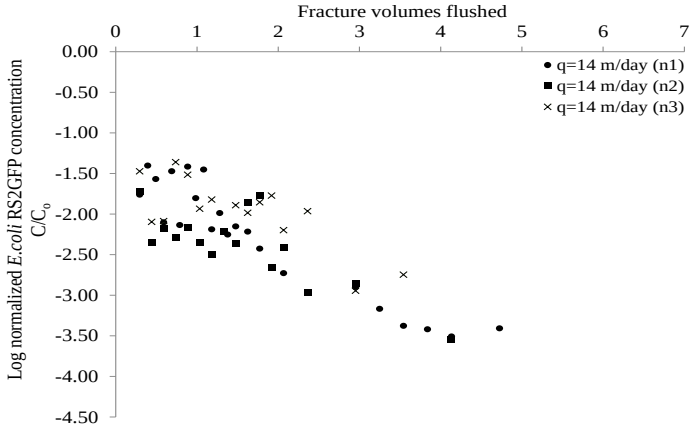

(b) q = 1cm·min^{-1}

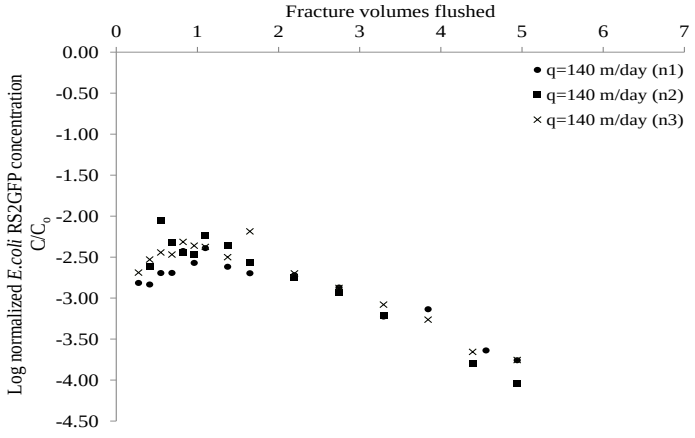

(c) q = 10cm·min^{-1}

Figure 7.1: Log-normalized median *E. coli* RS2-GFP BTCs for F1 at a)1.4m·d^{-1}, b)14m·d^{-1}, and c) 140m · d^{-1} (in triplicate).

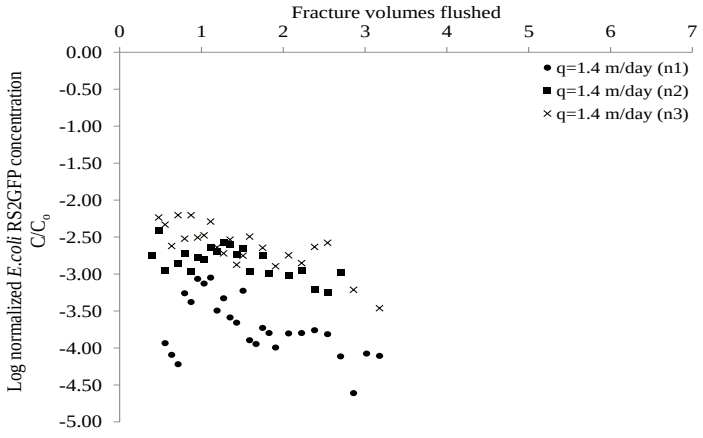

(a) q = 0.1cm·min^{-1}

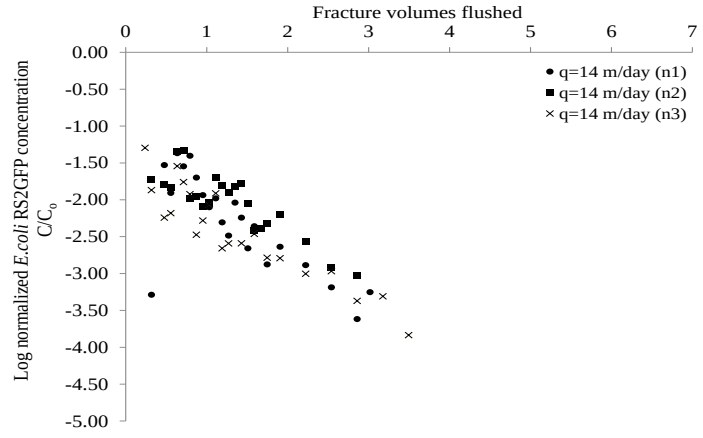

(b) q = 1cm·min^{-1}

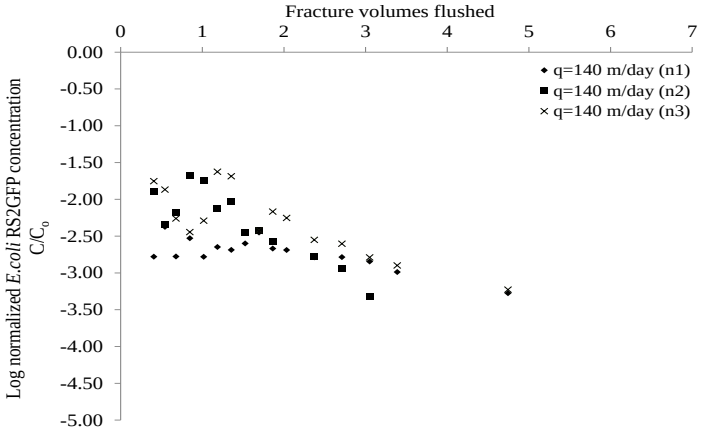

(c) q = 10cm·min^{-1}

Figure 7.2: Log-normalized median *E. coli* RS2-GFP BTCs for F2 at a)1.4m·d^{-1}, b)14m·d^{-1}, and c) 140m · d^{-1} (in triplicate).

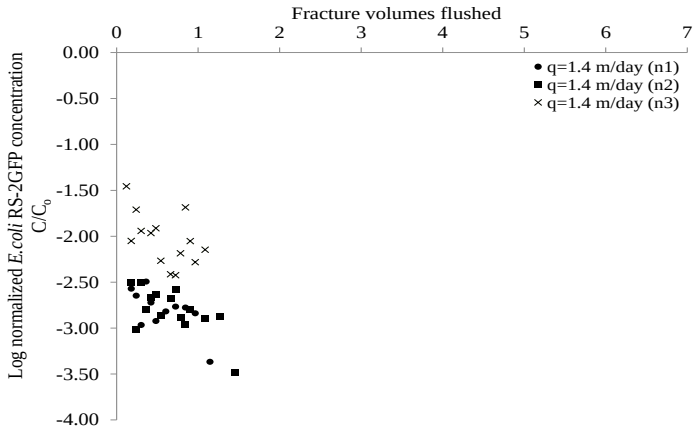

(a) q = 0.1cm·min^{-1}

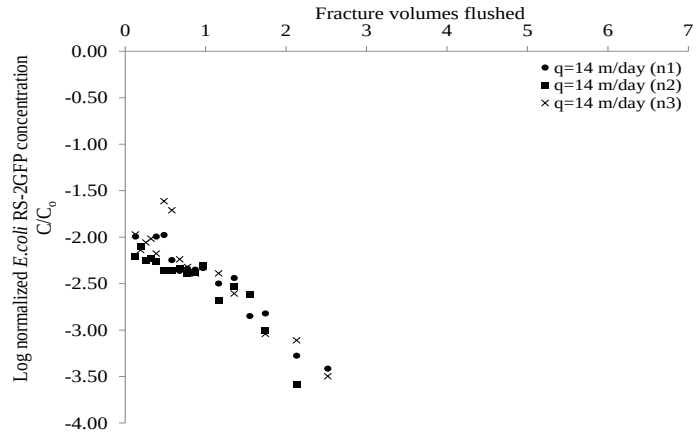

(b) q = 1cm·min^{-1}

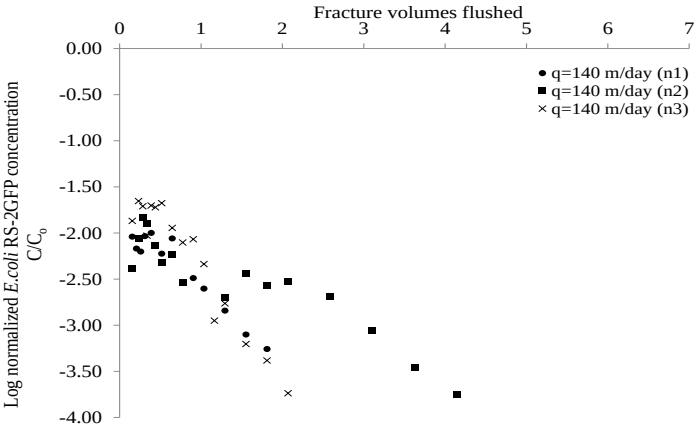

(c) q = 10cm·min^{-1}

Figure 7.3: Log-normalized median *E. coli* RS2-GFP BTCs for F3 at a)1.4m·d^{-1}, b)14m·d^{-1}, and c) 140m · d^{-1} (in triplicate).

Chapter 8

Appendix B

```
background_image = 'nameofbackgroundimage.tif';
test_image = 'nameofstackedimages.tif';

img_bg = im2double(imread(background_image));

yrange = 180:790;
xrange = 80:1090;

low_high = stretchlim(img_bg(yrange, xrange));
img_bg = imadjust(img_bg, low_high);
background = img_bg(yrange, xrange);

lowpass = fspecial('gaussian', 30, 10);

for i = 1:numel(imfinfo(test_image))
    img = im2double(imread(test_image, i));
    img = imadjust(img, low_high);
    frame = img(yrange, xrange);

    diff = background - frame;

    diff(find(diff < 0.025)) = 0; % 0.05 Change this if
                                  %exposure changes

    diff = medfilt2(diff, [7 7]);
    diff = imfilter(diff, lowpass);

    diff = (diff .^ 0.35) * 1.5; %(diff .^ 0.5) * 1.5 Change
                                 % this if exposure changes
    diff = repmat(diff, [1 1 3]);
    diff(:, :, 2) = 0;  % 1:Red 2:Green 3:Blue
    out = repmat(frame, [1 1 3]) - diff;

    img = repmat(img, [1 1 3]);
    img(yrange, xrange, :) = out;

    imwrite(out, ['out_' sprintf('%02d', i) '.png']); %just fracture
    %imwrite(img, ['img_' sprintf('%02d', i) '.png']); %frac & setup
end
```

Figure 8.1: Matlab code used for processing the photos of *E. coli* RS2-GFP transport through the epoxy fracture.

```
/* Before running the code below, using the tool bar, IMPORT the excel file (.xls) into the Sas work
space and call it "SAS_REGRESSION_DATA". */

PROC IMPORT OUT= WORK.SAS_REGRESSION_DATA  /* THIS IS TEMP SAS FILE NAME */
            DATAFILE= "C:\Users\Sandrina\Desktop\RegressionAugust2012.xls"    /* CHANGE THIS FILE
EXTENSION TO CALL ON FILE MAKE SURE .XLS*/
            DBMS=EXCEL REPLACE;
     RANGE="Sheet1$";
     GETNAMES=YES;
     MIXED=NO;
     SCANTEXT=YES;
     USEDATE=YES;
     SCANTIME=YES;
RUN;
PROC REG;
MODEL

LN_FRACTION_RETAINED = LN_SURFACE_CHARGE LN_IONIC_STRENGTH LN_SA_VOLUME LN_GRAV_ADVEC
LN_APERTURE_VARIABILITY LN_STRAINING_UF LN_STRAINING_UC LN_REYNOLDS_NUMBER LN_PECLET_NUMBER


/SELECTION=STEPWISE     /* STEPWISE FORWARD BACKWARD */
       SLENTRY=0.05     /* SIGNIFICANCE OF VARIABLE TO ENTER/EXIT MODEL*/
       SLSTAY=0.05
       ;

RUN;
*************************************************************************************************
PROC IMPORT OUT= WORK.SAS_REGRESSION_DATA  /* THIS IS TEMP SAS FILE NAME */
            DATAFILE= "E:\NOV18UPDATED_MODELING.xls"  /* CHANGE THIS FILE EXTENSION TO CALL ON FILE
MAKE SURE IT HAS EXTENSION: .XLS*/
            DBMS=EXCEL REPLACE;
     RANGE="Sheet1$";
     GETNAMES=YES;
     MIXED=NO;
     SCANTEXT=YES;
     USEDATE=YES;
     SCANTIME=YES;
RUN;
PROC REG;
MODEL

LN_FRACTION_RETAINED = LN_SURFACE_CHARGE LN_IONIC_STRENGTH LN_PECLET_NUMBER
/* WHERE THIS IS YOUR REDUCED MODEL AFTER REGRESSION ANALYSIS */

/CLB ALPHA=0.05   /* THIS PRODUCES CONFIDENCE LIMITS ON BETA VALUES */
VIF   /* THIS PRODUCES VARIANCE INFLATION FACTORS FOR EACH BETA VALUE */

       ;

RUN;
```

Figure 8.2: SAS code used to develop particulate retention model.

Table 8.1: Table of all the dimensionless numbers used in the multiple linear regression analysis. Each row represents values corresponding to one tracer experiment.

f_r	N_Q	N_{IS}	N_{geo}	$N_{Gr\text{-}Ad}$	N_{COV}	N_{bf}	N_{bc}	N_{Re}	N_{Pe}
0.214	5.17E-01	3.40E+06	2.74E+04	9.48E+10	1.60E-02	2.76E-05	4.42E-07	3.08E-03	9.73E+06
0.317	5.17E-01	3.40E+06	2.74E+04	9.48E+10	1.60E-02	2.76E-05	4.42E-07	3.08E-03	9.73E+06
0.688	5.17E-01	3.40E+06	2.74E+04	9.48E+08	1.60E-02	2.76E-05	4.42E-07	3.08E-02	9.73E+07
0.706	5.17E-01	3.40E+06	2.74E+04	9.48E+08	1.60E-02	2.76E-05	4.42E-07	3.08E-02	9.73E+07
0.309	5.17E-01	3.40E+06	2.74E+04	9.48E+08	1.60E-02	2.76E-05	4.42E-07	3.08E-02	9.73E+07
0.482	5.17E-01	3.40E+06	2.74E+04	9.48E+06	1.60E-02	2.76E-05	4.42E-07	3.08E-01	9.73E+08
0.570	5.17E-01	3.40E+06	2.74E+04	9.48E+06	1.60E-02	2.76E-05	4.42E-07	3.08E-01	9.73E+08
0.665	5.17E-01	3.40E+06	2.74E+04	9.48E+06	1.60E-02	2.76E-05	4.42E-07	3.08E-01	9.73E+08
0.860	5.17E-01	3.40E+06	2.16E+04	1.59E+11	7.51E-03	3.52E-05	2.64E-07	3.12E-03	1.17E+07
0.880	5.17E-01	3.40E+06	2.16E+04	1.59E+11	7.51E-03	3.52E-05	2.64E-07	3.12E-03	1.17E+07
0.780	5.17E-01	3.40E+06	2.16E+04	1.59E+11	7.51E-03	3.52E-05	2.64E-07	3.12E-03	1.17E+07
0.649	5.17E-01	3.40E+06	2.16E+04	1.59E+09	7.51E-03	3.52E-05	2.64E-07	3.12E-02	1.17E+08
0.391	5.17E-01	3.40E+06	2.16E+04	1.59E+09	7.51E-03	3.52E-05	2.64E-07	3.12E-02	1.17E+08
0.694	5.17E-01	3.40E+06	2.16E+04	1.59E+07	7.51E-03	3.52E-05	2.64E-07	3.12E-01	1.17E+09
0.554	5.17E-01	3.40E+06	2.16E+04	1.59E+07	7.51E-03	3.52E-05	2.64E-07	3.12E-01	1.17E+09
0.392	5.17E-01	3.40E+06	2.16E+04	1.59E+07	7.51E-03	3.52E-05	2.64E-07	3.12E-01	1.17E+09
0.890	5.17E-01	3.40E+06	5.69E+04	1.37E+11	2.30E-02	1.33E-05	3.07E-07	5.63E-03	1.47E+07
0.862	5.17E-01	3.40E+06	5.69E+04	1.37E+11	2.30E-02	1.33E-05	3.07E-07	5.63E-03	1.47E+07
0.329	5.17E-01	3.40E+06	5.69E+04	1.37E+09	2.30E-02	1.33E-05	3.07E-07	5.63E-02	1.47E+08
0.507	5.17E-01	3.40E+06	5.69E+04	1.37E+09	2.30E-02	1.33E-05	3.07E-07	5.63E-02	1.47E+08
0.241	5.17E-01	3.40E+06	5.69E+04	1.37E+09	2.30E-02	1.33E-05	3.07E-07	5.63E-02	1.47E+08
0.524	5.17E-01	3.40E+06	5.69E+04	1.37E+07	2.30E-02	1.33E-05	3.07E-07	5.63E-01	1.47E+09
0.438	5.17E-01	3.40E+06	5.69E+04	1.37E+07	2.30E-02	1.33E-05	3.07E-07	5.63E-01	1.47E+09
0.332	5.17E-01	3.40E+06	5.69E+04	1.37E+07	2.30E-02	1.33E-05	3.07E-07	5.63E-01	1.47E+09
0.233	5.68E+01	3.40E+06	1.63E+05	5.02E+07	4.13E-01	4.66E-06	1.92E-06	1.32E-01	4.14E+08
0.202	5.68E+01	3.40E+06	1.62E+05	3.85E+07	5.36E-01	4.68E-06	2.51E-06	1.32E-01	4.14E+08
0.377	5.68E+01	3.40E+06	1.61E+05	4.44E+08	4.15E-01	4.72E-06	1.96E-06	4.40E-02	1.38E+08
0.769	5.68E+01	3.40E+06	3.99E+05	1.05E+08	4.85E-01	1.90E-06	9.21E-07	2.67E-01	3.31E+08
0.493	5.68E+01	3.40E+06	4.16E+05	9.62E+07	5.50E-01	1.82E-06	1.00E-06	2.67E-01	3.31E+08
0.453	5.68E+01	3.40E+06	2.42E+05	1.01E+09	2.73E-01	3.14E-06	8.57E-07	8.88E-02	1.10E+08
0.325	8.45E+01	4.19E+01	4.35E+05	2.71E+07	3.67E-01	3.45E-06	1.27E-06	2.44E-01	2.72E+08
0.274	8.45E+01	4.19E+02	4.35E+05	2.71E+07	3.67E-01	3.45E-06	1.27E-06	2.44E-01	2.72E+08

Table 8.1: (cont.) Table of all the dimensionless numbers used in the multiple linear regression analysis. Each row represents values corresponding to one particulate tracer experiment.

f_r	N_Q	N_{IS}	N_{geo}	$N_{Gr\text{-}Ad}$	N_{COV}	N_{bf}	N_{bc}	N_{Re}	N_{Pe}
0.216	8.45E+01	4.19E+03	4.95E+05	1.38E+07	2.09E-01	3.03E-06	6.33E-07	6.52E-01	7.83E+08
0.066	8.45E+01	4.19E+01	4.80E+05	6.37E+06	1.87E-01	3.13E-06	5.85E-07	9.99E-01	1.20E+09
0.140	8.45E+01	4.19E+02	4.80E+05	6.37E+06	1.87E-01	3.13E-06	5.85E-07	9.99E-01	1.20E+09
0.128	8.45E+01	4.19E+03	4.80E+05	6.37E+06	1.87E-01	3.13E-06	5.85E-07	9.99E-01	1.20E+09
0.203	8.45E+01	4.19E+01	6.15E+05	5.11E+07	2.75E-01	2.44E-06	6.71E-07	3.66E-01	3.94E+08
0.191	8.45E+01	4.19E+02	6.15E+05	5.11E+07	2.75E-01	2.44E-06	6.71E-07	3.66E-01	3.94E+08
0.256	8.45E+01	4.19E+03	6.15E+05	5.11E+07	2.75E-01	2.44E-06	6.71E-07	3.66E-01	3.94E+08
0.099	8.45E+01	4.19E+01	5.85E+05	1.35E+07	2.53E-01	2.56E-06	6.49E-07	7.24E-01	7.81E+08
0.154	8.45E+01	4.19E+02	5.85E+05	1.35E+07	2.53E-01	2.56E-06	6.49E-07	7.24E-01	7.81E+08
0.192	8.45E+01	4.19E+03	5.85E+05	1.35E+07	2.53E-01	2.56E-06	6.49E-07	7.24E-01	7.81E+08
0.176	8.45E+01	4.19E+01	5.10E+05	7.18E+06	1.76E-01	2.94E-06	5.18E-07	1.11E+00	1.20E+09
0.183	8.45E+01	4.19E+03	5.10E+05	7.18E+06	1.76E-01	2.94E-06	5.18E-07	1.11E+00	1.20E+09
0.826	5.17E-01	3.40E+06	6.47E+04	2.60E+08	3.17E-02	1.17E-05	3.72E-07	1.11E-01	4.05E+08
0.594	5.17E-01	3.40E+06	6.47E+04	2.34E+09	3.17E-02	1.17E-05	3.72E-07	3.69E-02	1.35E+08
0.930	5.17E-01	3.40E+06	6.47E+04	9.35E+09	3.17E-02	1.17E-05	3.72E-07	1.85E-02	6.76E+07
0.446	5.17E-01	3.40E+06	3.27E+04	1.78E+08	2.34E-02	2.32E-05	5.43E-07	9.00E-02	3.39E+08
0.430	5.17E-01	3.40E+06	3.27E+04	1.60E+09	2.34E-02	2.32E-05	5.43E-07	3.00E-02	1.13E+08
0.888	5.17E-01	3.40E+06	3.27E+04	6.40E+09	2.34E-02	2.32E-05	5.43E-07	1.50E-02	5.65E+07
0.220	7.69E-01	5.32E-01	6.47E+04	2.69E+08	3.17E-02	5.05E-07	1.60E-08	1.11E-01	1.75E+07
0.240	7.69E-01	5.32E-01	3.27E+04	1.84E+08	2.34E-02	1.00E-06	2.34E-08	9.00E-02	1.46E+07
0.159	7.69E-01	5.32E-01	3.27E+04	1.84E+08	2.34E-02	1.00E-06	2.34E-08	9.00E-02	1.46E+07
0.409	7.69E-01	5.32E-01	3.27E+04	1.66E+09	2.34E-02	1.00E-06	2.34E-08	3.00E-02	4.87E+06

Table 8.2: Table of all the dimensionless numbers used to verify the predictive model. Each row represents values corresponding to one particulate tracer experiment.

f_r	N_Q	N_{IS}	N_{geo}	$N_{Gr\text{-}Ad}$	N_{COV}	N_{bf}	N_{bc}	N_{Re}	N_{Pe}
0.466	5.17E-01	3.40E+06	2.74E+04	9.48E+10	1.60E-02	2.76E-05	4.42E-07	3.08E-03	9.73E+06
0.649	5.17E-01	3.40E+06	2.16E+04	1.59E+09	7.51E-03	3.52E-05	2.64E-07	3.12E-02	1.17E+08
0.503	5.17E-01	3.40E+06	5.69E+04	1.37E+11	2.30E-02	1.33E-05	3.07E-07	5.63E-03	1.47E+07
0.290	5.68E+01	3.40E+06	1.72E+05	1.29E+09	6.12E-01	4.41E-06	2.70E-06	2.20E-02	6.89E+07
0.593	5.68E+01	3.40E+06	1.72E+05	3.49E+09	2.26E-01	4.41E-06	9.97E-07	4.44E-02	5.51E+07
0.237	8.45E+01	4.19E+03	4.05E+05	8.13E+06	2.90E-01	3.70E-06	1.08E-06	4.83E-01	5.39E+08
0.194	8.45E+01	4.19E+02	4.95E+05	5.25E+07	2.16E-01	3.03E-06	6.54E-07	3.29E-01	3.95E+08
0.176	8.45E+01	4.19E+01	5.10E+05	7.18E+06	1.76E-01	2.94E-06	5.18E-07	1.11E+00	1.20E+09
0.920	5.17E-01	3.40E+06	6.47E+04	2.60E+08	3.17E-02	1.17E-05	3.72E-07	1.11E-01	4.05E+08
0.446	5.17E-01	3.40E+06	3.27E+04	1.78E+08	2.34E-02	2.32E-05	5.43E-07	9.00E-02	3.39E+08
0.559	7.69E-01	5.32E-01	3.27E+04	6.62E+09	2.34E-02	1.00E-06	2.34E-08	1.50E-02	2.44E+06

Chapter 9

Appendix C

Table 9.1: *E. coli* RS2-GFP recoveries from experiments conducted in the replica fracture.

q [m/day]	*E. coli* Recovery [%]	Standard Deviation [%]
5	64	-
15	72	1.5
30	82	6.63
60	83	-
150	73	-

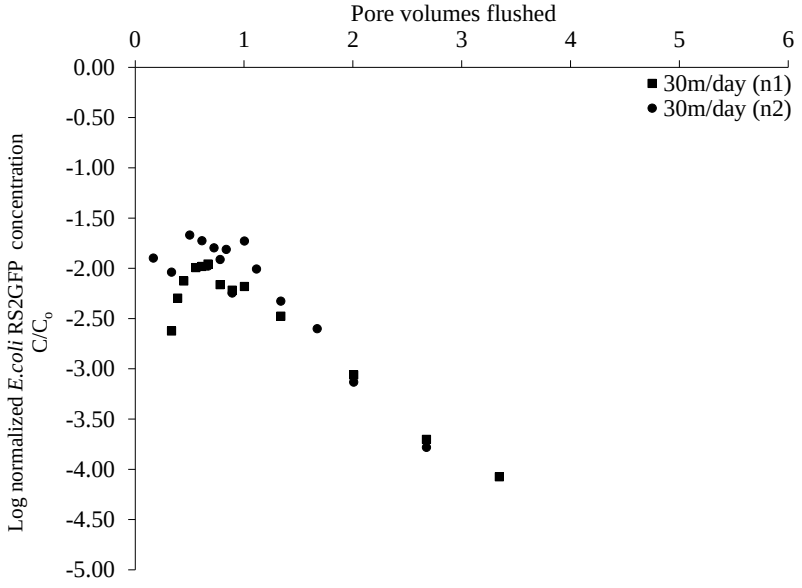

Figure 9.1: *E. coli* RS2-GFP BTC for RF at $30\mathrm{m} \cdot \mathrm{d}^{-1}$ (in duplicate).